MINISTRY OF AVIATION

AERONAUTICAL RESEARCH COUNCIL

REPORTS AND MEMORANDA

The Theory of Interference Effects on Dynamic Measurements in Slotted-Wall Tunnels at Subsonic Speeds and Comparisons with Experiment

By H. C. Garner, A. W. Moore and K. C. Wight

The Theory of Interference Effects on Dynamic Measurements in Slotted-Wall Tunnels at Subsonic Speeds and Comparisons with Experiment

By H. C. Garner, A. W. Moore and K. C. Wight

Summary.

Experiment has already shown that the aerodynamic damping on half-span models in pitching oscillation is subject to interference effects that may exceed 30 per cent in slotted-wall tunnels at subsonic speeds. An explanatory theory is presented with numerous illustrations and comparisons with measured data. The basic assumptions demand a small ratio of model span to tunnel breadth, small frequency parameter and open instead of slotted boundaries; nevertheless, the effects of span, frequency and slot geometry are considered theoretically, as well as those of tunnel shape, planform, model size, Mach number and pitching axis.

Further experiments have been made to check the theory, and conclusions are drawn from studies in four different tunnels with their slots sealed and open. Direct comparison between prediction and measurement is consistently good with slots sealed and in most cases with slots open. For a particular tunnel large discrepancies in the latter case are attributed to viscous effects that cause a wall with too narrow slots to behave like a closed boundary; wall interference then changes sign, is less severe, but can no longer be detected by sealing the slots. Although the theory clarifies the problem, the usefulness of slotted-wall tunnels for dynamic measurements is open to question when corrections are very large.

With inviscid flow the following conclusions are drawn from the theory: (a) that the lift-damping due to pitching is subject to even more serious interference than the direct pitching damping, (b) that it may be impracticable to obtain adequate reduction in the wall corrections simply by testing smaller models, (c) that complete or more slender models are less seriously affected than half-models of moderate aspect ratio, (d) that with horizontal models in rectangular tunnels the best remedy is to have slotted side-walls but closed roof and floor.

LIST OF CONTENTS

LIST OF TABLES

LIST OF ILLUSTRATIONS

1. *Introduction.*

The original concept of a slotted-wall tunnel appears to have been motivated by the desire to reduce wall interference. There are many instances where blockage and lift interference in subsonic flow are altered in sign when closed walls are replaced by open boundaries. Indeed, great reductions in blockage interference led to the design of transonic tunnels with slotted or perforated walls, so as to avoid the choking encountered in closed tunnels at high subsonic speeds. This important development and its manifold implications are fully described by Goethert[1]. Slotted or perforated walls are now accepted as an essential feature of transonic wind-tunnel testing, for these alone permit the Mach number to be varied from subsonic to supersonic without change in the tunnel geometry. It is seldom possible to eliminate simultaneously both blockage and lift interference, but in steady flow a compromise can be reached whereby measured results require only small corrections.

The use of wind tunnels for oscillatory aerodynamics predates the development of suitable lifting-surface theories. Although these now exist for many purposes in both subsonic and supersonic flow, theoretical progress is unlikely to be fruitful in the transonic speed range. Moreover, the unsteady aerodynamic characteristics of slender or bluff shapes, with flow separation, remain largely beyond the scope of established theory which is unlikely to supplant the need for dynamic testing, even at subcritical Mach numbers. The correlation between theoretical calculation and wind-tunnel measurement has been discussed by Acum[2]. Most experiments in compressible flow achieve only quite low values of the frequency parameter, so that Multhopp's[3] subsonic lifting-surface theory often forms the basis of comparison. Wall-interference effects are usually ignored, and under favourable conditions there is evidence of reasonable agreement between linearized theory and uncorrected experiment.

The first indication of excessive interference effects from slotted walls in oscillatory experiments was discovered in 1960 by Bratt and Wight whilst checking the unexpectedly low pitching damping reported in Ref. 4. In the course of measuring pitching derivatives on a half-model M-wing in the NPL 25 in. $\times$ 20 in. Tunnel with eleven longitudinal slots in the roof and floor, they progressively reduced the number of slots until the tunnel was completely closed. Fig. 1 shows large smooth changes in the observed pitching damping at Mach numbers $M = 0.60, 0.80, 0.90$ and 0.95. The effect of the slots increases as M increases until tunnel choking sets a lower limit to the number of slots. It is typical, not only of the M-wing, that the damping can change by 30 per cent or more. There is confirmation of slotted-wall interference in the NPL $9\frac{1}{2}$ in. $\times$ $9\frac{1}{2}$ in. Tunnel from the measurements of Ref. 5. The full evidence from previous experiments has been reviewed by Wight[6] (1964). Although the effect of sealing the slots in the

4

NPL 36 in. × 14 in. Tunnel is observed to be small, the likelihood of large effects in many other tunnels constitutes a threat to the validity of dynamic measurements until an acceptable explanation is found.

Several attempts to explain the phenomenon have proved negative. One possibility, that the large slotted-wall interference might be associated with standing transverse waves, has been ruled out by a theoretical study, due to Acum[7], of acoustic resonance. He shows that the critical frequency parameter for resonance is higher for slotted walls than for closed walls and well outside the experimental range. In another investigation (Ref. 8, Part I) Rushton has considered the oscillatory flow at individual slots by an electrical analogue. The theoretical problem is reduced to two dimensions by confining attention to the distant wake; the results give no reason to doubt the validity of the boundary conditions at the slotted walls. A more likely explanation was thought to stem from resonances or other disturbances in the plenum chamber surrounding the slots or from the step at the downstream end of the slots. Molyneux[9] refers to random disturbances of this kind, but subsequent attempts to measure unsteady pressures in the plenum chamber have shown negligible fluctuations due to the oscillatory motion of the model in the working section.

A recent note by two of the present authors[10] gives a brief account of an extension to the classical theory of lift interference, that offers a convincing explanation of the cases where the aerodynamic forces are particularly sensitive to the sealing of the slots. Ref. 10 is superseded by this fuller presentation of the theory. In essence it is assumed that the model is of small span and oscillates at low frequency in subsonic flow, and that the slotted walls may be replaced by open boundaries, as will be given some justification at the end of Section 2. Under these conditions the sinusoidal interference upwash is expressible as a polynomial in the streamwise distance. For a particular tunnel boundary three interference parameters are sufficient and these are formulated for rectangular cross-sections (Section 3.1.). A dominant role is played by one particular parameter that only occurs in oscillatory flow. Application of lifting-surface theory[3] leads to straightforward relationships between aerodynamic quantities in the tunnel and those in the free stream which are dependent on the Mach number, planform and pitching axis (Section 3.2.). On the basis of the steady lift interference it is suggested that rough estimates of the effects of slot geometry and model span may be made; in Section 4.2. also, the theoretical effect of small frequency is described and in Section 5.3. its application is discussed. There is no attempt to investigate wall interference at transonic speeds when many of the approximations lose their justification.

The theory supports the evidence in Ref. 6 for the NPL 25 in. × 20 in. Tunnel with slots both open and sealed, as indicated by the arrows in Fig. 1. Numerical results in Section 4.1. show that the wall interference on pitching damping is highly dependent on the location of pitching axis. Recent experiments (Section 5.2.) in the NPL $9\frac{1}{2}$ in. × $9\frac{1}{2}$ in. Tunnel confirm this and show reasonable agreement with the theoretical predictions. The basis of comparison is to combine the lifting-surface and wall-interference theories to calculate oscillatory forces on the model in the wind tunnel. In practice it may be desirable to divorce the wall-interference theory from lifting-surface theory, and in Section 6 corrections are applied to measured aerodynamic derivatives as if lifting-surface theory were untrustworthy or not available. It must be recognised, however, that these corrections are often large and may well be less accurate than the technique of measurement. In formulating the slotted-wall interference theory it is assumed that the flow is inviscid, but Section 7 gives a qualitative discussion of possible effects of non-ideal flow through the slots. This appears to provide the most likely source of discrepancies between theory and experiment for the NPL 36 in. × 14 in. Tunnel with slots open (Section 5.1.), for which only the theory gives large interference effects due to sealing of the slots. One important corollary is that the corrections may be quite large, even when sealing of the slots hardly influences the measurements.

The concluding remarks in Section 8 give a more detailed guide to the salient features of the report.

2. Theoretical Treatment of Slotted Walls.

It is supposed that there are uniformly spaced longitudinal slots, that the tunnel cross-section is constant and of unlimited streamwise extent, and that the boundary conditions may be linearized. Then in a flow of velocity potential $(Ux + \phi)$ the condition

$$\partial\phi/\partial n = 0 \text{ at a solid wall or a slot} \tag{1}$$

ensures zero outflow across a closed portion of the tunnel boundary. The requirement of constant pressure at an open portion is linearized to give $\partial\phi/\partial x = 0$; then, since the uniform flow is undisturbed far upstream, integration with respect to streamwise distance x gives

$$\phi = 0 \text{ at a free boundary or a slot.} \tag{2}$$

Both conditions apply in steady or unsteady flow.

Although these mixed boundary conditions are easily formulated, mathematical solutions of Laplace's equation for ϕ in steady flow with the necessary singularities at the edge of each slot are very few. Solutions exist for circular tunnels with equidistant slots, but conformal transformation to rectangular tunnel boundaries would give irregular slot spacing of no practical interest. Therefore the usual approach for rectangular tunnels with walls of uniform slot spacing is to replace equations (1) and (2) by a single homogeneous boundary condition to be satisfied at all points of a slotted wall. The idea was first developed by Davis and Moore[11] (1953) from a suggestion of Dr. A. Busemann. The homogeneous condition may be written as

$$\phi + K\frac{\partial\phi}{\partial n} = 0, \tag{3}$$

where for slots of width a and periodic spacing d in a tunnel of height h the constant K is given by the non-dimensional slot parameter

$$F = \frac{2K}{h} = \frac{2d}{\pi h}\log_e\cosec\frac{\pi a}{2d}. \tag{4}$$

There is evidence in Ref. 11 that the calculated lift interference on small wings in circular tunnels with eight or more discrete slots can be reproduced closely by means of the homogeneous condition (3). Solutions by electrical analogue for rectangular tunnels with discrete slots and conditions (1) and (2) have been obtained by Rushton in Part II of Ref. 8; when there are six slots in the roof and also in the floor, the equivalence of condition (3) is established likewise.

Equations (3) and (4) define the equivalent homogeneous boundary condition for an 'ideal' slotted wall such that viscous effects in the slots can be neglected. Baldwin, Turner and Knechtel[12] have proposed a more general condition

$$\frac{\partial\phi}{\partial x} + K\frac{\partial^2\phi}{\partial x\partial n} + \frac{1}{P}\frac{\partial\phi}{\partial n} = 0, \tag{5}$$

where the porosity parameter P regulates the pressure drop through the slots from tunnel to plenum chamber in proportion to the outflow. By analogy with perforated walls $(K = 0)$ the import of β/P in compressible flow $(\beta^2 = 1 - M^2)$ is fairly well understood from theoretical and experimental studies in steady flow (Ref. 1). But there is little apparent progress towards the evaluation of β/P when viscous slot flow is thought to be significant. At the end of Appendix A of Ref. 12 it is argued that there is a lower limit to the open area ratio a/d below which the mathematical basis for the slot parameter K is unreliable; it is likely, however, that before this limit is approached the porosity parameter P will assume overriding importance.

The boundary condition corresponding to equation (5) in oscillatory flow is not known with certainty, but it is plausible to take

$$\left(\frac{\partial}{\partial x} + \frac{i\omega}{U}\right)\left(\bar{\phi} + K\frac{\partial\bar{\phi}}{\partial n}\right) + \frac{1}{P}\frac{\partial\bar{\phi}}{\partial n} = 0, \tag{6}$$

6

where, in the usual notation, ϕ is written as the real part of $\bar{\phi}\exp(i\omega t)$. Ref. 13 is one of very few mathematical solutions based on such a boundary condition; Drake used equation (6) with $K = 0$ and P real to represent a perforated wall, but perhaps P should be complex so as to permit a phase lag between the pressure drop and the outflow across the wall. For ideal slots ($P \to \infty$) equation (6) integrates to give

$$\bar{\phi}+K\frac{\partial\bar{\phi}}{\partial n} = 0, \tag{7}$$

since $\bar{\phi}$ is identically zero as $x \to -\infty$ upstream. Otherwise equation (6) cannot be integrated to become independent of the frequency ω, and therefore viscous slot flow may lie beyond the scope of the theoretical treatment in Section 3. But when equations (3) and (7) hold, there is a simple integral relationship between the steady and oscillatory upwash fields due to wall interference.

Unfortunately the state of knowledge of the steady interference upwash field in slotted-wall tunnels is incomplete. The known results are virtually confined to the transverse plane containing the lifting element itself. The information concerning the streamline curvature, that is the streamwise gradient of the interference upwash, is exceedingly limited. The experimental evidence of large slotted-wall interference is from tests on half-models in rectangular tunnels with slotted roof and floor. On the reflection-plane principle, with models mounted on solid side-walls the tunnel breadth is effectively doubled and particular interest attaches to breadth to height ratios b/h as high as 2·5. Holder[14] has obtained the most relevant values of the steady interference parameter

$$\delta_0 = \frac{\rho U C}{2L}\frac{\partial\phi_i}{\partial z} \tag{8}$$

at the position of an element of lift L on the tunnel axis. Here ρ and U are respectively the density and speed of the undisturbed stream, C is the cross-sectional area of the tunnel, z is measured vertically upwards and the interference potential ϕ_i is given by

$$\phi = \phi_m+\phi_i, \tag{9}$$

where ϕ_m corresponds to the same element of lift L in the absence of wall constraint. Holder's results for small wings in duplex and square tunnels with slotted roof and floor are plotted in carpet form in Figs. 2 and 3 with allowance for compressibility. For both shapes of tunnel δ_0 is presented in terms of the modified slot and porosity parameters $(1+F)^{-1}$ and $\left(1+\dfrac{\beta}{P}\right)^{-1}$. In each case δ_0 varies from a negative value for open roof and floor when both parameters are unity to a positive value for the completely closed tunnel when either of the parameters is zero.

The NPL tunnels correspond to slot parameters from equation (4) in the range $0.05 < F < 0.11$, so that roughly $0.90 < (1+F)^{-1} < 0.95$ and, apart from the effects of porosity, the slotted walls operate much like open boundaries even when the open area ratio $a/d = 1/11$. A good approximation to unsteady slotted-wall interference can therefore be sought by considering rectangular tunnels with open roof and floor, for which the steady interference upwash field is amenable to analysis (Section 3.1.). Allowance for the slot parameter $(1+F)^{-1}$ may be estimated on the basis of Figs. 2 and 3. Similar interpolation with respect to the porosity parameter $\left(1+\dfrac{\beta}{P}\right)^{-1}$ has little theoretical justification, but the importance of this parameter for particular tunnels is discussed in Section 7.

3. Method of Interference Correction.

The basic idea underlying most applications of oscillatory wall interference is the relation between the steady acceleration potential and the unsteady velocity potential due to Goodman[15] (1953). His

7

result for linearized incompressible flow of arbitrary frequency in any closed tunnel may be written in the form

$$\bar{\phi}(x,y,z) = \int_{-\infty}^{x} \exp\left[\frac{i\omega(\xi-x)}{U}\right] \frac{\partial \phi_0(\xi,y,z)}{\partial \xi} d\xi.$$ (10)

Here ϕ_0 is the velocity potential due to a steady horse-shoe vortex of small span and the real part of $\bar{\phi}\exp(i\omega t)$ is the velocity potential in phase with the oscillating strength of the corresponding semi-infinite vortex doublet. Equation (10) is not restricted to closed tunnels, but it is sufficient that the boundary conditions on ϕ_0 and $\bar{\phi}$ are the same in the respective steady and unsteady problems. This is true in equations (1) and (2) for tunnels with longitudinal slots; equally well, with ideal slots, ϕ_0 and $\bar{\phi}$ satisfy the homogeneous conditions (3) and (7) respectively. The more general condition (6) is dependent on frequency when the porosity parameter P is non-zero and finite; in such cases the method may not be applicable.

The result in equation (10) is also derived by Acum and Garner in Section 3 of Ref. 16, and they go on to explain how the relation can be generalized to the case of low-frequency subsonic compressible flow. They show that

$$\phi_1 = \bar{\phi}\exp\left(-\frac{i\omega M^2 x}{\beta^2 U}\right)$$

satisfies the linear differential equation

$$\frac{\partial \phi_1}{\partial (x/\beta)} + \frac{i\omega\phi_1}{\beta U} = \frac{\partial \phi_0}{\partial (x/\beta)}.$$

By means of the integrating factor $\exp(i\omega x/\beta^2 U)$ it follows that

$$\bar{\phi}(x,y,z) = \int_{-\infty}^{x/\beta} \exp\left[\frac{i\omega\xi}{\beta U} - \frac{i\omega x}{U}\right] \frac{\partial \phi_0(\xi,y,z)}{\partial \xi} d\xi,$$ (11)

where $\bar{\phi}$ refers to the oscillatory compressible flow but ϕ_0 remains the steady velocity potential in incompressible flow due to the semi-infinite vortex doublet. An identical relation for elementary horse-shoe vortices of finite span forms the basis of Acum's[17] general theory of oscillatory wall interference for closed rectangular tunnels. Similarly in Ref. 18 he has treated the problem of slowly oscillating slender wings in subsonic wind tunnels.

Equation (11) holds for the velocity potential with or without wall constraint, and therefore for the complex interference potential $\bar{\phi}_i$ and the interference upwash $\bar{w}_i = \partial\bar{\phi}_i/\partial z$. Expansion to first order in frequency gives along the axis of the tunnel

$$\bar{w}_i(x) = \int_{-\infty}^{x/\beta} \left[1 + \frac{i\omega\xi}{\beta U} - \frac{i\omega x}{U}\right] \frac{dw_{i0}}{d\xi} d\xi,$$ (12)

where $w_{i0}(\xi)$ is the steady interference upwash in incompressible flow. Corresponding to a lifting element L at the position $\xi = 0$ on the tunnel axis we write

$$w_{i0}(\xi) = \frac{2L}{\rho U C} \delta(\xi) \text{ for all } \xi$$ (13)

or

$$w_{i0}(\xi) = \frac{2L}{\rho UC} \left[\delta_0 + \frac{\delta_1 \xi}{h} + O\left(\frac{\xi}{h}\right)^3 \right] \text{ for small } \xi, \tag{14}$$

each a more general form of equation (8). On integration by parts equation (12) gives

$$\bar{w}_i(x) = w_{i0}(x/\beta) + \frac{i\omega}{U} \left[\frac{M^2 x}{\beta^2} w_{i0}(x/\beta) - \frac{1}{\beta} \int_{-\infty}^{x/\beta} w_{i0}(\xi) d\xi \right] .$$

Hence by equations (13) and (14)

$$\bar{w}_i(x) = \frac{2L}{\rho UC} \left[\left(\delta_0 + \frac{\delta_1 x}{\beta h} \right) + \frac{i\omega h}{U} \left(\frac{\delta_0'}{\beta} - \frac{\delta_0 x}{h} + \frac{\delta_1 x^2 (2M^2 - 1)}{2\beta^3 h^2} + O\left(\frac{x}{\beta h}\right)^3 \right) \right] , \tag{15}$$

where

$$\delta_0' = -\frac{1}{h} \int_{-\infty}^{0} \delta(\xi) d\xi. \tag{16}$$

Equation (15) is similar to the expressions used in Refs. 16 and 18, but it includes the extra term in x^2. This imaginary term, also omitted in the preliminary account of the present work in Ref. 10, will be seen to provide contributions to the aerodynamic forces of the same order as some of those arising from the real term in δ_1.

Although primarily concerned with a closed circular tunnel, Ref. 16 also contains in Table A.II the three interference parameters δ_0, δ_1 and δ_0' for closed rectangular tunnels. Although δ_0 and δ_1 are known for other types of rectangular tunnel, there is no information concerning δ_0' from equation (16). It will be seen in Section 3.1 that its formulation is not quite straightforward in the case of practical interest when there are closed side-walls and open roof and floor. Although δ_0' is very small for the larger ratios b/h appropriate to half-models in closed rectangular tunnels, the corresponding values of δ_0' for open roof and floor are found to be fairly large. This, coupled with the fact that the contribution to $\bar{w}_i(x)$ in equation (15) is inversely proportional to a linear dimension of the tunnel, will provide large interference effects. The interpretation of $\bar{w}_i(x)$ is conveniently handled by the techniques of linearized lifting-surface theory for low frequency. Because equation (15) is so simple, the formulation in Section 3.2. is straightforward. Apart from the terms in δ_1, the oscillatory pitching derivatives with wall constraint only involve oscillatory and rotary pitching derivatives in a free stream.

3.1. Interference Parameters.

Of the three interference parameters in equation (15), the two occurring in steady flow are well documented. For small lifting wings centrally placed in rectangular tunnels δ_0 and δ_1 are respectively $\frac{1}{2}\delta$ and $\frac{1}{2}\delta'$, as defined and formulated for closed walls by Glauert in equations (9.01) to (9.02) and (11.1) to (11.4) of Ref. 19. Following Figs. 7 and 8 of Ref. 19, we consider rectangular tunnels of the types (1) to (4) each giving a doubly infinite array of images in the transverse plane at positions $(y,z) = (mb, nh)$, where m and n extend over all positive and negative integral values excluding the pair $(0,0)$ corresponding to the wing itself. The signs of the image doublets are

$$\left. \begin{array}{ll} j = j^{(1)} = (-1)^n & \text{for a completely closed tunnel} \\[4pt] j = j^{(2)} = (-1)^m & \text{for a completely open tunnel} \\[4pt] j = j^{(3)} = (-1)^{m+n} & \text{for open sides, closed roof and floor} \\[4pt] j = j^{(4)} = 1 & \text{for closed sides, open roof and floor} \end{array} \right\} . \tag{17}$$

Thus the interference parameters for steady flow are

$$\delta_0 = \frac{bh}{8\pi} \sum_{-\infty}^{\infty} \sideset{}{'}\sum (j) \frac{m^2b^2 - n^2h^2}{(m^2b^2 + n^2h^2)^2} \tag{18}$$

and

$$\delta_1 = \frac{bh^2}{8\pi} \sum_{-\infty}^{\infty} \sideset{}{'}\sum (j) \frac{m^2b^2 - 2n^2h^2}{(m^2b^2 + n^2h^2)^{5/2}}, \tag{19}$$

where $\sum\sum'_{-\infty}^{\infty}$ denotes that (m,n) takes all possible integral pairs except $(0,0)$. It must be recognised that, although equation (19) is absolutely convergent, the double summation for δ_0 is not. The treatment of equation (18) for rectangular tunnels of type (4) when $j = 1$ needs special care and is fully discussed in Ref. 20; this type of mixed boundary is crucial to the study of wall interference in the NPL slotted tunnels.

The upwash interference parameter δ_0 can be expressed as a single series in several ways. For example, corresponding to the four types of rectangular tunnel listed in equations (17) there are respective formulae

$$\left. \begin{aligned}
\delta_0 &= \delta_0^{(1)} = \frac{\pi h}{24b} + \frac{\pi h}{b} \sum_{n=1}^{\infty} \frac{n}{e^{2n\pi h/b} + 1} \\[2ex]
\delta_0 &= \delta_0^{(2)} = -\frac{\pi h}{48b} - \frac{\pi h}{2b} \sum_{n=1}^{\infty} \frac{2n-1}{e^{(2n-1)\pi h/b} - 1} \\[2ex]
\delta_0 &= \delta_0^{(3)} = -\frac{\pi h}{48b} + \frac{\pi h}{2b} \sum_{n=1}^{\infty} \frac{2n-1}{e^{(2n-1)\pi h/b} + 1} \\[2ex]
\delta_0 &= \delta_0^{(4)} = -\frac{1}{4} + \frac{\pi h}{24b} - \frac{\pi h}{b} \sum_{n=1}^{\infty} \frac{n}{e^{2n\pi h/b} - 1}
\end{aligned} \right\} \quad . \tag{20}$$

There are three useful auxiliary equations concerning $\delta_0^{(4)}$ (λ) where $\lambda = h/b$, namely

$$\left. \begin{aligned}
\delta_0^{(4)}(1/\lambda) &= -\frac{1}{4} - \delta_0^{(4)}(\lambda) \\[2ex]
\delta_0^{(4)}(\tfrac{1}{2}\lambda) &= \delta_0^{(2)}(\lambda) + \delta_0^{(4)}(\lambda) \\[2ex]
\delta_0^{(4)}(2\lambda) &= \delta_0^{(1)}(\lambda) + \delta_0^{(4)}(\lambda)
\end{aligned} \right\} \quad , \tag{21}$$

the first of which is given incorrectly in Ref. 19 and follows from Ref. 20. Values of δ_0 from each of equations (20) are plotted against b/h in Fig. 4.

The streamline curvature parameter δ_1 from equation (19) may be evaluated for the four types of rectangular tunnel from the convergent series

$$\left.\begin{array}{l} \delta_1 = \delta_1^{(1)} = \dfrac{\pi}{24} + \dfrac{h^2}{4\pi b^2}\left[\displaystyle\sum_{m=1}^{\infty}\dfrac{1}{m^3} + \displaystyle\sum_{n=1}^{\infty}(-1)^n S_1\left(\dfrac{nh}{b}\right)\right] \\[3ex] \delta_1 = \delta_1^{(2)} = \dfrac{h^2}{4\pi b^2}\left[\displaystyle\sum_{m=1}^{\infty}\dfrac{(-1)^m}{m^3} + \displaystyle\sum_{n=1}^{\infty} S_2\left(\dfrac{nh}{b}\right)\right] \\[3ex] \delta_1 = \delta_1^{(3)} = \dfrac{h^2}{4\pi b^2}\left[\displaystyle\sum_{m=1}^{\infty}\dfrac{(-1)^m}{m^3} + \displaystyle\sum_{n=1}^{\infty}(-1)^n S_2\left(\dfrac{nh}{b}\right)\right] \\[3ex] \delta_1 = \delta_1^{(4)} = -\dfrac{\pi}{12} + \dfrac{h^2}{4\pi b^2}\left[\displaystyle\sum_{m=1}^{\infty}\dfrac{1}{m^3} + \displaystyle\sum_{n=1}^{\infty} S_1\left(\dfrac{nh}{b}\right)\right] \end{array}\right\} , \qquad (22)$$

where

$$\sum_{m=1}^{\infty}\dfrac{1}{m^3} = 1.2020_5, \qquad \sum_{m=1}^{\infty}\dfrac{(-1)^m}{m^3} = -0.9015_5,$$

and

$$\left.\begin{array}{l} S_1(\mu) = \dfrac{2}{\mu^2} + \displaystyle\sum_{m=-\infty}^{\infty}\dfrac{m^2 - 2\mu^2}{(m^2 + \mu^2)^{5/2}} \\[3ex] S_2(\mu) = \displaystyle\sum_{m=-\infty}^{\infty}(-1)^m\dfrac{m^2 - 2\mu^2}{(m^2 + \mu^2)^{5/2}} \end{array}\right\} . \qquad (23)$$

The most convenient evaluation of $S_1(\mu)$ and $S_2(\mu)$ is by transformation into more rapidly convergent series of modified Bessel functions, as derived by Olver in Ref. 21. Hence

$$\left.\begin{array}{l} S_1(\mu) = -\dfrac{8\pi}{\mu}\displaystyle\sum_{p=1}^{\infty}\left[p\,K_1(2p\pi\mu) + 2p^2\pi\mu K_0(2p\pi\mu)\right] \\[3ex] S_2(\mu) = -\dfrac{4\pi}{\mu}\displaystyle\sum_{p=1}^{\infty}\left[(2p-1)K_1\{(2p-1)\pi\mu\} + (2p-1)^2\pi\mu K_0\{(2p-1)\pi\mu\}\right] \end{array}\right\} , \qquad (24)$$

where

$$K_0(x) = \int_1^\infty e^{-xt}(t^2-1)^{-\frac{1}{2}}dt$$

$$K_1(x) = x \int_1^\infty e^{-xt}(t^2-1)^{\frac{1}{2}}dt$$

$S_2(\mu)$ may be identified with the function f' in Table A.I of Ref. 16. Corresponding to the last two equations (21), superposition of the image systems leads to useful auxiliary relations

$$\delta_1^{(4)}(\tfrac{1}{2}\lambda) = \delta_1^{(2)}(\lambda) + \delta_1^{(4)}(\lambda)$$

$$\delta_1^{(4)}(2\lambda) = 2\delta_1^{(1)}(\lambda) + 2\delta_1^{(4)}(\lambda)$$

$$(25)$$

Values of δ_1 from each of equations (22) are plotted against b/h in Fig. 5.

From the Appendix to Ref. 16 and in the notation of equations (17) to (19), the steady interference upwash w_{i0} of equation (13) is

$$w_{i0}(\xi) = \frac{2L}{\rho U C}\frac{bh}{8\pi} \sum_{-\infty}^{\infty}\sum' (j) \left[\frac{m^2b^2-n^2h^2}{(m^2b^2+n^2h^2)^2}\left(1+\frac{\xi}{r}\right) - \frac{n^2h^2\xi}{(m^2b^2+n^2h^2)r^3} \right]$$

$$(26)$$

with $r^2 = \xi^2 + m^2b^2 + n^2h^2$. Hence by equations (13) and (16)

$$\delta_0' = -\frac{b}{8\pi}\sum_{-\infty}^{\infty}\sum' (j)\frac{m^2b^2}{(m^2b^2+n^2h^2)^{3/2}} .$$

$$(27)$$

For the first three types of rectangular tunnel equation (27) may be used, provided that a summation with terms of alternating sign is carried out first. Following the Appendix to Ref. 16, we have for a completely closed tunnel

$$\delta_0'^{(1)} = -\frac{b^2}{4\pi h^2}\sum_{m=1}^{\infty} mf\left(\frac{mb}{h}\right) ,$$

$$(28)$$

where

$$f(\mu) = \sum_{n=-\infty}^{\infty}\frac{(-1)^n\mu}{(n^2+\mu^2)^{3/2}} = 4\pi\sum_{p=1}^{\infty}(2p-1)K_1\{(2p-1)\pi\mu\}$$

$$(29)$$

12

is given in Table A.I of Ref. 16. The corresponding expression for a completely open tunnel is

$$\delta_0'^{(2)} = -\frac{1}{4\pi} \sum_{n=-\infty}^{\infty} G\left(\frac{nh}{b}\right),$$

(30)

where

$$G(\mu) = \sum_{m=1}^{\infty} \frac{(-1)^m m^2}{(m^2+\mu^2)^{3/2}}$$

$$= \frac{1}{2}\left[\frac{1}{|\mu|} - \mu f(\mu)\right] - \frac{1}{2} \int_{|\mu|}^{\infty} \left[\frac{1}{\kappa^2} - f(\kappa)\right] d\kappa$$

$$= 2 \sum_{p=1}^{\infty} \left[K_0\{(2p-1)\pi\mu\} - (2p-1)\pi\mu K_1\{(2p-1)\pi\mu\}\right]$$

(31)

by a procedure similar to that of Ref. 21. The result for tunnels with open sides and closed roof and floor is more closely related to equation (28), and it is easily shown that

$$\delta_0'^{(3)} = \frac{b^2}{4\pi h^2} \sum_{m=1}^{\infty} (-1)^m m f\left(\frac{mb}{h}\right).$$

(32)

Equation (27) is divergent when $j = 1$ and a different approach is necessary to evaluate the unsteady interference parameter $\delta_0'^{(4)}$ for the important fourth type of rectangular tunnel.

Simple superposition of image systems leads to auxiliary equations

$$\left.\begin{array}{l} \delta_0'^{(4)}\left(\tfrac{1}{2}\lambda\right) = \delta_0'^{(2)}(\lambda) + \delta_0'^{(4)}(\lambda) \\[2mm] \delta_0'^{(4)}(2\lambda) = \tfrac{1}{2}\delta_0'^{(1)}(\lambda) + \tfrac{1}{2}\delta_0'^{(4)}(\lambda) \end{array}\right\}$$

(33)

corresponding to equations (25). Equations (33) are not invalidated by the divergence of equation (27) when $j = 1$ and can be used to extend a table of $\delta_0'^{(4)}$ provided that $\delta_0'^{(1)}$ and $\delta_0'^{(2)}$ have already been calculated. Fig. 6 illustrates how a table of $\delta_0'^{(4)}$ can be started. Consider four rectangular tunnels

A of type (4) having breadth b and height h,

B of type (4) having breadth $2b$ and height $2h$,

C of type (1) having breadth b and height h,

D of type (2) having breadth b and height $2h$.

Convergence can then be achieved by taking the linear combination $-A + 4B \equiv C + 2D$ shown in Fig. 6. For elements of the same lift at the centres of these tunnels, the steady interference upwashes along the centrelines satisfy the equation

$$-w_{iA}(x) + 4w_{iB}(x) = w_{iC}(x) + 2w_{iD}(x).$$

(34)

13

Since the cross-sectional areas of the four tunnels are in the ratio 1 : 4 : 1 : 2 and their respective heights are in the ratio 1 :2 :1 :2, it follows from the definitions of the three interference parameters in equations (13), (14) and (16) that

$$
\left.\begin{aligned}
-\delta_{0A}+\delta_{0B} &= \delta_{0C}+\delta_{0D} \\
-2\delta_{1A}+\delta_{1B} &= 2\delta_{1C}+\delta_{1D} \\
-\delta'_{0A}+2\delta'_{0B} &= \delta'_{0C}+2\delta'_{0D}
\end{aligned}\right\} \quad . \tag{35}
$$

The wing is of small span and the parameters for tunnels A and B are identical. Therefore the relations (35) may be rewritten in the notation of equations (21), (25) and (33) as

$$
\left.\begin{aligned}
0 &= \delta_0^{(1)}(\lambda)+\delta_0^{(2)}(2\lambda) \\
-\delta_1^{(4)}(\lambda) &= 2\delta_1^{(1)}(\lambda)+\delta_1^{(2)}(2\lambda) \\
\delta_0'^{(4)}(\lambda) &= \delta_0'^{(1)}(\lambda)+2\delta_0'^{(2)}(2\lambda)
\end{aligned}\right\} \quad . \tag{36}
$$

The first of these, though irrelevant here, appears to be a new result and is clearly true in Fig. 4. The second supplements equations (25) and the third enables $\delta_0'^{(4)}$ to be calculated from equation (28) as it stands and equation (30) with the values of nh/b doubled. Both $\delta_0'^{(2)}$ and $\delta_0'^{(4)}$ behave like $(4\pi\lambda)^{-1}$ when $b/h = 1/\lambda$ exceeds about 1·5.

The curves of δ_0' against b/h in Fig. 7 for the four types of rectangular tunnel have been determined from equations (28) to (33) and (36). Two striking features of Fig. 7 are the different orders of magnitude of δ_0' for broad tunnels according to the type of roof and floor, and the result that $\delta_0'^{(3)}$ for open sides and closed roof and floor remains fairly small over the whole range of b/h. It is desirable to understand why δ_0' is so small for completely closed tunnels of large breadth to height ratio while both δ_0 and δ_1 from Figs. 4 and 5 are increasing positive functions of b/h. The steady interference upwashes from equation (26) with $j = j^{(1)} = (-1)^n$ and $j = j^{(4)} = 1$ have therefore been evaluated for duplex tunnels ($b = 2h$) without the approximation in equation (14). It is seen in Fig. 8 that at roughly one tunnel height downstream of the lifting element in the completely closed tunnel $\delta = \rho U C w_{i0}/2L$ attains a maximum value appreciably greater than that in the distant wake; correspondingly, ahead of the element $\delta(\xi)$ becomes negative before tending asymptotically to zero as $\xi \to -\infty$. For the case of open roof and floor it is necessary to sum equation (26) by columns, first with respect to n (Ref. 20), and by contrast with the completely closed tunnel δ behaves monotonically against streamwise distance. The results show that, although $-\delta_0^{(4)}$ is less than twice $\delta_0^{(1)}$, the integral $\delta_0'^{(4)}$ from equation (16) is practically 40 times $-\delta_0^{(1)}$ for in this case there is near cancellation of positive and negative contributions to the integral. The significance of $\delta_0'^{(4)}$ is by far the most important factor in the explanation of the large interference effects on damping derivatives from half-model tests. In retrospect, however, it is the more remarkable that the leading imaginary term in equation (15) should so nearly disappear for broad rectangular tunnels with closed roof and floor. Slotted side-walls may well be preferable to a slotted roof and floor from the standpoint of lift interference; indeed for type (3) of equation (17) Figs. 4, 5 and 7 show that there is a range of shape just narrower than square for which each of the three interference parameters has magnitude less than 0·04.

3.2. Corrections to Pitching Derivatives.

The interference upwash is specified by equation (15), provided that the parameters δ_0, δ_1 and δ_0' are known (Section 3.1.) and that the wing can be represented as a distribution of lifting elements

$$
L(\xi)d\xi = [L_R(\xi)+i\bar{v}L_I(\xi)]d\xi \tag{37}
$$

14

along the axis of the tunnel. The frequency parameter $\bar{v} = \omega\bar{c}/U$ is based on the geometric mean chord of the wing and is supposed to be small. Then

$$\bar{w}_i(x) = \frac{2}{\rho U C} \int_0^l \left[\delta_0 + \frac{\delta_1(x-\xi)}{\beta h} + \frac{i\bar{v}h}{\bar{c}} \left\{ \frac{\delta_0'}{\beta} - \frac{\delta_0(x-\xi)}{h} + \frac{\delta_1(x-\xi)^2 (2M^2-1)}{2\beta^3 h^2} \right\} \right] L(\xi)d\xi$$

(38)

where $0 \leqslant \xi \leqslant l$ denotes the streamwise extent of the wing. If the lift, pitching moment and second moment are defined by

$$\left.\begin{aligned} \tfrac{1}{2}\rho U^2 S(C_{LR} + i\bar{v}C_{LI}) &= \int_0^l L(\xi)d\xi \\[2mm] \tfrac{1}{2}\rho U^2 S\bar{c}(C_{mR} + i\bar{v}C_{mI}) &= -\int_0^l L(\xi)\xi d\xi \\[2mm] \tfrac{1}{2}\rho U^2 S\bar{c}^2(C_{mR}^* + i\bar{v}C_{mI}^*) &= -\int_0^l L(\xi)\xi^2 d\xi \end{aligned}\right\} ,$$

(39)

then from equation (38) to first order in $\bar{v}$

$$\frac{\bar{w}_i(x)}{U} = \frac{S}{C} \left\{ \delta_0 C_{LR} + \frac{\delta_1\bar{c}}{\beta h}\left(\frac{x}{\bar{c}} C_{LR} + C_{mR} \right) \right\}$$

$$+ \frac{i\bar{v}S}{C} \left\{ \frac{\delta_0' h}{\beta\bar{c}} C_{LR} + \delta_0 \left(-\frac{x}{\bar{c}} C_{LR} - C_{mR} + C_{LI} \right) \right.$$

$$\left. + \frac{\delta_1\bar{c}}{\beta h}\left(\frac{1-2\beta^2}{2\beta^2} \left[\left(\frac{x}{\bar{c}}\right)^2 C_{LR} + \frac{2x}{\bar{c}} C_{mR} - C_{mR}^* \right] + \frac{x}{\bar{c}} C_{LI} + C_{mI} \right) \right\} .$$

(40)

In the case of oscillatory pitching motion it is desirable to express $\bar{w}_i/U$ directly in terms of the measured pitching derivatives. If θ_0 and $x = x_0$ denote the amplitude and axis of oscillation, then the first two equations (39) are equivalent to

$$\left.\begin{aligned} C_{LR} &= 2\theta_0 l_\theta \text{ and } C_{mR} = 2\theta_0 \left(m_\theta - \frac{x_0}{\bar{c}} l_\theta \right) \\[2mm] C_{LI} &= 2\theta_0 l_{\dot\theta} \text{ and } C_{mI} = 2\theta_0 \left(m_{\dot\theta} - \frac{x_0}{\bar{c}} l_{\dot\theta} \right) \end{aligned}\right\} .$$

(41)

Unfortunately the second moment coefficient C_{mR}^* cannot be related to measurement, and it is expedient to make the rough approximation that

$$-C_{mR}^* = C_{mR}^2/C_{LR}.$$

(42)

Although equation (42) seems likely to underestimate C_{mR}^* by some 20 per cent, the approximation is equivalent to the assumption that the real part of the lift $L_R(\xi)$ is concentrated at the aerodynamic centre

15

$$\xi = \bar{x} = -\frac{C_{mR}\bar{c}}{C_{LR}} = x_0 - \frac{m_\theta \bar{c}}{l_\theta} \quad . \tag{43}$$

Thus

$$\frac{\overline{w}_i(x)}{U} = \frac{2\theta_0 S}{C} \left[\delta_0 l_\theta + \frac{\delta_1 \bar{c}}{\beta h} \left(m_\theta + \frac{x - x_0}{\bar{c}} l_\theta \right) \right.$$

$$+ i\bar{v} \left\{ \frac{\delta_0' h}{\beta \bar{c}} l_\theta + \delta_0 \left(l_\theta - m_\theta - \frac{x - x_0}{\bar{c}} l_\theta \right) \right.$$

$$\left. \left. + \frac{\delta_1 \bar{c}}{\beta h} \left(m_\theta + \frac{x - x_0}{\bar{c}} l_\theta + \frac{1 - 2\beta^2}{2\beta^2} \left(\frac{x - \bar{x}}{\bar{c}} \right)^2 l_\theta \right) \right\} \right] \quad , \tag{44}$$

where l_θ, m_θ, $l_{\dot\theta}$, $m_{\dot\theta}$ and $\bar{x}$ refer to uncorrected wind-tunnel data denoted hereafter by the subscript T.

The interference upwash is made equivalent to incremental forces that theoretically cancel it. We first take the motion of oscillatory pitching with an upward displacement of the wing

$$z = -\theta_0(x - x_0) \cos \omega t, \tag{45}$$

which leads to the complex upwash and force coefficients

$$\left.\begin{array}{l} \dfrac{\overline{w}}{U} = -\theta_0 \left[1 + \dfrac{i\bar{v}(x - x_0)}{\bar{c}} \right] \\[2ex] \overline{C}_L = 2\theta_0(l_\theta + i\bar{v}l_{\dot\theta}) \\[2ex] \overline{C}_m = 2\theta_0(m_\theta + i\bar{v}m_{\dot\theta}) \end{array}\right\} \quad . \tag{46}$$

To first order in frequency parameter the corresponding steady quantities from rotary pitching motion of angular velocity $q = i\omega\theta_0$ may be written as

$$\left.\begin{array}{l} \dfrac{\overline{w}}{U} = -\dfrac{i\theta_0 \bar{v}(x - x_0)}{\bar{c}} \\[2ex] \overline{C}_L = 2i\theta_0 \bar{v}l_q \\[2ex] \overline{C}_m = 2i\theta_0 \bar{v}m_q \end{array}\right\} \quad . \tag{47}$$

Equation (44) is therefore put in the form

$$\frac{\overline{w}_i(x)}{U} = \frac{2\theta_0 S}{C} \left[\delta_0(l_\theta)_T \left\{ 1 + \frac{i\bar{v}(x - x_0)}{\bar{c}} \right\} + \frac{\delta_1 \bar{c}}{\beta h} \left\{ (m_\theta)_T + (l_\theta)_T \frac{x - x_0}{\bar{c}} \right\} \right]$$

$$+ \frac{2i\bar{v}\theta_0 S}{C} \left[\frac{\delta_0' h}{\beta \bar{c}} (l_\theta)_T + \delta_0 \left\{ (l_{\dot\theta})_T - (m_\theta)_T - 2(l_\theta)_T \frac{x - x_0}{\bar{c}} \right\} \right.$$

$$\left. + \frac{\delta_1 \bar{c}}{\beta h} \left\{ (m_{\dot\theta})_T + (l_\theta)_T \frac{x - x_0}{\bar{c}} + \frac{1 - 2\beta^2}{2\beta^2} (l_\theta)_T \left(\frac{x - \bar{x}_T}{\bar{c}} \right)^2 \right\} \right] \quad , \tag{48}$$

where the subscript T denotes the tunnel value with wall constraint. The first term of equation (48) is exactly cancelled by equation (46) with pitching amplitude $(2\theta_0 S/C)\delta_0(l_\theta)_T$ and is therefore contributing $(2S/C)\delta_0(l_\theta)_T l_\theta$ to the derivative $(l_\theta)_T$, for example. Thus, from equations (46) to (48) we may write

$$
\left.
\begin{aligned}
(l_\theta)_T - l_\theta &= \frac{2S}{C}\left[\left\{\delta_0(l_\theta)_T + \frac{\delta_1\bar{c}}{\beta h}(m_\theta)_T\right\}l_\theta + \frac{\delta_1\bar{c}}{\beta h}(l_\theta)_T l_q\right] \\[2ex]
(m_\theta)_T - m_\theta &= \frac{2S}{C}\left[\left\{\delta_0(l_\theta)_T + \frac{\delta_1\bar{c}}{\beta h}(m_\theta)_T\right\}m_\theta + \frac{\delta_1\bar{c}}{\beta h}(l_\theta)_T m_q\right]
\end{aligned}
\right\} \tag{49}
$$

and

$$
\left.
\begin{aligned}
(l_{\dot\theta})_T - l_{\dot\theta} &= \frac{2S}{C}\left[\left\{\delta_0(l_{\dot\theta})_T + \frac{\delta_1\bar{c}}{\beta h}(m_\theta)_T\right\}l_\theta + \frac{\delta_1\bar{c}}{\beta h}(l_\theta)_T l_q\right. \\[2ex]
&\quad \left. + \frac{\delta_0' h}{\beta\bar{c}}(l_\theta)_T l_\theta + \delta_0\left\{(l_\theta)_T(l_{\dot\theta} - 2l_q) - (m_\theta)_T l_\theta\right\} + \frac{\delta_1\bar{c}}{\beta h}F_L\right] \\[2ex]
(m_{\dot\theta})_T - m_{\dot\theta} &= \frac{2S}{C}\left[\left\{\delta_0(l_{\dot\theta})_T + \frac{\delta_1\bar{c}}{\beta h}(m_\theta)_T\right\}m_\theta + \frac{\delta_1\bar{c}}{\beta h}(l_\theta)_T m_q\right. \\[2ex]
&\quad \left. + \frac{\delta_0' h}{\beta\bar{c}}(l_\theta)_T m_\theta + \delta_0\left\{(l_\theta)_T(m_{\dot\theta} - 2m_q) - (m_\theta)_T m_\theta\right\} + \frac{\delta_1\bar{c}}{\beta h}F_m\right]
\end{aligned}
\right\} \quad, \tag{50}
$$

where the quantities F_L and F_m arising from the second and last terms of equation (48) are rather lengthy and require analysis by lifting-surface theory (Ref. 3).

For this purpose it is convenient to quote Ref. 22, where in equations (39) the pitching derivatives are formulated. In the present notation

$$
\left.
\begin{aligned}
l_\theta &= \frac{1}{2\beta}I_{L1} \\[2ex]
m_\theta &= \frac{1}{2\beta}\left[I_{m1} + \frac{x_0}{\bar{c}}I_{L1}\right] \\[2ex]
l_{\dot\theta} &= \frac{1}{2\beta}\left[\frac{\beta^2 - M^2}{\beta^2}I_{L2} + \frac{1}{\beta^2}I_{L3} - \frac{M^2}{\beta^2}I_{m1} - \frac{x_0}{\bar{c}}I_{L1}\right] \\[2ex]
m_{\dot\theta} &= \frac{1}{2\beta}\left[\frac{\beta^2 - M^2}{\beta^2}I_{m2} + \frac{1}{\beta^2}I_{m3} + \frac{M^2}{\beta^2}I_{m1}^*\right. \\[2ex]
&\quad \left. + \frac{x_0}{\bar{c}}\left\{\frac{\beta^2 - M^2}{\beta^2}I_{L2} + \frac{1}{\beta^2}I_{L3} - \frac{1}{\beta^2}I_{m1}\right\} - \left(\frac{x_0}{\bar{c}}\right)^2 I_{L1}\right]
\end{aligned}
\right\} \quad, \tag{51}
$$

where the coefficients are defined in equations (33) of Ref. 22 and the numeral subscript relates to the appropriate steady distribution of incidence

$$\begin{rcases} \alpha_1 = 1 \\[4pt] \alpha_2 = x/\bar{c} \\[4pt] \alpha_3 \quad \text{from equation (23) of Ref. 22 with } \alpha = \alpha_1 \\[4pt] \alpha_4 = (x/\bar{c})^2 \\[4pt] \alpha_5 \quad \text{from equation (23) of Ref. 22 with } \alpha = \alpha_2 \end{rcases} \quad (52)$$

from equations (37) of Ref. 22. Likewise from Section 7.1. of Ref. 3 the rotary pitching derivatives are

$$\begin{rcases} l_q = \dfrac{1}{2\beta}\left[I_{L2} - \dfrac{x_0}{\bar{c}} I_{L1} \right] \\[14pt] m_q = \dfrac{1}{2\beta}\left[I_{m2} + \dfrac{x_0}{\bar{c}}(I_{L2} - I_{m1}) - \left(\dfrac{x_0}{\bar{c}}\right)^2 I_{L1} \right] \end{rcases} \quad (53)$$

All five of the distributions in equations (52) are required to formulate F_L and F_m in equations (50). By a straightforward analysis, based on Refs. 3 and 22, it can be shown that

$$\begin{aligned}
F_L &= \left\{ (m_\theta)_T - \frac{x_0}{\bar{c}}(l_\theta)_T \right\} \left\{ \frac{1}{2\beta^3} I_{L3} - \frac{M^2}{2\beta^3} I_{L2} - \frac{M^2}{2\beta^3} I_{m1} \right\} \\[8pt]
&\quad + (l_\theta)_T \left\{ \frac{1}{2\beta^3} I_{L5} - \frac{M^2}{2\beta^3} I_{L4} - \frac{M^2}{2\beta^3} I_{m2} \right\} \\[8pt]
&\quad + \frac{1-2\beta^2}{4\beta^3}(l_\theta)_T \left\{ I_{L4} - \frac{2\bar{x}_T}{\bar{c}} I_{L2} + \left(\frac{\bar{x}_T}{\bar{c}}\right)^2 I_{L1} \right\} \\[12pt]
F_m - \frac{x_0}{\bar{c}} F_L &= \left\{ (m_\theta)_T - \frac{x_0}{\bar{c}}(l_\theta)_T \right\} \left\{ \frac{1}{2\beta^3} I_{m3} - \frac{M^2}{2\beta^3} I_{m2} + \frac{M^2}{2\beta^3} I^*_{m1} \right\} \\[8pt]
&\quad + (l_\theta)_T \left\{ \frac{1}{2\beta^3} I_{m5} - \frac{M^2}{2\beta^3} I_{m4} + \frac{M^2}{2\beta^3} I^*_{m2} \right\} \\[8pt]
&\quad + \frac{1-2\beta^2}{4\beta^3}(l_\theta)_T \left\{ I_{m4} - \frac{2\bar{x}_T}{\bar{c}} I_{m2} + \left(\frac{\bar{x}_T}{\bar{c}}\right)^2 I_{m1} \right\}
\end{aligned} \quad \right\} \quad (54)$$

It will be noted that the second factor in curly brackets in the first term of F_L is simply $(l_\theta - l_q)$ and relates to the part of the second term of equation (48) that is independent of x; the remaining contributions from this and the final terms of equation (48) are equivalent to distortions of the wing in longitudinal bending.

For the present investigation it is convenient to solve equations (49) and (50) for the unknowns $(l_\theta)_T$, $(m_\theta)_T$, $(l_\theta)_T$ and $(m_\theta)_T$. We assume theoretical values of the derivatives from equations (51) and (53) without wall constraint and predict the wind-tunnel values to compare with those measured in the NPL slotted-wall tunnels. Thus

$$\begin{rcases} (l_\theta)_T \left(1 - \dfrac{2S}{C}\delta_0 l_\theta - \dfrac{2S}{C}\dfrac{\delta_1 \bar{c}}{\beta h} l_q \right) + (m_\theta)_T \left(-\dfrac{2S}{C}\dfrac{\delta_1 \bar{c}}{\beta h} l_\theta \right) = l_\theta \\[14pt] (l_\theta)_T \left(-\dfrac{2S}{C}\delta_0 m_\theta - \dfrac{2S}{C}\dfrac{\delta_1 \bar{c}}{\beta h} m_q \right) + (m_\theta)_T \left(1 - \dfrac{2S}{C}\dfrac{\delta_1 \bar{c}}{\beta h} m_\theta \right) = m_\theta \end{rcases} \quad (55)$$

18

and

$$(l_{\dot{\theta}})_T \left(1 - \frac{2S}{C}\delta_0 l_\theta - \frac{2S}{C}\frac{\delta_1\bar{c}}{\beta h}l_q\right) + (m_{\dot{\theta}})_T \left(-\frac{2S}{C}\frac{\delta_1\bar{c}}{\beta h}l_\theta\right) = l_{\dot{\theta}} + \frac{2S}{C}\lambda_i$$

$$(l_{\dot{\theta}})_T \left(-\frac{2S}{C}\delta_0 m_\theta - \frac{2S}{C}\frac{\delta_1\bar{c}}{\beta h}m_q\right) + (m_{\dot{\theta}})_T \left(1 - \frac{2S}{C}\frac{\delta_1\bar{c}}{\beta h}m_\theta\right) = m_{\dot{\theta}} + \frac{2S}{C}\mu_i$$

$$\left. \right\} \quad (56)$$

where

$$\lambda_i = \frac{\delta'_0 h}{\beta\bar{c}}(l_{\dot{\theta}})_T l_\theta + \delta_0 \left[(l_{\dot{\theta}})_T(l_{\dot{\theta}} - 2l_q) - (m_{\dot{\theta}})_T l_\theta \right] + \frac{\delta_1\bar{c}}{\beta h}F_L$$

$$\mu_i = \frac{\delta'_0 h}{\beta\bar{c}}(l_{\dot{\theta}})_T m_\theta + \delta_0 \left[(l_{\dot{\theta}})_T(m_{\dot{\theta}} - 2m_q) - (m_{\dot{\theta}})_T m_\theta \right] + \frac{\delta_1\bar{c}}{\beta h}F_m$$

$$\left. \right\} \quad (57)$$

with F_L and F_m from equations (54). The formal identity of the left hand sides of the pairs of simultaneous equations (55) and (56) helps the computation. In most of the calculations the full equations (57) have been used, but the terms in F_L and F_m are not of primary importance and have been omitted in a few instances. In such cases there is no advantage in simplifying the left hand sides as originally proposed in Ref. 10.

Solutions for the corrected derivatives l_θ, m_θ, $l_{\dot{\theta}}$ and $m_{\dot{\theta}}$ in terms of the wind-tunnel values are not possible with the full equations. But when the terms in F_L and F_m are omitted, equations (49) and (50) yield

$$l_\theta \left\{ 1 + \frac{2S}{C}\delta_0(l_\theta)_T + \frac{2S}{C}\frac{\delta_1\bar{c}}{\beta h}(m_\theta)_T \right\} = (l_\theta)_T \left\{ 1 - \frac{2S}{C}\frac{\delta_1\bar{c}}{\beta h}l_q \right\}$$

$$m_\theta \left\{ 1 + \frac{2S}{C}\delta_0(l_\theta)_T + \frac{2S}{C}\frac{\delta_1\bar{c}}{\beta h}(m_\theta)_T \right\} = (m_\theta)_T - (l_\theta)_T\frac{2S}{C}\frac{\delta_1\bar{c}}{\beta h}m_q$$

$$l_{\dot{\theta}} \left\{ 1 + \frac{2S}{C}\delta_0(l_\theta)_T \right\} = (l_\theta)_T \left\{ 1 - \frac{2S}{C}\delta_0 l_\theta - \frac{2S}{C}\frac{\delta_1\bar{c}}{\beta h}l_q \right\} - (m_\theta)_T\frac{2S}{C}\frac{\delta_1\bar{c}}{\beta h}l_\theta$$

$$\qquad\qquad - (l_\theta)_T\frac{2S}{C}\left\{ \frac{\delta'_0 h}{\beta\bar{c}}l_\theta - 2\delta_0 l_q \right\} + (m_\theta)_T\frac{2S}{C}\delta_0 l_\theta$$

$$m_{\dot{\theta}} \left\{ 1 + \frac{2S}{C}\delta_0(l_\theta)_T \right\} = -(l_\theta)_T\frac{2S}{C}\left\{ \delta_0 m_\theta + \frac{\delta_1\bar{c}}{\beta h}m_q \right\} + (m_\theta)_T\left\{ 1 - \frac{2S}{C}\frac{\delta_1\bar{c}}{\beta h}m_\theta \right\}$$

$$\qquad\qquad - (l_\theta)_T\frac{2S}{C}\left\{ \frac{\delta'_0 h}{\beta\bar{c}}m_\theta - 2\delta_0 m_q \right\} + (m_\theta)_T\frac{2S}{C}\delta_0 m_\theta$$

$$\left. \right\} \quad (58)$$

Equations (58) represent the best practical procedure for correcting a set of measured values $(l_\theta)_T$, $(m_\theta)_T$, $(l_{\dot{\theta}})_T$ and $(m_{\dot{\theta}})_T$. It must be anticipated that, due to various causes, these may be significantly different from those predicted by equations (55) to (57). Although theoretical values of the oscillatory derivatives need play no part in the practical interference correction, theoretical or empirical values of l_q and m_q must be known. It is no great task to obtain the aerodynamic coefficients in equations (53), but the flow may be such that theoretical values of the rotary derivatives are quite untrustworthy and no estimates are available. Then it becomes necessary to omit terms from each of equations (58) and to incur some loss of accuracy, but the corrections are still worth applying (Section 6).

19

4. Application of Method.

The method of interference correction described in the preceding sections is completely general as regards wing planform, pitching axis and subsonic Mach number. Although the three interference parameters have only been formulated for tunnels of rectangular shape in Section 3.1., the method applies in principle to any cross-section for which the parameters are known, for example a closed circular tunnel (Ref. 16); the bipolar shape appropriate to a half-model in a circular tunnel with reflection plane is considered crudely in Section 5.3. Furthermore, the restriction that the model is placed centrally on the axis of the tunnel is unnecessary, provided that the interference parameters can be adjusted. Most of the present calculations are for tunnels with solid side-walls, and Table 1 gives the values of δ_0, δ_1 and δ'_0 that are used. With the aid of Figs. 4, 5 and 7 it is just as easy to consider tunnels where the side-walls or all four walls are open. The mathematical analysis of Section 3.2. concludes with a procedure for correcting measured pitching derivatives to free-stream conditions. Practical situations when there are insufficient experimental data are considered in Section 6. Although the analysis is specifically for dynamic measurements of pitching derivatives, a similar approach could be used for cases of control-surface oscillation and other longitudinal wing motion.

The Algol programme of Ref. 22 is particularly convenient for the evaluation of the required theoretical aerodynamic data, and the coefficients used in the present calculations are listed in Table 2. In Section 4.1. the predicted effects of tunnel shape, pitching axis, Mach number and model size are examined for the two limiting cases of rectangular tunnels with open or closed roof and floor. Strictly the application to slotted-wall tunnel rests on a further assumption that the interference parameters δ_1 and δ'_0 are linearly related to δ_0 as the slot geometry is varied. The curves for δ_0 for ideal slotted roof and floor in Figs. 2 and 3 enable this to be done, and in this respect it is fortunate that the slot parameter $(1 + F)^{-1}$ from equation (4) usually lies close to the limiting value of unity for open roof and floor. A similar assumption enables us to estimate the effect of model span through changes in the steady interference parameter δ_0. These two approximate extensions of the basic method are discussed in Section 4.2., where also rigorous allowance for the effect of a small frequency parameter is described.

4.1. Examples of Theoretical Predictions.

The interference parameters are listed in Table 1 for five rectangular tunnels which include three NPL tunnels with half-models and intermediate breadth to height ratios. With the aid of the aerodynamic coefficients in Table 2, illustrative theoretical results at the three Mach numbers 0, 0·6 and 0·8 have been obtained for the unswept tapered planform shown in Fig. 9. Predictions for this and four other planforms are compared with experiment and discussed further in Sections 5 to 7.

With fixed Mach number $M = 0·8$ and area ratio of planform to tunnel cross-section $S/C = 0·1$, the effect of b/h on the pitching derivatives about the mid-chord axis is shown in Figs. 9 to 12. The constant free-stream values with no wall constraint are calculated from equations (51). The lift derivative l_θ in Fig. 9 is subject to wall corrections of the order ± 10 per cent according as the roof and floor are open or closed, more for the broader shapes and less for those near square. By contrast, wall interference on the cross-damping derivative $l_{\dot\theta}$ produces the full and broken curves in Fig. 10 that differ by about four times the free-stream value of the derivative over the whole range $0·8 < b/h < 2·6$. This at once establishes the seriousness of the predicted interference effect. For open roof and floor the sign of the derivative is affected, and the corrections are greatest for the broadest shapes of tunnel; the nearly square tunnels show a similar magnitude of interference whether the roof and floor are open or closed. This is roughly the trend shown by the dominant interference parameter δ'_0 in Fig. 7. The direct pitching derivatives m_θ and $m_{\dot\theta}$ in Figs. 11 and 12 show much the same behaviour as l_θ and $l_{\dot\theta}$ respectively. The wall interference is again of opposite sign for the two wall conditions; the quasi-steady aerodynamic centre from equation (43) moves aft in the closed tunnels and forward with open roof and floor by small distances up to $0·014\bar{c}$ in the broader tunnels, but by much less for nearly square cross-sections. The wall interference on m_θ varies in magnitude from nearly 15 to 50 per cent and is consistent with observation in the NPL 25 in. × 20 in. Tunnel ($b/h = 1·905$).

The relative importance of the individual terms in equations (57) is illustrated in Fig. 13, firstly by including only the leading terms in δ'_0 and secondly by ignoring the final terms in F_L and F_m. It has already

20

been remarked that the unsteady interference parameter δ_0' is of paramount importance in broad tunnels with open roof and floor. Here, with $b/h = 1.905$, the major part of the wall interference on the pitching damping is obtained over the whole range of pitching axis in the first approximation when δ_0 and δ_1 are both excluded from the right hand sides of equations (56). Again, in Fig. 13, the major part of the deficiency in the first approximation is removed when in the second approximation the terms in δ_0 are added. Although the final terms in δ_1 are worth including, their omission can be justified when, as in the practical procedure of equations (58), a real advantage accrues.

Perhaps the most striking feature of Fig. 13 is the extent to which the wall interference on m_θ increases as the pitching axis moves aft. The change in the sign of the corrections as the pitching axis crosses a position near the aerodynamic centre is not surprising, since μ_i in the second of equations (57) is dominated by its first term; therefore $(m_\theta)_T - m_\theta$ is expected to have the sign of m_θ when δ_0' is positive. But it is noticeable how the secondary terms contribute to increase this difference for the rearward axes. The feature is not confined to the high Mach number 0·8, as a similar effect is apparent for $M = 0.6$ in Fig. 14. The latter illustrates that, for $b/h = 1.905$, the smaller interference effect from the completely closed tunnel is found over the whole range of pitching axis.

Figs. 15 and 16 show two other aspects of the calculated wall interference on forces in quadrature with the pitching motion, which follow qualitatively from the terms in δ_0'. The curves of l_θ against Mach number in Fig. 15 are drawn as quadratic functions of $1/\beta$ through the calculated results for $M = 0$, 0·6 and 0·8; for the different wall conditions they are seen to diverge as M increases. The leading term in the first of equations (57) is roughly proportional to l_θ^2/β, and the interference is seen to grow slightly more rapidly than the factor $1/\beta$. As model size increases, the contribution from the same leading term to the right hand side of the first equation (56) is proportional to $(2S/C)(h/\bar{c})$, and therefore to $(S/C)^{1/2}$. This effect is apparent for open roof and floor and a rearward pitching axis in the lower diagram of Fig. 16. The value of δ_0' is so much smaller for the closed tunnel, that the full curve of l_θ exhibits for small S/C the more familiar linear dependence shown by the lift derivative l_θ in the upper diagram. The conclusion is reached that, unless δ_0' is quite small, it is impracticable to reduce wall interference on dynamic measurements to negligible proportions by diminishing model size. When $S/C = 0.02$, for example, the wall interference with open roof and floor on l_θ in Fig. 16 at $M = 0.6$ is about 2 per cent while that on l_θ is no less than 50 per cent. This poses a serious threat to the validity of oscillatory experiments on half-models in rectangular tunnels with slotted roof and floor.

4.2. Approximate Generalizations.

From the boundary conditions for ideal longitudinal slots in Section 2 it follows that the present method of interference correction is applicable. It turns out in practice that the geometric slot parameter F is nearly small enough to be ignored. This is fortunate as there appear to be no reliable calculations of δ_1 and δ_0' for rectangular slotted-wall tunnels; the best approach is perhaps by finite difference methods, and to this end Rushton has extended the electrical analogue of Ref. 8 to three dimensions. Unless values of δ_1 and δ_0' are available, knowledge of δ_0 from Refs. 11, 12 and 14 must suffice. It will be assumed that, as F is varied, δ_1 and δ_0' are linear functions of δ_0. Thus, in the notation of Section 3.1, as δ_0 varies between the extremes of $\delta_0^{(4)}$ when $F = 0$ and $\delta_0^{(1)}$ when $F = \infty$, we take

$$\delta_1 = \delta_1^{(4)} + \frac{\delta_0 - \delta_0^{(4)}}{\delta_0^{(1)} - \delta_0^{(4)}}(\delta_1^{(1)} - \delta_1^{(4)}) \tag{59}$$

and a similar equation for δ_0'. The last term of equation (59) is in the nature of a small and approximate correction. Detailed calculation is perhaps superfluous here, so for simplicity the same equation (59) is used for the derivatives themselves and the factor involving δ_0 is deduced from the full curves on the extreme left of Figs. 2 and 3. The resulting long-dashed curves in Figs. 12, 14 and 15 show the effect to be significant but not large. In practical application it is advisable to determine $\delta_0^{(1)}$, $\delta_0^{(4)}$, δ_0, $\delta_1^{(1)}$, $\delta_1^{(4)}$, $\delta_0'^{(1)}$ and $\delta_0'^{(4)}$ and hence δ_1 and δ_0' on the principle of equation (59), and then to use equations (58).

While interference calculations for oscillating wings of large span are possible (Ref. 17), they are excessively laborious in practice, even when small frequency is assumed. Yet it is known that span ratio $2s/b$ can have a marked effect on δ_0. The usual practice in steady flow is to evaluate the spanwise distribution of interference upwash along a uniformly loaded lifting line of semi-span s,

$$w_i = \frac{2L}{\rho U C}\,\delta_0(y,s).$$ (60)

Then $\delta_0(0,0)$ is replaced by the average value

$$(\delta_0)_U = \int_0^1 \delta_0(y,s)d(y/s)$$ (61)

for uniform spanwise loading, or preferably for elliptic spanwise loading

$$(\delta_0)_E = \frac{16}{\pi^2}\int_0^1\!\!\int_0^1 \delta_0(y,t)\left\{1-\left(\frac{y}{s}\right)^2\right\}^{\frac{1}{2}}\left(\frac{t}{s}\right)^2\left\{1-\left(\frac{t}{s}\right)^2\right\}^{-\frac{1}{2}}d\left(\frac{y}{s}\right)d\left(\frac{t}{s}\right).$$ (62)

A convenient procedure for evaluating $(\delta_0)_E$ is that used by Glauert for circular tunnels in Section 6 of Ref. 19. The function $\delta_0(y,t)$ is expressed as a polynomial in even powers of the two variables

$$\delta_0(y,t) = \sum\sum a_{mn}(2y/b)^{2m}(2t/b)^{2n}.$$ (63)

Then from equations (62) and (63)

$$(\delta_0)_E = 4\sum\sum a_{mn}\frac{E_m E_n}{2m+1}\left(\frac{2s}{b}\right)^{2m+2n},$$ (64)

where

$$E_p = \frac{1.3.5\ldots(2p+1)}{2.4.6\ldots(2p+2)}\text{ for } p = 0,1,2,\ldots.$$

Now for closed sides and open roof and floor it can be shown that

$$\delta_0^{(4)}(y,t) = -\frac{b^2}{8\pi(y^2-t^2)} + \frac{b}{16t}\sum_{m=-\infty}^{\infty}\left[\coth\frac{\pi(y-mb-t)}{b} - \coth\frac{\pi(y-mb+t)}{b}\right],$$ (65)

and numerical values of a_{mn} may be found. Calculations with $m,n = 0,1,\ldots.4$ give the broken curves of $(\delta_0)_E$ against $2s/b$ in Fig. 17 for square and duplex tunnels. The full curves for completely closed tunnels are based on Table 6 of Ref. 19. The effect of wing span is clearly more important in the broader tunnel when the theory for small span can be expected to overestimate the wall interference for both types of roof and floor. It is questionable to what extent the factor $(\delta_0)_E/\delta_0$ can be applied to δ_1 and δ_0' and so to the increments to the derivatives, but this simple device indicates the order of magnitude of the effect on l_θ and $l_{\dot\theta}$ in Fig. 16. When $S/C = 0.1$ in Fig. 16, the span ratio $2s/b = 0.48$. While for larger spans it

22

would seem desirable to examine the interference parameter δ_0' more thoroughly, the factor $(\delta_0)_E/\delta_0$ may well be adequate up to this size of model. Then its effect is comparable with that of the geometrical slot parameter discussed earlier.

The third generalization of the method concerns the frequency parameter. It has been demonstrated from lifting-surface theory by Garner and Milne[23], that in the limit as frequency tends to zero there are very simple expressions for the rates of change of damping derivatives with respect to frequency parameter. In the present notation equations (18) and (19) of Ref. 23 become

$$\left.\begin{array}{l} \dfrac{\partial}{\partial \bar{v}}(l_{\dot\theta}) = \dfrac{1}{16} A l_\theta^2 \\[3mm] \dfrac{\partial}{\partial \bar{v}}(m_{\dot\theta}) = \dfrac{1}{16} A l_\theta m_\theta \end{array}\right\} \quad, \tag{66}$$

where A is the aspect ratio. The results hold for any uniform subsonic free stream. Now, if $\bar{K}(x-x', y-y', z-z')$ denotes the kernel function of the integral relation between upwash and lift distribution, as in equation (1) of Ref. 23, under the constraint of rectangular tunnel boundaries $\bar{K}$ is simply replaced by

$$\bar{K}_T(x-x', y-y', z-z') = \sum_{-\infty}^{\infty}\sum (j)\bar{K}(x-x', y-y'-mb, z-z'-nh), \tag{67}$$

where j is defined in equations (17). The analysis of Ref. 23 follows with $\bar{K}$ replaced by $\bar{K}_T$, since the additional terms in equation (67) do not influence the singularity in the expansion for small frequency that leads to equation (66). Hence

$$\left.\begin{array}{l} \dfrac{\partial}{\partial \bar{v}}(l_{\dot\theta})_T = \dfrac{1}{16} A(l_\theta)_T^2 \\[3mm] \dfrac{\partial}{\partial \bar{v}}(m_{\dot\theta})_T = \dfrac{1}{16} A(l_\theta)_T(m_\theta)_T \end{array}\right\} \quad. \tag{68}$$

By equations (56) and (68) the slope as well as the limiting value of the damping derivatives can be predicted to compare with experimental values plotted against frequency parameter. The results in equations (68) can also be derived from equations (54) to (57) by applying equations (66) and noting that in equations (52) only α_3 and α_5 are affected and the corresponding coefficients satisfy

$$\left.\begin{array}{l} \dfrac{\partial}{\partial \bar{v}}\left\{\dfrac{1}{2\beta^3} I_{L3}\right\} = \dfrac{1}{16} A l_\theta^2 \\[3mm] \dfrac{\partial}{\partial \bar{v}}\left\{\dfrac{1}{2\beta^3}\left(I_{m3} + \dfrac{x_0}{\bar{c}} I_{L3}\right)\right\} = \dfrac{1}{16} A l_\theta m_\theta \\[3mm] \dfrac{\partial}{\partial \bar{v}}\left\{\dfrac{1}{2\beta^3} I_{L5}\right\} = \dfrac{1}{16} A l_\theta\left(l_q + \dfrac{x_0}{\bar{c}} l_\theta\right) \\[3mm] \dfrac{\partial}{\partial \bar{v}}\left\{\dfrac{1}{2\beta^3}\left(I_{m5} + \dfrac{x_0}{\bar{c}} I_{L5}\right)\right\} = \dfrac{1}{16} A m_\theta\left(l_q + \dfrac{x_0}{\bar{c}} l_\theta\right) \end{array}\right\} \quad. \tag{69}$$

Practical applications of equations (68) are discussed in Section 5.3.

5. *Measured and Predicted Pitching Derivatives.*

The survey of available experimental evidence prepared by Wight[6] indicated that dynamic measurements might not always be subject to the large wall interference effects shown in Fig. 1. The tunnel-model configurations were too few for a definite pattern to emerge, but the additional results from the present experimental investigation enable a satisfactory comparison with theory to be made with a systematic variation of the most important parameters involved.

The effect of tunnel shape is assessed from experiments done mainly in the three NPL tunnels shown in Fig. 18, each having a slotted roof and floor. The cross-sectional areas of the two larger tunnels are approximately equal, whilst the 25 in. × 20 in. Tunnel and the $9\frac{1}{2}$ in. × $9\frac{1}{2}$ in. Tunnel are of more similar cross-sectional shape. It should be noted that the actual working-section heights h, measured between the slotted walls, are less than the nominal heights which describe the original tunnels with solid liners fitted. In addition, the effective breadth (b) of each of the tunnels is twice the actual breadth since all the tests are made with a half-model mounted on a solid side-wall. This configuration is equivalent to one in which a full-span model is tested in a tunnel of twice the breadth. The effective breadth to height ratios of the tunnels are indicated, and these show that the 36 in. × 14 in. Tunnel behaves as if it is nearly square and the 25 in. × 20 in. Tunnel behaves as if it is nearly duplex. The two rigid half-models of M-wing and unswept-wing planform shown in Fig. 18 were both tested in each of the two larger tunnels, and most of the present tests were done with the rigid half-delta-model of aspect ratio $A = 2.64$ in the $9\frac{1}{2}$ in. × $9\frac{1}{2}$ in. Tunnel. This model was also used in a brief experimental programme in the 18 in. × 14 in. Tunnel, and a few additional tests in the $9\frac{1}{2}$ in. × $9\frac{1}{2}$ in. Tunnel were made with the half-delta-model of aspect ratio $A = 3$. The motion was restricted to single degree of freedom pitching, and in most cases only pitching moment derivatives were measured for subsonic Mach numbers in the range $0.4 \leqslant M \leqslant 0.9$. The facilities in the $9\frac{1}{2}$ in. × $9\frac{1}{2}$ in. Tunnel allowed a variation in the position of the pitching axis. In every case, measurements were obtained with all the slots open and with all the slots closed.

In Section 5.1., the previous results for models in the 36 in. × 14 in. Tunnel and the 25 in. × 20 in. Tunnel are compared with theory. Similar comparisons with measured derivatives from the present investigation in the $9\frac{1}{2}$ in. × $9\frac{1}{2}$ in. Tunnel are discussed in Section 5.2. The theoretical derivatives for each tunnel condition are determined from equations (55) to (57), and a good assessment of the accuracy of the theory is obtained. Satisfactory correlation is found for the 25 in. × 20 in. Tunnel and the $9\frac{1}{2}$ in. × $9\frac{1}{2}$ in. Tunnel, but there are unresolved discrepancies in the case of the 36 in. × 14 in. Tunnel where, by contrast with experiment, the theory predicts very large changes due to scaling the slots. The present experiments cover frequency parameters in the range $0.03 < \bar{v} < 0.28$. As discussed in Section 4.2., some theoretical allowance can be made for such small frequency parameters, and evidence to support this is found in Section 5.3. There is also an approximate analysis for a half-model in low-speed closed and open circular tunnels with reflection planes, and measurements in the range $0.37 < \bar{v} < 1.35$ are considered.

5.1. *Evidence from Previous Tests.*

We first discuss the experimental results obtained several years ago in the 25 in. × 20 in. Tunnel and the 36 in. × 14 in. Tunnel. For the M-wing in the former tunnel with varying numbers of slots, Fig. 1 shows a systematic variation of the pitching damping derivative with the slot parameter $(1 + F)^{-1}$ for several Mach numbers. For $M = 0.8$, a smooth extrapolated curve is drawn through the experimental points to give an estimated value for a tunnel with an open roof and floor. For this tunnel condition and for a completely closed tunnel theoretical values of the derivative, based on equations (55) to (57) without the terms in F_L and F_m, are shown. These are the best that can be obtained from available theoretical data[24] and correspond to the second approximation in Fig. 13 which is expected to give satisfactory values. It is evident that the change in $-m_{\dot{\theta}}$ between the two extreme conditions is predicted reasonably well. Although not shown, the pitching stiffness derivative is less sensitive to wall interference, but the changes of order 10 per cent are in reasonable accord with theory.

Seriously large interference effects were also found when a more conventional unswept wing was tested in the 25 in. × 20 in. Tunnel. Pitching-moment derivatives were measured as for the M-wing tests but results were obtained for only two tunnel-wall conditions, namely all the slots open and all the slots sealed. Values of the damping derivative for oscillations about a mid-chord pitching axis are plotted

against Mach number in Fig. 19. The theoretical treatment by means of equations (55) to (57) is applied and the predicted values are in good agreement with the experimental results. With slots sealed the results closely follow the trend of the theoretical curve but consistently show a slight reduction in magnitude. This is the sort of difference that may arise from any linearized theory which neglects the wing thickness and the boundary layers of the half-model and the side-wall on which it is mounted. A comparison between experimental and theoretical values with slots open shows remarkably similar agreement when the relatively small correction for slot parameter is included. In accord with the predictions of Section 4.1., the difference between the measured values increases with Mach number by a factor just greater than $1/\beta$.

Some results for the same unswept wing pitching in the 36 in. $\times$ 14 in. Tunnel are given in Figs. 20 and 21 which show the variation with Mach number of the two in-quadrature derivatives $m_{\dot\theta}$ and $l_{\dot\theta}$. Comparison of Figs. 19 and 20 shows that the theory predicts practically the same overall differences in $m_{\dot\theta}$ due to sealing the slots in the two tunnels, but for the 36 in. $\times$ 14 in. Tunnel ($b/h = 0.91$), closed and open roof and floor give approximately equal and opposite effects. These contrast the corresponding results in the broader 25 in. $\times$ 20 in. Tunnel ($b/h = 1.90_5$) where the open roof and floor contributed a very large proportion of the wall interference. The results for the lift derivative $l_{\dot\theta}$ in Fig. 21 indicate a particularly large interference effect with slots sealed, which is confirmed in magnitude and trend by the experimental results. Measurements with slots open are not as predicted, being of the opposite sign and quite near the theoretical curve for slots sealed. This discrepancy is discussed fully in Section 7.

The present theory satisfactorily explains the large interference effects observed when the unswept wing was tested in the 25 in. $\times$ 20 in. Tunnel, even when the sealing of the slots caused the pitching damping to double in value. With reference back to Fig. 14, it is predicted that these effects would become even larger if the pitching axis were moved downstream. Unfortunately, the previous tests were restricted to the one pitching axis, but the present measurements on a delta wing in the $9\frac{1}{2}$ in. $\times$ $9\frac{1}{2}$ in. Tunnel will be seen to indicate that this prediction is probably correct.

5.2. *Present Experimental Evidence.*

The present tests in the $9\frac{1}{2}$ in. $\times$ $9\frac{1}{2}$ in. Tunnel involve two rigid half-span models of cropped-delta planform of aspect ratios 2·64 and 3, described in Ref. 5 as 'Arrowhead No. 1' and 'Delta No. 1' respectively. As in the previous tests, boundary-layer transition was fixed by a roughness band near the leading edge. The oscillating rig is basically the model mounting shown in Fig. 6 of Ref. 25; no reflection plate was used, but the models were fitted with root fences. A few modifications have been made: the incidence-compensating spring and the eddy-current damping facility were removed, and two new cover plates and a new model mounting platform were fitted. With this platform three locations of pitching axis can be used, $x_0 = 0.31\bar{c}$, $0.65\bar{c}$ and $1.04\bar{c}$ for the $A = 2.64$ delta wing and $x_0 = 0.55\bar{c}$, $0.96\bar{c}$ and $1.42\bar{c}$ for the $A = 3$ delta wing. The bulk of the experiments have been done with the $A = 2.64$ delta, for which the centre axis passes very close to the aerodynamic centre whilst the other two axis positions are as far upstream and downstream as practicable. Pitching-moment derivatives have been determined for Mach numbers in the range $0.38 \leqslant M \leqslant 0.78$ about each of the three axis positions with all slots open and with all slots sealed, but no lift derivatives could be measured with the apparatus. The frequency of oscillation is varied from 12 c/sec to 85 c/sec by using four torsion bars of different stiffnesses with masses added when appropriate. A decaying oscillation technique is used to determine the damping derivative. The decaying signal, recorded electronically as described by Wight and Nixon[26], is analysed by Bratt's electronic integration method, described in Section 5.1.1. of Ref. 27, to give a value of $m_{\dot\theta}$. The stiffness derivative m_θ is determined by measuring directly the change in frequency of oscillation from still-air to wind-on conditions and applying equation (26) of Ref. 27. Mean values from at least three separate decaying oscillations were determined. With the exceptions mentioned in Section 5.3., the scatter about the mean values of both damping and stiffness derivatives was of the order ± 3 per cent. This was acceptable in view of the expected large interference effects. Measured values of the stiffness derivative and the damping derivative are given in Tables 3 and 4 respectively; for reasons given in Section 5.3., the data plotted in Figs. 22 to 25 correspond to the averaged m_θ for the two lowest frequencies and the averaged $-m_{\dot\theta}$ for the two highest frequencies.

Calculations have been made for the Mach numbers 0, 0·661 and 0·866 for which aerodynamic coefficients are available in Table 2. Figs. 22 and 23 show m_θ against axis position and Mach number for the $A = 2\cdot64$ delta wing, and in each case there is convincing agreement between the measured variation and that predicted by equation (55). Apart from a range of axis position near the aerodynamic centre of the model where the interference is small, m_θ is numerically larger with slots sealed than with slots open and the interference effect increases linearly as the axis position is moved away from the aerodynamic centre. This is illustrated in Fig. 22 for the Mach number $M = 0\cdot66$ used in the theoretical calculations; the experimental results are interpolated. Fig. 23 shows a small increase with Mach number in both calculated and measured wall interference.

The corresponding variation of the damping derivative with axis position and Mach number is shown in Figs. 24 and 25. The allowance for slot parameter is very small and has not been plotted. By means of equations (55) to (57) it is predicted in Fig. 24 that m_θ will be subject to much larger wall interference for a downstream pitching axis than for an upstream one. This trend is similar to that shown in Fig. 14 for the unswept half-wing in the 25 in. × 20 in. Tunnel. However, in the present case very small interference corrections to m_θ are predicted for an upstream pitching axis, and the theoretical curves for the closed tunnel and for open roof and floor do not intersect. This is contrary to the predictions for the unswept half-wing in Fig. 14 and to experiment in Fig. 24 where the effect of sealing the slots is of opposite sign for downstream and upstream pitching axes. With the slots sealed, the measured values are consistently just below the theoretical curve. The results with slots open are in fair agreement with calculation, but for the forward axis the predicted value is exceeded. This disparity is found over a range of Mach number in Fig. 25, where for the pitching axis $x_0 = 0\cdot31\bar{c}$ the calculated interference effect due to sealing the slots is evidently too small and of wrong sign.

Although the corresponding comparison for the second delta wing ($A = 3$) in Fig. 26 shows better agreement, the calculated slotted-wall interference effect is still rather small. The reason for this discrepancy is not clear, but it may be associated with the approximations made in the small-wing interference theory. For the delta wings oscillating about rearward pitching axes the δ_0' terms are an order of magnitude larger than the other terms on the right hand sides of equations (57). The neglected terms can therefore be regarded as a further order of magnitude smaller and a good agreement between theory and experiment is expected. With forward pitching axes, the δ_0' terms are only dominant for small models. The cumulative effect of the neglected terms may now become significant if the area ratio S/C is too large. Support for this idea can be gleaned from the fact that the smaller of the two models in Fig. 26 ($S/C = 0\cdot107$) gives appreciably better comparisons than the larger model ($S/C = 0\cdot137$) in Fig. 25. There is further evidence in Fig. 27, which shows some results for the $A = 2\cdot64$ delta wing in the 18 in. × 14 in. Tunnel with the much smaller area ratio $S/C = 0\cdot042$. For the same forward pitching axis that was used in the $9\frac{1}{2}$ in. × $9\frac{1}{2}$ in. Tunnel, the magnitude and sign of the effect of sealing the slots is now in accord with theory. For the rearward pitching axis, Figs. 25 and 27 show that this effect only decreases roughly in proportion to $(S/C)^{1/2}$, as anticipated at the end of Section 4.1.

The effect of Mach number is shown in Figs. 25 to 27. Results for the middle pitching axis were obtained for the $A = 2\cdot64$ delta wing but have not been plotted as the measurements were insensitive to the slotted-wall condition. For the forward pitching axis in Fig. 26, the predicted effect of sealing the slots decreases at the higher Mach numbers. This unusual trend arises because the constraints for the two wall conditions are of the same sign and that for slots sealed increases more rapidly with Mach number. With slots sealed all the experimental points are consistent apart from possible discrepancies for wing thickness and boundary layers of model and side-wall; the last of these probably explains the larger discrepancies in Fig. 27, since the boundary layer then extends over much of the model. As half-model size is reduced, this type of discrepancy is likely to become serious before the slotted-wall interference is acceptably small. A general increase in wall interference with Mach number is indicated for the rearward axis positions and the interference effect can be seriously large. For the $A = 3$ delta with $x_0 = 1\cdot420\bar{c}$ in Fig. 26 for instance, the measured value of the damping derivative at $M = 0\cdot78$ drops from 0·63 with slots sealed to 0·17 with slots open. This large drop is predicted extremely well by the theory which gives a corresponding drop from 0·70 to 0·25. The calculated free-stream value of 0·62 indicates that the bulk of the large effect stems from slotted-wall interference.

5.3. *Effect of Frequency Parameter.*

Results have been obtained for several frequencies of oscillation giving frequency parameters in the range $0.03 < \bar{v} < 0.28$. Typical variations with frequency parameter for the Mach number $M = 0.58$ are shown in Fig. 28. At the lowest frequencies of about 12 c/sec, the amplitude of the decaying oscillations was subject to considerable fluctuation, possibly due to the high turbulence in the $9\frac{1}{2}$ in. $\times$ $9\frac{1}{2}$ in. Tunnel. The values of the damping derivative from repeated experiments at the lowest frequency were therefore considerably scattered about the mean value shown in Table 4. Conversely, less confidence is placed in the values of the stiffness derivative measured at the highest frequency. In this case, the system is sharply tuned and the change in frequency from still-air to wind-on conditions is very small, being of the same order as the stability of the apparatus. Since the derivatives m_θ and $-m_{\dot\theta}$ vary little with frequency, mean values from the two lowest frequencies in Table 3 and from the two highest frequencies in Table 4 have been used in Section 5.2.

Under free-stream conditions the initial rate of change of damping derivatives with frequency parameter may be calculated from an exact theoretical result of Garner and Milne[23]. As discussed in Section 4.2., the same principle holds under wall constraint and equations (68) are derived. For the range of frequency parameter shown in Fig. 28, the measured values of $-m_{\dot\theta}$ follow the predicted linear trend. With a forward pitching axis (m_θ negative) there is a general increase in the values of $-m_{\dot\theta}$ with increasing frequency and, also in accord with the second of equations (68), there is a corresponding decrease for a rearward pitching axis (m_θ positive). Theoretically the pitching stiffness is known to be independent of small changes in frequency parameter, and the constant values of m_θ in Fig. 28 are calculated from the present wall-interference theory. There is apparently no measurable effect of frequency on the values of m_θ over the range of $\bar{v}$ available. The drop in the value for the highest frequency with slots sealed was not observed at other Mach numbers. It seems that at least for $\bar{v} < 0.2$ a variation in frequency of oscillation has little effect on the magnitude of tunnel interference.

A much wider range of frequency parameter is covered by Guyett and Curran[28] in their measurements of pitching-moment derivatives about the leading edge of a rectangular half-model. The wing was mounted on a reflection plane near the floor of a closed circular tunnel, so that the configuration is equivalent to a complete wing in a closed bipolar tunnel. Guyett[29] has supplied unpublished values of m_θ and $m_{\dot\theta}$ for the corresponding open circular tunnel with reflection plane and the results in Fig. 29 show important changes due to interference. The steady interference upwash parameter $(\delta_0)_U$ from equation (61) is analysed by Kondo[30] for uniformly loaded wings in this shape of tunnel, but the interference parameters δ_1 and δ_0' have not been formulated. However, from Figs. 4, 5 and 7 the interference parameters δ_0, δ_1 and δ_0' can be obtained for small wings in closed or open rectangular tunnels of the same breadth to height ratio $b/h = 1.866$. As suggested in Section 4.2., a correction factor $(\delta_0)_U/\delta_0$ is applied to each interference parameter so that δ_0 is the same as $(\delta_0)_U$ in the bipolar tunnel; for the particular span $0.598b$, $(\delta_0)_U = 0.0853$ and -0.2382 respectively for the closed and open bipolar tunnels. Despite the use of such a crude approximation there is remarkable agreement between the measured and predicted values of m_θ. The predictions are less satisfactory for the pitching damping, although an interference effect of the correct sign is indicated. Since the model has a forward pitching axis and a very large area ratio $S/C = 0.24$, the cause of the discrepancies is thought to be similar to that discussed in Section 5.2. for the delta wings. The predicted variation in $m_{\dot\theta}$ with frequency is calculated from the second of equations (68). In view of the possible error in the magnitude of the theoretical interference effect, only the gradients of those curves should be considered. Unfortunately, there are no experimental results at a suitably low frequency for comparison. It is interesting that the measured differences in the values of the derivatives show little effect of frequency on tunnel-wall interference until the frequency parameter is of order unity.

6. *Practical Correction for Wall Interference.*

It is not always easy or convenient to calculate theoretical values of aerodynamic derivatives, especially for complete aircraft or under conditions of separated flow. For the present purpose of confirming the validity of the interference theory, tests were made on wing models amenable to a theoretical study and the interference theory is suitably formulated in equations (54) to (57). However, in a practical application

it is desirable to calculate corrections to measured derivatives to give corresponding values in an unconstrained flow. The equations are inverted with suitable approximations, and equations (58) can be used to determine the free-stream pitching derivatives from their measured values if the rotary derivatives l_q and m_q in an unconstrained flow can be estimated. If, however, l_q and m_q are not available, great simplification is necessary. All but the dominant terms are then neglected in equations (58), so that

$$
\left.
\begin{aligned}
l_\theta &= (l_\theta)_T \left[1 + \frac{2S}{C} \delta_0 (l_\theta)_T \right]^{-1} \\[2ex]
m_\theta &= (m_\theta)_T \left[1 + \frac{2S}{C} \delta_0 (l_\theta)_T \right]^{-1} \\[2ex]
l_{\dot\theta} &= \left[(l_{\dot\theta})_T - \frac{2S}{C} (l_\theta)_T \frac{\delta_0' h}{\beta \bar c} l_\theta \right] \left[1 + \frac{2S}{C} \delta_0 (l_\theta)_T \right]^{-1} \\[2ex]
m_{\dot\theta} &= \left[(m_{\dot\theta})_T - \frac{2S}{C} (l_\theta)_T \frac{\delta_0' h}{\beta \bar c} m_\theta \right] \left[1 + \frac{2S}{C} \delta_0 (l_\theta)_T \right]^{-1}
\end{aligned}
\right\} , \qquad (70)
$$

where the subscript T denotes a derivative measured in the wind tunnel.

The accuracy of the corrections determined from equations (58) or (70) may be assessed by applying them to the calculated tunnel values of the derivatives. Figs. 30 and 31 show theoretical curves of pitching damping against axis position, respectively for the unswept half-wing at $M = 0.80$ in the slotted 25 in. $\times$ 20 in. Tunnel and for the delta ($A = 2.64$) at $M = 0.66$ in the $9\frac{1}{2}$ in. $\times 9\frac{1}{2}$ in. Tunnel. In both cases the corrected values of $m_{\dot\theta}$ from the alternative equations (58) and (70) are compared with the original theoretical calculation without wall constraint. The simpler set of equations gives a fairly good approximation to the original curve, but in both Figs. 30 and 31 there is only a narrow range of pitching axis for which equations (58) do not improve the approximation. Nevertheless, for a practical application, the simpler approximation gives a fair guide to the magnitude of wall constraint. The presence of large interference can be detected readily by equations (70), whilst a small correction implies that the wall-interference effect is small. In either case more accurate estimates can be obtained by equations (58), provided that satisfactory values of the rotary derivatives are available.

The choice of procedure will be influenced by the type of model and the scope of the measurements; four different situations and methods are summarized below.

(1) If a reasonable degree of confidence can be placed in the theory of Ref. 3, equations (58) should be used when all four derivatives are measured. If, however, only $(m_\theta)_T$ and $(m_{\dot\theta})_T$ are measured, then l_θ, $l_{\dot\theta}$, l_q and m_q may be calculated by Ref. 3 or Ref. 22 so that the four equations (58) determine $(l_\theta)_T$, m_θ, $(l_{\dot\theta})_T$ and $m_{\dot\theta}$ respectively.

(2) When the unconstrained flow is qualitatively beyond the scope of lifting-surface theory and all four pitching derivatives are measured, wall interference should be evaluated by equations (70) since calculated free-stream values of l_q and m_q are untrustworthy.

(3) If only the pitching-moment derivatives, $(m_\theta)_T$ and $(m_{\dot\theta})_T$ are measured about two axes $x_0 = x_1$ and $x_0 = x_2$, say, and the frequency parameter is small, the lift derivatives can be deduced. It follows from equations (51) that

$$
\left.
\begin{aligned}
(l_\theta)_{T1} &= (l_\theta)_{T2} = \frac{(m_\theta)_{T2} - (m_\theta)_{T1}}{(x_2 - x_1)/\bar c} \\[2ex]
(l_{\dot\theta})_{T1} - (m_\theta)_{T2} &= \frac{(m_{\dot\theta})_{T2} - (m_{\dot\theta})_{T1}}{(x_2 - x_1)/\bar c} = (l_{\dot\theta})_{T2} - (m_\theta)_{T1}
\end{aligned}
\right\} \qquad (71)
$$

According to the type of flow, method (1) or (2) may then be used.

28

(4) If $(m_\theta)_T$ and $(m_{\dot\theta})_T$ are measured about a single axis, no corrections can be applied without empirical or theoretical aid. But there should be little difficulty in estimating l_θ, so that $(l_\theta)_T$ and hence m_θ and $m_{\dot\theta}$ can be evaluated from equations (70).

Method (3) is appropriate for calculating lift derivatives from the present measurements of direct pitching derivatives in the $9\frac{1}{2}$ in. $\times$ $9\frac{1}{2}$ in. Tunnel. In Fig. 32a, values of $(l_{\dot\theta})_T$ deduced from the second of equations (71) are compared with theoretical curves given by equations (54) to (57). There is reasonable agreement between the estimated and predicted tunnel values, and both sets give a further indication of dramatically large interference in a typical experimental configuration. The result of correcting the deduced values by methods (1) and (2) is illustrated in Fig. 32b. Since the terms omitted in method (2) give contributions of opposite sign for the two wall conditions, the corrected values, shown as small dots, are less convincing than the comparisons in Fig. 32a. Method (1) is quite satisfactory, since the corrected experimental values from the tunnel with slots sealed, shown as solid circles, lie very close to the theoretical interference-free curve whilst the corresponding open circles corresponding to open slots are displaced from it by amounts consistent with Fig. 32a. It follows that a reasonable estimate of the corrected lift is possible, even when only the pitching-moment derivatives are measured and the results are particularly sensitive to the tunnel boundary condition.

7. *Non-Ideal Slotted Walls.*

It has been shown that the present theory successfully predicts the tunnel-wall interference effects in both the 25 in. $\times$ 20 in. Tunnel and the $9\frac{1}{2}$ in. $\times$ $9\frac{1}{2}$ in. Tunnel. The predictions are confirmed experimentally for the 36 in. $\times$ 14 in. Tunnel with slots sealed, but with slots open the correlation disappears. Indeed, in Figs. 20 and 21 for the unswept wing, $m_{\dot\theta}$ and $l_{\dot\theta}$ vary with Mach number as if the interference effect of the slotted walls were more like that of a sealed wall. Fig. 12, showing the typical effect of a variation in tunnel cross-sectional shape for a fixed area, includes measured values of $m_{\dot\theta}$ in the 36 in. $\times$ 14 in. Tunnel ($b/h = 0.91$) and the 25 in. $\times$ 20 in. Tunnel ($b/h = 1.90_5$) and demonstrates clearly that it is the former tunnel with slots open which is not behaving as expected. Corresponding results for m_θ, given in Fig. 11, show much less interference effect and are harder to interpret, as the measured values do not agree particularly well with the theoretical curves. Nevertheless, they confirm that the effect of sealing the slots of the 36 in. $\times$ 14 in. Tunnel is much smaller than the predicted difference, whereas a similar comparison for the 25 in. $\times$ 20 in. Tunnel shows better agreement. The authors believe that the behaviour of the 36 in. $\times$ 14 in. Tunnel with slots open can be explained by the action of viscosity at the slotted walls.

Although no allowance for viscosity can be made in the present theory, the appropriate change of boundary condition in steady flow has been discussed in Section 2 and the typical behaviour of δ_0 is shown in Figs. 2 and 3. If the porosity parameter β/P is changed from zero to be of order unity in a square tunnel, for instance, there is a significantly large change in δ_0 from -0.125 for an open roof and floor to a small value of positive sign as for a closed tunnel. A similar result is obtained for an ideal slotted tunnel ($P \to \infty$) with $(1 + F)^{-1}$ of order 0.5, so that in steady flow viscosity reduces the effective open area ratio of a slotted wall. It might also be anticipated that, as the Mach number approaches unity and $\beta \to 0$, the porosity parameter β/P becomes small and an ideal slotted condition with negligible viscous effects is approached. The oscillatory results obtained in the 36 in. $\times$ 14 in. Tunnel show both these trends. In Figs. 20 and 21 there are very small changes in the derivatives due to sealing the slots at low Mach numbers. However, as M increases, there is an increasing difference between the values measured with the two slot conditions, the results with slots open falling away from those with slots sealed towards values appropriate to an ideal slotted roof and floor. This suggests that with changing β/P the unsteady interference upwash may behave like δ_0.

The 36 in. $\times$ 14 in. Tunnel and the 25 in. $\times$ 20 in. Tunnel have the same open area ratio (0.091) and the same number of slots (11). The slots in the 36 in. $\times$ 14 in. Tunnel are therefore narrower than those in the 25 in. $\times$ 20 in. Tunnel, and it is physically reasonable that viscosity could affect the former tunnel more than the broader 25 in. $\times$ 20 in. Tunnel. A similarity parameter is desirable to indicate the sensitivity of slotted-wall configurations to viscous effects, and Goethert's[1] study of perforated walls in steady flow

29

may offer a clue. The linearized steady boundary condition at a perforated wall from equation (5) with $K = 0$ is equivalent to proportionality between the pressure drop through the wall and the velocity normal to it, viz.,

$$\delta p = \frac{\rho U}{P}\, v_n.$$

(72)

Goethert suggests that the ratio of boundary-layer displacement thickness δ^* to hole diameter D is important, and that viscous effects on P are likely to grow suddenly as δ^*/D increases above about 0·75. Evidence of such a critical value from Ref. 1 is reproduced in Fig. 33. For Mach numbers of 0·75 and 0·80, the pressure drop δp across the wall is related to the mass outflow ρv_n through a perforated wall of open area ratio 0·225, (a) when $D = \frac{1}{16}$ in. and the wall is $\frac{1}{16}$ in. thick and (b) when the thickness is the same but $D = \frac{1}{2}$ in. With the larger holes, the pressure drop increases linearly with increasing mass outflow in Fig. 33b, so that by equation (72) the effective parameter

$$\frac{\beta}{P} = \frac{\beta}{2}\frac{\partial(\delta p/\frac{1}{2}\rho_\infty U^2)}{\partial(\rho v_n/\rho_\infty U)} \doteq 0\cdot4.$$

(73)

The smaller perforations again give $\beta/P \doteq 0\cdot4$ when the mass-flow parameter in Fig. 33a exceeds 0·03 ; below this there is an abrupt change and the pressure drop shows considerable scatter but tends to remain constant. The perforated wall is thus behaving almost as if it were solid corresponding to a large value of β/P in place of equation (73). For small mass flow and small perforations when δ^*/D is large, Goethert suggests that viscous effects govern the wall characteristics. With increasing mass outflow δ^*/D decreases until it reaches some critical value near 0·75 below which the viscous effects disappear rapidly and β/P is determined by the wall geometry. For the wall with perforations eight times larger, the boundary layer will be smaller relative to hole size and will give a subcritical value of δ^*/D throughout Fig. 33b.

A rapid increase in the effect of viscosity in a slotted tunnel similar to that shown in Fig. 33 could explain the drastic discrepancy in Fig. 12 for the 36 in. × 14 in. Tunnel ($h/h = 0\cdot91$) with slots open. As the boundary-layer displacement thickness δ^* has little meaning in this case, it is tentatively suggested that viscous effects in a slot of width a may grow in proportion to the ratio l_u/a where l_u is the distance between the model and the upstream end of the working section ; future work may well show that plenum-chamber depth, amongst other factors, is important in this respect. The 'Δ ratio' of the measured change to the predicted change in m_0 due to sealing the slots is plotted against l_u/a in Fig. 34 for delta and unswept tapered wings with rearward pitching axes in the three slotted tunnels shown in Fig. 18. As a further check, some results have been obtained from the NPL 18 in. × 14 in. Tunnel with full slots and with slot width crudely narrowed by about 30 per cent by means of tape. This reduction in slot width produces a negligible change in the geometric slot parameter $(1 + F)^{-1}$ from 0·91 to 0·90. From Fig. 34 it is clear that the Δ ratio is dramatically reduced from about 1 when l_u/a is small to low values when l_u/a is large and the slot width is relatively small. Although the analysis in Fig. 34 for $M = 0\cdot6$ and $M = 0\cdot8$ involves variations of numerous parameters, two significant points emerge. Firstly, the 36 in. × 14 in. Tunnel gives small Δ ratios, whereas the 18 in. × 14 in. Tunnel with identical slots and 30 per cent shorter upstream working section gives Δ ratios of about two thirds. Secondly, when the slot width in the 18 in. × 14 in. Tunnel is narrowed to give l_u/a roughly equivalent to the 36 in. × 14 in. Tunnel, the Δ ratio falls by 26 per cent at $M = 0\cdot6$ and by 16 per cent at $M = 0\cdot8$. Fig. 34, although inconclusive, may provide a plausible explanation of the results in the 36 in. × 14 in. Tunnel. The slotted wall appears to behave as if it were practically closed, not because of small open area ratio, but because of the small relative slot width a/l_u, which may be associated with low porosity in terms of the parameter β/P. Indeed, the fall in Δ ratio is noticeably less at the higher Mach number when β/P is expected to be smaller.

Unfortunately it is difficult to estimate a value of P for steady flow in a tunnel with slotted walls. A further difficulty arises with unsteady flow because it is possible that there is a phase lag between the pressure drop and the mass outflow. In the present theory, it is assumed that viscous effects are small. As discussed in Section 3, the simple relationship (12) between the steady and the unsteady upwash

30

interference may not hold without this assumption. If, however, β/P is very large for slotted tunnels, the present corrections for closed walls should be adequate. Most of the present experimental data can be explained satisfactorily on the basis of very small or very large β/P although the few results from the 18 in. × 14 in. Tunnel suggest that an intermediate condition can exist. Further work is planned to investigate experimentally the effect of an artificial increase in the viscous effects at a slot; it is necessary to establish that such an increase can greatly reduce the change in measured damping due to sealing the slots.

8. *Concluding Remarks.*

(1) It is shown that large wall-interference effects on dynamic measurements observed with half-models in slotted tunnels can be satisfactorily explained by an extension to the classical theory of steady lift interference. With the assumptions of relatively small model span, small frequency parameter and open instead of slotted boundaries, the method gives theoretical pitching damping derivatives whose values are confirmed by experiment in two NPL tunnels, even when the changes due to sealing the slots exceed 30 per cent (Sections 5.1. and 5.2.).

(2) The large effects with slotted roof and floor are shown to stem from the parameter δ'_0 which represents the wall-interference upwash in quadrature with the pitching motion of the model. For the crucial case of rectangular tunnels with closed side-walls and open roof and floor, particular care is needed in the formulation and evaluation of δ'_0 (Section 3.1.). This parameter alone determines the major effects of tunnel shape, model size, Mach number and pitching axis on the damping derivatives (Section 4.1.).

(3) Subsonic lifting-surface theory is used to interpret the interference upwash as incremental forces on the model (Section 3.2.). Equations (54) to (57) are then derived such that values of the pitching derivatives in a tunnel can be predicted for direct comparison with experiment. Approximations to these equations are inverted to give equations (58) which are recommended for practical application. Measured derivatives can thus be corrected for wall interference with little or no reference to lifting-surface theory (Section 6). As a crude, but instructive, approximation the incremental corrections to the damping derivatives are concisely

$$
\left.
\begin{aligned}
l_{\dot\theta} - (l_{\dot\theta})_T &= -\frac{4 s \delta'_0}{\beta b} (l_\theta)_T^2 \\[2ex]
m_{\dot\theta} - (m_{\dot\theta})_T &= -\frac{4 s \delta'_0}{\beta b} (l_\theta)_T (m_\theta)_T.
\end{aligned}
\right\}
\qquad (74)
$$

(4) In some respects the present method is more general than the formulae suggest (Section 4). In particular, approximate allowance may easily be made for the geometric slot parameter and for the ratio of wing span to tunnel breadth (Section 4.2). The first order effect of frequency parameter on the damping derivatives under wall constraint is given very simply in equations (68) which should cover the range of frequency parameter normally encountered in slotted-wall tunnels. Limited experimental confirmation of the frequency effect is found (Section 5.3).

(5) The location of the pitching axis is shown to have a significant effect on the predicted interference correction to pitching damping in tunnels with slotted roof and floor. For a forward axis the theory apparently underestimates the fairly small correction. When the axis is moved downstream of the aerodynamic centre, the sign of the interference changes and its magnitude grows very rapidly and often in accord with experiment. The lift-damping due to pitching is subject to such serious corrections that its sign may change (Section 4.1).

(6) For a given area of working section, the wall interference on half-models in tunnels with slotted roof and floor is greatest when the effective breadth to height ratio is large. In such cases it may not be practicable to diminish model size as a means of reducing the interference to negligible proportions. The merit of these tunnels for dynamic measurements is open to question. When interference corrections of 50 per cent or greater are involved, the present theory, approximate as it is, goes a long way towards

removing the uncertainty. Nevertheless the corrected derivative must often be far less accurate than the measuring techniques used in the experiment. Somewhat smaller corrections are anticipated for complete models in slotted tunnels, especially when the planform is more slender.

(7) A possible remedy is to use tunnels with slotted side-walls and closed roof and floor (Section 3.1.). Then each of the interference parameters, especially δ_0', remains small over a range of cross-sectional shapes of practical importance. Orlik-Rückemann and Laberge[31] have published a few experimental data for this configuration in subsonic flow; they give no results with slots sealed, but report that the effect of sealing the slots seems to be small.

(8) When the slots are relatively narrow, viscous effects within the slots may change the interference effects fundamentally (Section 7). For atmospheric tunnels it appears likely that inviscid flow may be assumed unless the length of working section upstream of the model exceeds about 300 slot widths. If, however, this length exceeds about 500 slot widths and the Mach number is not too large, then there is limited evidence to suggest that the slotted wall may be treated as a closed boundary. In the latter case, there may still be significant interference effects not revealed by sealing the slots.

(9) Provided that viscous effects can be well understood and controlled, they could offer a possibility of reducing wall interference to an acceptable magnitude. Further work in slotted tunnels is needed to explore this possibility.

(10) The interference effects on dynamic measurements in other types of ventilated tunnel need to be studied theoretically and experimentally. Solutions by electrical analogue (Ref. 8) may greatly assist theoretical prediction, but experimental work to establish reliable unsteady boundary conditions could be more crucial.

LIST OF SYMBOLS

a	Width of slot
A	Aspect ratio of wing $= 2s/\bar{c}$
b	Effective breadth of tunnel
$\bar{c}$	Geometric mean chord of wing $= S/2s$
C	Cross-sectional area of tunnel
C_L	Lift$/\frac{1}{2}\rho U^2 S$, $\bar{C}_L e^{i\omega t}$
C_m	Nose-up pitching moment$/\frac{1}{2}\rho U^2 S\bar{c}$
C_m^*	Second pitching moment$/\frac{1}{2}\rho U^2 S\bar{c}^2$
$\bar{C}_L$	Complex lift coefficient
$\bar{C}_m$	Complex pitching-moment coefficient
d	Periodic spacing of slots
D	Hole diameter of perforated wall
f	Function defined in equation (29)
F	Non-dimensional slot parameter in equation (4)
F_L, F_m	Functions defined in equations (54)
G	Function in equation (31)
h	Height of tunnel
i	$(-1)^{\frac{1}{2}}$
I_{Lr}	Equivalent C_L for incidence α_r ($r = 1,2,\ldots 5$)
I_{mr}	Equivalent C_m for incidence α_r ($r = 1,2,\ldots 5$)
I_{mr}^*	Equivalent C_m^* for incidence α_r ($r = 1,2$)
j	Sign according to the appropriate equation (17)
K	Geometric slot parameter in equation (4)
$\bar{K}$	Kernel function of integral equation (Section 4.2.)
K_0, K_1	Modified Bessel functions of the second kind in equations (24)
l_q	Rotary pitching derivative of lift in equations (47) and (53)
$l_\theta, l_{\dot{\theta}}$	Derivatives of lift due to pitching in equations (46) and (51)
L	Lift, streamwise distribution of lift
m	Integer defining column of images $y = mb$
m_q	Direct rotary pitching derivative in equations (47) and (53)
$m_\theta, m_{\dot{\theta}}$	Direct pitching derivatives in equations (46) and (51)
M	Mach number of undisturbed stream
n	Outward normal distance from tunnel boundary

The symbols I_{Lr}, I_{mr}, I_{mr}^* are defined in equations (33) of Ref. 22

n	Integer defining row of images $z = nh$
p	Pressure
P	Porosity parameter in equations (5) and (72)
q	Steady rate of pitching
s	Semi-span of wing
S	Area of planform of wing
S_1, S_2	Functions in equations (23) and (24)
t	Time
t	Semi-span of elementary horse-shoe vortex
U	Velocity of undisturbed stream
v_n	Velocity normal to perforated wall
$\bar{w}$	Complex upward component of velocity
w_i	Interference upwash velocity, $\bar{w}_i e^{i\omega t}$
$\bar{w}_i$	Complex interference upwash velocity
w_{i0}	Steady interference upwash velocity in incompressible flow
x	Streamwise distance from root leading edge, from lifting element in Section 3
$\bar{x}$	Aerodynamic centre of wing in equation (43)
x_0	Value of x at pitching axis
y	Spanwise distance from wing root
z	Upward distance from centre of tunnel
α_r	Steady distributions of incidence in equations (52)
β	$(1 - M^2)^{\frac{1}{2}}$
δ	Non-dimensional steady interference upwash in equation (13)
δ^*	Displacement thickness of boundary layer
δ_0	Steady upwash interference parameter in equation (8), (20) or (60)
δ_1	Steady streamline curvature parameter in equations (14) and (22)
δ_0'	Unsteady upwash interference parameter in equations (16) and (27)
$(\delta_0)_E$	Mean δ_0 for elliptic spanwise loading in equation (62)
$(\delta_0)_U$	Mean δ_0 for uniform spanwise loading in equation (61)
δp	Pressure drop across perforated wall
θ_0	Amplitude of pitching oscillation
λ	h/b
$\bar{\nu}$	Frequency parameter $= \omega \bar{c}/U$

34

ξ	Streamwise distance, variable to replace x	
ρ	Local density of stream (Section 7)	
ρ_∞	Density of undisturbed stream (Section 7)	
ϕ	Perturbation velocity potential, $\bar{\phi}e^{i\omega t}$	
$\bar{\phi}$	Complex perturbation velocity potential	
ϕ_0	ϕ corresponding to steady horse-shoe vortex in incompressible flow	
ϕ_i	Interference velocity potential	
ω	Angular frequency of oscillation	
(1)	Superscript denoting closed tunnel	
(2)	Superscript denoting open tunnel	
(3)	Superscript denoting open sides, closed roof and floor	
(4)	Superscript denoting closed sides, open roof and floor	
A	Subscript denoting tunnel A of type (4) in Fig. 6	
B	Subscript denoting tunnel B of type (4) in Fig. 6	
C	Subscript denoting tunnel C of type (1) in Fig. 6	
D	Subscript denoting tunnel D of type (2) in Fig. 6	
I	Subscript denoting imaginary part in equations (37) and (39)	
R	Subscript denoting real part in equations (37) and (39)	
T	Subscript denoting derivative with tunnel-wall constraint	

REFERENCES

No.	Author(s)	Title, etc.
1	B. H. Goethert	*Transonic wind tunnel testing.* AGARDograph 49. Pergamon Press. 1961.
2	W. E. A. Acum	The comparison of theory and experiment for oscillating wings. A.R.C. C.P.681. March, 1962.
3	H. C. Garner	Multhopp's subsonic lifting-surface theory of wings in slow pitching oscillations. A.R.C. R. & M. 2885. July, 1952.
4	J. B. Bratt and K. C. Wight	Measurements of pitching oscillation derivatives at subsonic and transonic speeds for an *M*-wing (Interim Report). A.R.C.21 661. February, 1960.

REFERENCES—*(contd.)*

No.	Author(s)	Title, etc.

5   C. J. W. Miles and
K. B. Bridgman

Measurements of the direct pitching oscillation derivatives for three cropped delta and three arrowhead planforms at subsonic and transonic speeds.
A.R.C. R. & M. 3397. August, 1962.

6   K. C. Wight

A review of slotted-wall wind-tunnel interference effects on oscillating models in subsonic and transonic flows.
J. R. Aeronaut. Soc. Vol. 68, pp. 670–674. October, 1964.

7   W. E. A. Acum

A simplified approach to the phenomenon of wind-tunnel resonance.
A.R.C. R. & M. 3371. April, 1962.

8   K. R. Rushton

Studies of slotted-wall interference using an electrical analogue. Part I. The electrical analogue to steady and oscillating flow in slotted-wall tunnels. Part II. Particular examples of slotted-wall tunnel interference.
A.R.C. R. & M. 3452. June, 1965.

9   W. G. Molyneux

Wind tunnel interference in dynamic measurements.
R.A.E. Tech. Report 64069.
A.R.C. 26 673. November, 1964.
Presented at a short course on the use of flexible models in aero-elastic research at the Von Karman Institute of Fluid Dynamics. May, 1964.

10   H. C. Garner and
A. W. Moore

Notes on unsteady slotted-wall tunnel interference.
N.P.L. Aero Note 1039.
A.R.C. 27 486. November, 1965.

11   D. D. Davis and D. Moore

Analytical study of blockage- and lift-interference corrections for slotted tunnels obtained by the substitution of an equivalent homogeneous boundary for the discrete slots.
NACA RM L53E07b (NACA/TIB/3792). June, 1953.

12   B. S. Baldwin, J. B. Turner
and E. D. Knechtel

Wall interference in wind tunnels with slotted and porous boundaries at subsonic speeds.
NACA Tech. Note 3176. May, 1954.

13   D. G. Drake

Wind-tunnel interference for oscillating wings at transonic speeds.
A.R.C. 21 489. December, 1959.

14   D. R. Holder

Upwash interference on wings of finite span in a rectangular wind tunnel with closed side walls and porous-slotted floor and roof.
A.R.C. R. & M. 3395. November, 1963.

15   T. R. Goodman

The upwash correction for an oscillating wing in a wind tunnel.
J.Aero.Sci. Vol. 20, pp. 383–386, 406. 1953.

16   W. E. A. Acum and
H. C. Garner

Approximate wall corrections for an oscillating swept wing in a wind tunnel of closed circular section.
A.R.C. C.P. 184. January, 1954.

36

REFERENCES—*(contd.)*

No.	Author(s)	Title, etc.

17   W. E. A. Acum   ..   ..   Wall corrections for wings oscillating in wind tunnels of closed rectangular section.
A.R.C. R. & M. 3312. January, 1958.

18   W. E. A. Acum   ..   ..   A note on the estimation of the effect of wind tunnel walls on the forces on slowly oscillating slender wings.
A.R.C. C.P. 707. April, 1963.

19   H. Glauert   ..   ..   ..   Wind-tunnel interference on wings, bodies and airscrews.
A.R.C. R. & M. 1566. 1933.

20   H. C. Garner, D. R. Holder ..   An anomaly in the theory of tunnel-wall interference on a lifting wing.
and W. E. A. Acum   *Aeronaut.Q.* Vol. XIV, pp. 31–40. 1963.

21   F. W. J. Olver ..   ..   ..   Transformation of certain series occurring in aerodynamic interference calculations.
Q.J.Mech.Appl.Math. Vol. 2, pp. 452–457. 1949.

22   H. C. Garner and D. A. Fox ..   Algol 60 programme for Multhopp's low-frequency subsonic lifting-surface theory.
A.R.C. R. & M. 3517. April, 1966.

23   H. C. Garner and   ..   ..   Asymptotic expansion for transient forces from quasi-steady subsonic wing theory.
R. D. Milne   *Aeronaut.Q.* Vol. XVII, pp. 343–350. 1966.

24   H. C. Garner and   ..   ..   Theoretical subsonic derivatives for an oscillating M-wing.
W. E. A. Acum   A.R.C. R. & M. 3214. January, 1959.

25   L. Woodgate, ...   Measurement of the pitching-moment derivatives for rigid tapered wings of hexagonal planform oscillating in supersonic flow.
J. F. M. Maybrey and
C. Scruton   A.R.C. R. & M. 3294. March, 1961.

26   K. C. Wight and   ..   ..   Measurements of the direct oscillatory derivatives for a linear bending mode on four rigid half-span models at subsonic and transonic speeds, in closed and slotted tunnels.
Miss J. A. Nixon   A.R.C. R. & M. 3376. March, 1963.

27   J. B. Bratt   ..   ..   ..   Wind-tunnel techniques for the measurement of oscillatory derivatives.
A.R.C. R. & M. 3319. August, 1960.

28   P. R. Guyett and   ..   ..   Aerodynamic derivative measurements on a rectangular wing of aspect ratio 3·3.
J. K. Curran   A.R.C. R. & M. 3171. March, 1958.

29   P. R. Guyett ..   ..   ..   Private communication. October, 1965.

30   K. Kondo   ..   ..   ..   The wall interference of wind tunnels with boundaries of circular arcs.
Aero. Res. Inst. (Univ. of Tokyo) Report 126. 1935.

31   K. J. Orlik-Rückemann and ..   Static and dynamic longitudinal stability characteristics of a series of delta and sweptback wings at supersonic speeds.
J. G. LaBerge   N.R.C. (Canada) Aero. Report LR–396. January, 1966.

TABLE 1

Interference Parameters for Small Half-Models in Rectangular Tunnels.

NPL Tunnel	Effective b/h	Completely closed			Open roof and floor		
		δ_0	δ_1	$-\delta'_0$	$-\delta_0$	$-\delta_1$	δ'_0
36 in. × 14 in.	0·911	0·1472	0·2546	0·0428	0·1097	0·1547	0·0694
	1·250	0·1213	0·2277	0·0218	0·1621	0·2364	0·0989
	1·667	0·1231	0·2542	0·0087	0·2181	0·3187	0·1325
25 in. × 20 in.	1·905	0·1322	0·2809	0·0050	0·2493	0·3644	0·1516
9½ in. × 9½ in.	2·468	0·1632	0·3556	0·0012	0·3230	0·4722	0·1964

TABLE 2

Aerodynamic Coefficients for Various Planforms* and Mach Numbers.

	Unswept tapered wing $A = 4\cdot329$ $\Lambda = 15$ deg			Delta wing $A = 2\cdot64$ $\Lambda = 33\cdot7$ deg		
	$M = 0$	$M = 0\cdot6$	$M = 0\cdot8$	$M = 0$	$0\cdot6614$	$0\cdot8660$
I_{L1}	3·821	3·467	2·968	2·965	2·465	1·820
I_{L2}	4·051	3·715	3·221	3·568	3·016	2·284
I_{L3}	−0·415	0·126	0·608	0·526	0·786	0·858
I_{L4}	4·622	4·269	3·733	4·497	3·843	2·957
I_{L5}	−0·869	−0·294	0·242	0·201	0·555	0·724
$-I_{m1}$	1·911	1·714	1·447	1·853	1·541	1·143
$-I_{m2}$	2·483	2·298	2·022	2·666	2·294	1·788
$-I_{m3}$	0·216	0·490	0·715	0·670	0·817	0·825
$-I_{m4}$	3·152	2·965	2·661	3·687	3·232	2·586
$-I_{m5}$	−0·031	0·264	0·521	0·499	0·706	0·775
$-I^*_{m1}$	1·265	1·123	0·933	1·432	1·181	0·867
$-I^*_{m2}$	1·928	1·796	1·593	2·347	2·037	1·611

*In Table 2, Λ denotes the angle of leading-edge sweepback.

TABLE 2—(contd.)

	Delta wing A = 3 Λ = 45 deg				M-wing A = 5·02	Rect. A = 3·35
	$M = 0$	$M = 0.6$	$M = 0.8$	$M = 0.9165$	$M = 0.8$	$M = 0$
I_{L1}	3·099	2·706	2·222	1·626	1·909	3·332
I_{L2}	4·669	4·123	3·437	2·570	−0·026	2·575
I_{L3}	0·423	0·656	0·788	0·766	0·118	0·062
I_{L4}	7·284	6·478	5·453	4·139		2·184
I_{L5}	0·098	0·499	0·777	0·858		−0·315
$-I_{m1}$	2·856	2·526	2·110	1·580	−0·705	0·756
$-I_{m2}$	4·851	4·353	3·707	2·852	0·566	0·951
$-I_{m3}$	0·632	0·844	0·962	0·926	0·077	0·378
$-I_{m4}$	8·079	7·317	6·308	4·941		0·955
$-I_{m5}$	0·464	0·828	1·077	1·126		0·157
$-I^{*}_{m1}$	3·128	2·777	2·334	1·764	0·787	0·363
$-I^{*}_{m2}$	5·704	5·157	4·439	3·468		0·555

TABLE 3

Stiffness Derivative m_θ for the Half-Delta-Model $A = 2.64$ in the NPL $9\frac{1}{2}$ in. × $9\frac{1}{2}$ in. Tunnel.

M	$\bar{v}$	Slots open			Slots sealed		
		$x_0 = 0.31\bar{c}$	$x_0 = 0.65\bar{c}$	$x_0 = 1.04\bar{c}$	$x_0 = 0.31\bar{c}$	$x_0 = 0.65\bar{c}$	$x_0 = 1.04\bar{c}$
0·38	0·29	−0·614	—	0·630	−0·697	—	0·410
0·58	0·19	−0·712	—	0·569	−0·694	—	0·604
0·78	0·15	−0·641	—	0·609	−0·788₅	—	0·626
0·38	0·19	−0·524	−0·006	0·552	−0·589	−0·026	0·638
0·48	0·15	−0·529	−0·014	0·541	−0·619	−0·024	0·636
0·58	0·12₅	−0·523	−0·013	0·556	−0·622	−0·016₅	0·648
0·68	0·11	−0·492	−0·008	0·556₅	−0·651	−0·015₅	0·668
0·78	0·09₅	−0·488	−0·011	0·566	−0·698₅	−0·016	0·696
0·38	0·09	−0·427		0·519	−0·586	—	0·606
0·58	0·06	−0·468		0·559	−0·609₅	—	0·636
0·78	0·04₅	−0·482		0·581	−0·658	—	0·695
0·38	0·06	−0·475		0·552	−0·559	—	0·643₅
0·58	0·04	−0·486		0·572	−0·591	—	0·672₅
0·78	0·03	−0·498		0·579	−0·681	—	0·715₅

TABLE 4

Damping Derivative $-m_{\dot{\theta}}$ *for the Half-Delta-Model A $= 2\cdot64$ in the NPL $9\frac{1}{2}$ in. $\times$ $9\frac{1}{2}$ in. Tunnel.*

M	$\bar{v}$	Slots open			Slots sealed		
		$x_0 = 0\cdot31\bar{c}$	$x_0 = 0\cdot65\bar{c}$	$x_0 = 1\cdot04\bar{c}$	$x_0 = 0\cdot31\bar{c}$	$x_0 = 0\cdot65\bar{c}$	$x_0 = 1\cdot04\bar{c}$
0·38	0·29	1·058	—	0·042	1·011	—	0·144
0·58	0·19	1·145	—	0·058	1·025	—	0·231
0·78	0·15	1·291	—	0·133	1·164	—	0·462
0·38	0·19	1·054	0·375	0·020	0·962	0·406	0·177
0·48	0·15	1·130	0·383	0·020	0·956	0·391	0·199
0·58	0·12$_5$	1·178	0·426	0·037	0·957	0·426$_5$	0·257$_5$
0·68	0·11	1·298	0·480$_5$	0·103$_5$	1·032	0·480	0·309
0·78	0·09$_5$	1·352	0·583	0·209	1·149	0·617	0·479$_5$
0·38	0·09	1·174	—	0·027	0·964	—	0·164
0·58	0·06	1·118	—	0·119	0·887	—	0·273
0·78	0·04$_5$	1·198$_5$	—	0·412	1·003	—	0·537
0·38	0·06	1·356	—	0·076	1·337	—	0·200$_5$
0·58	0·04	1·084	—	0·099	1·126	—	0·229
0·78	0·03	1·128	—	0·331	1·052$_5$	—	0·728
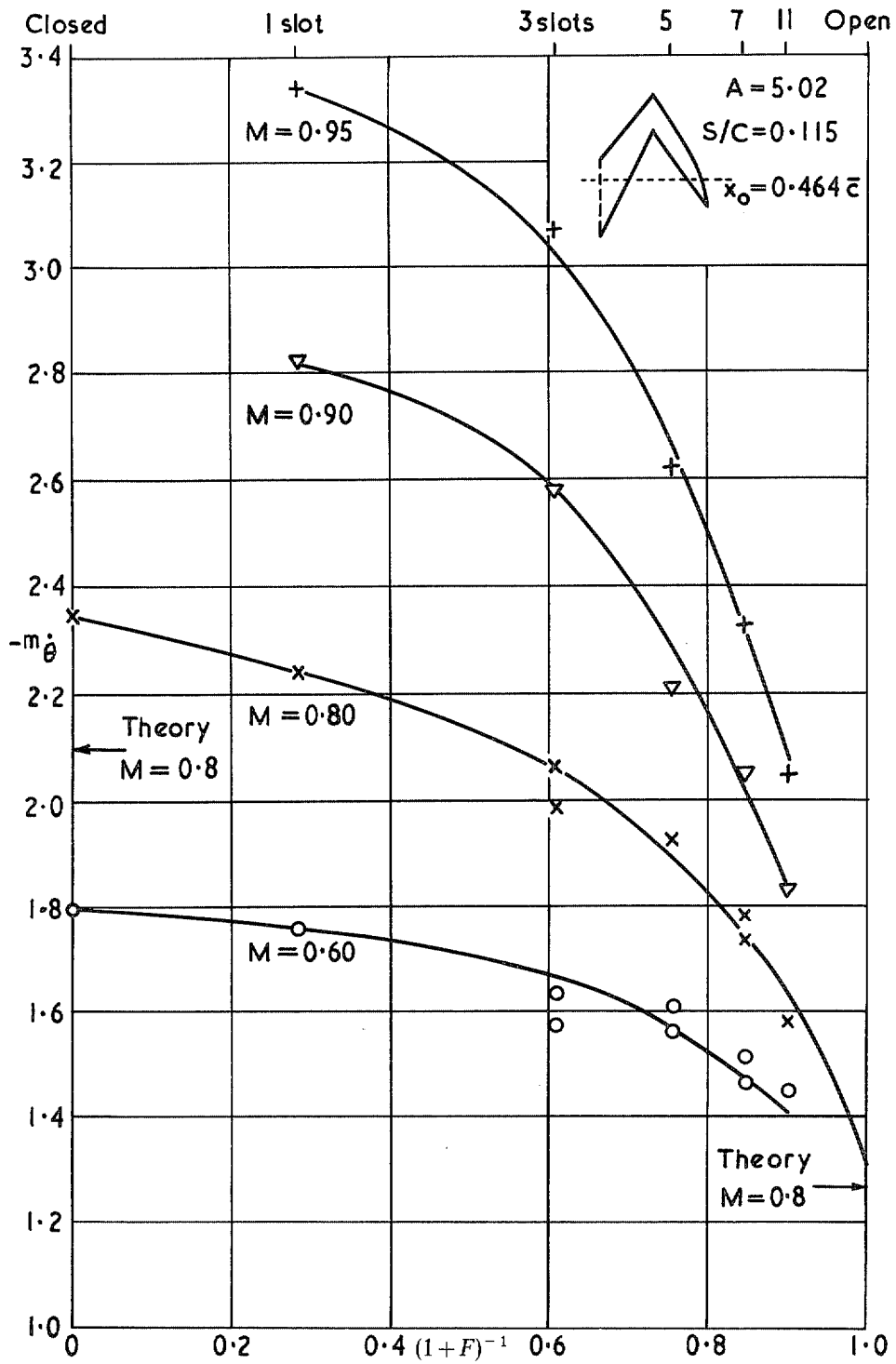
FIG. 1. Pitching damping of a half M-wing in the 25 in. × 20 in. Tunnel with varying numbers of longitudinal slots.
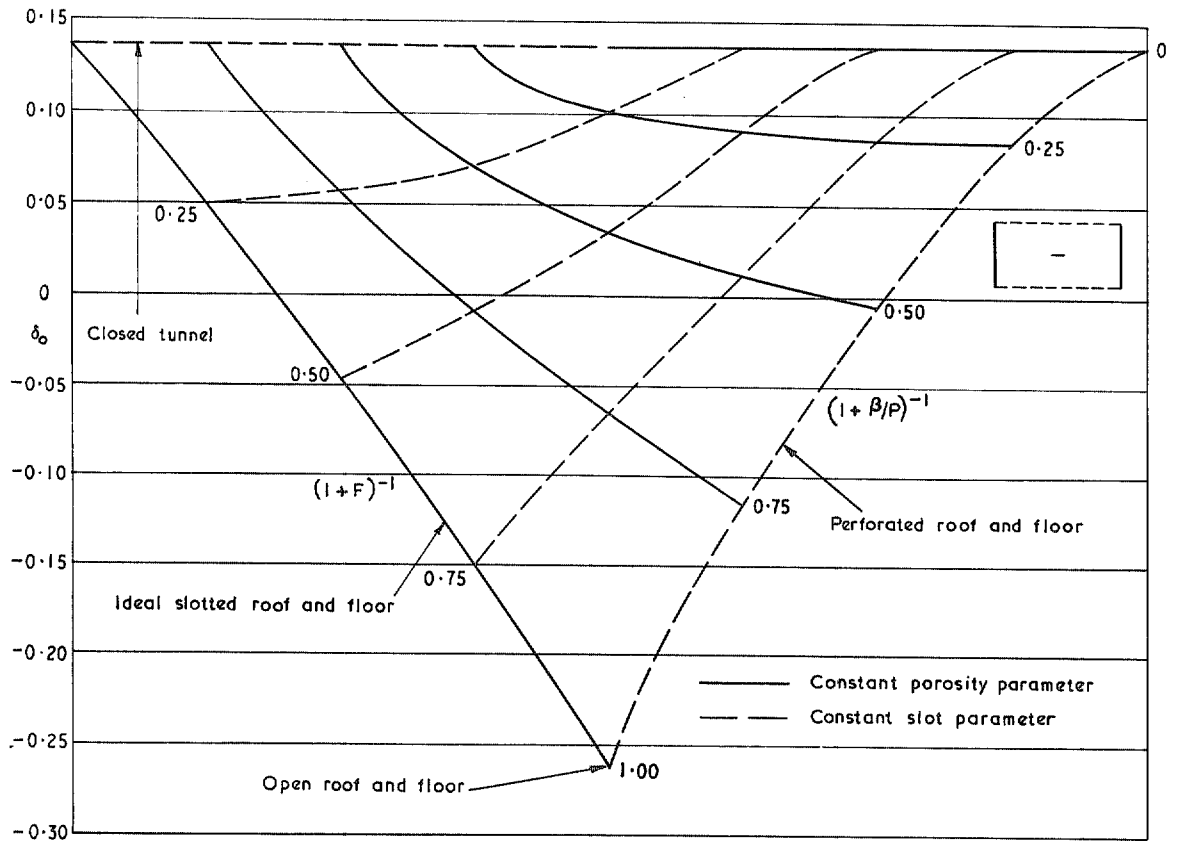
FIG. 2. Steady lift interference parameter in duplex tunnels with ventilated roof and floor (Ref. 14).
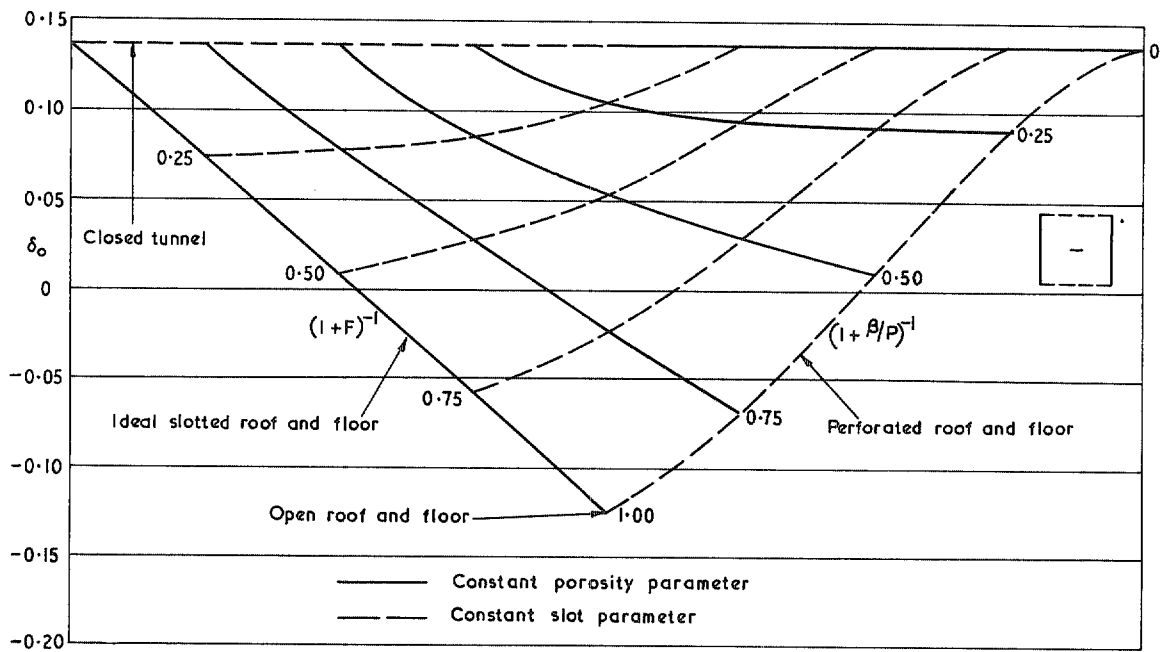
FIG. 3. Steady lift interference parameter in square tunnels with ventilated roof and floor (Ref. 14).

42
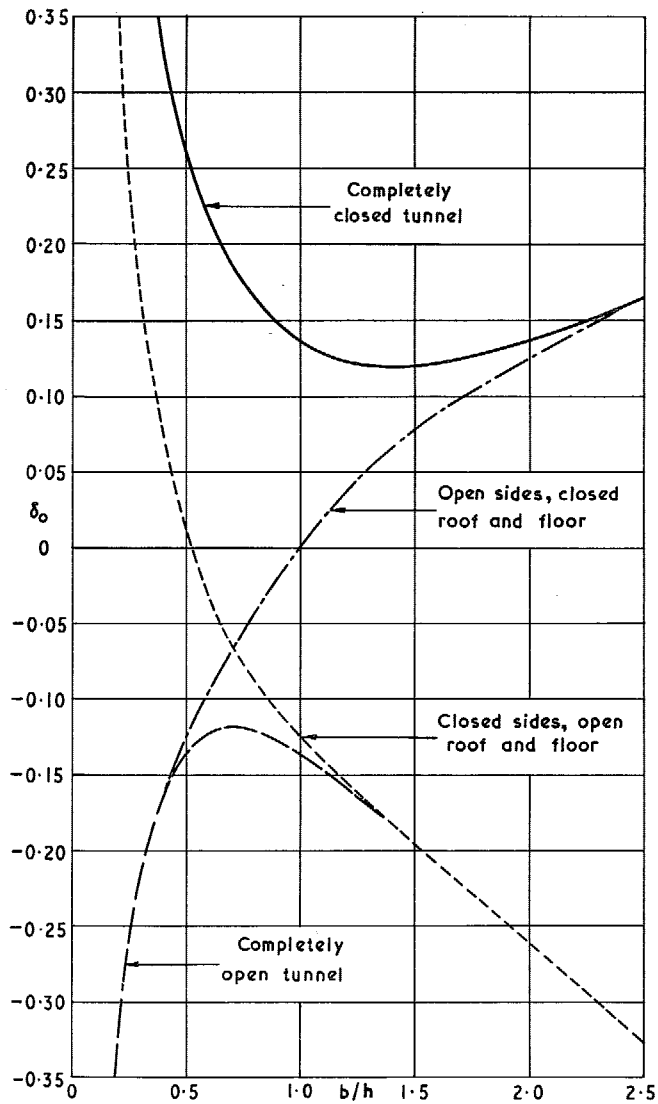
FIG. 4. Steady upwash interference parameter for small wings in different types and shapes of rectangular tunnel.
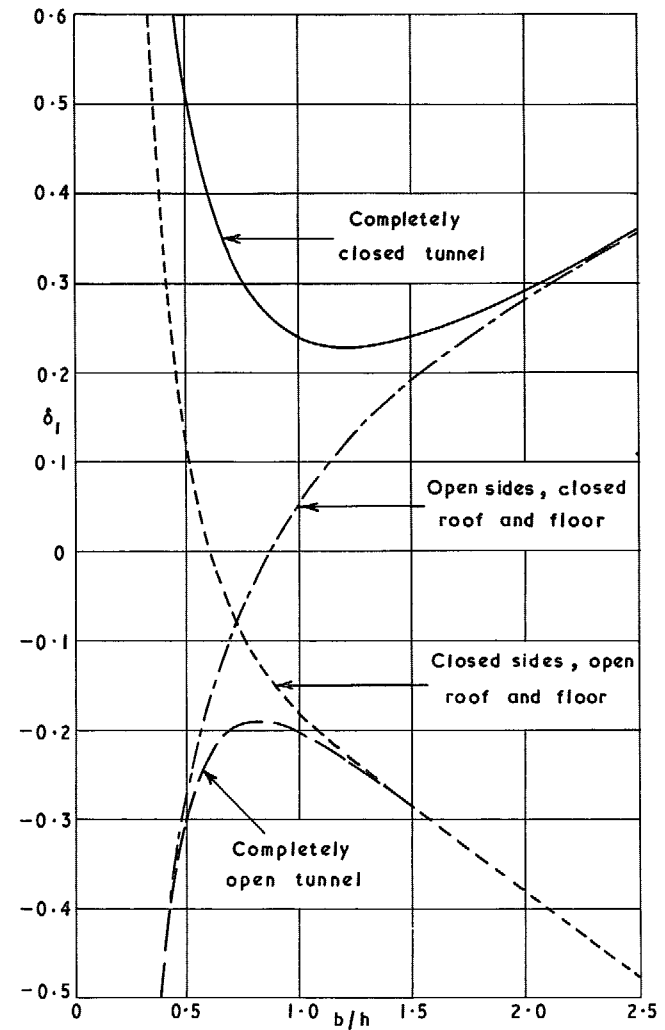
FIG. 5. Steady streamline curvature parameter for small wings in different types and shapes of rectangular tunnel.
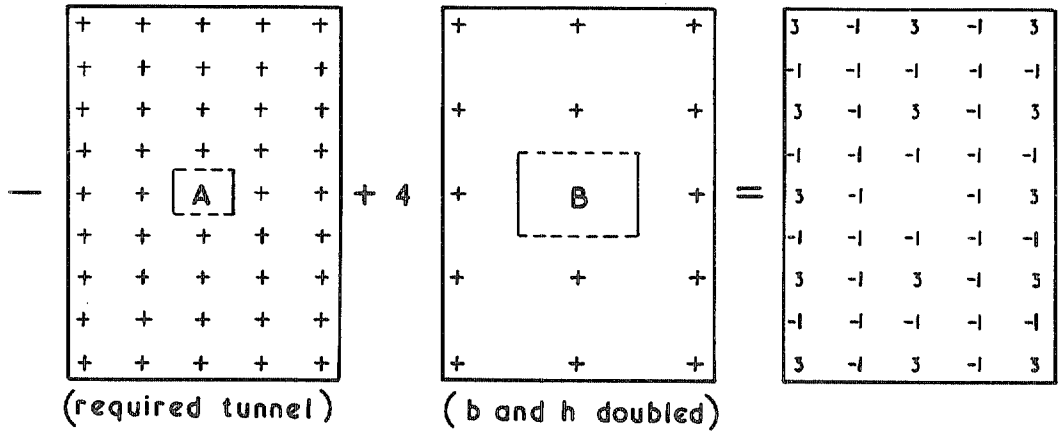
(required tunnel) (b and h doubled)
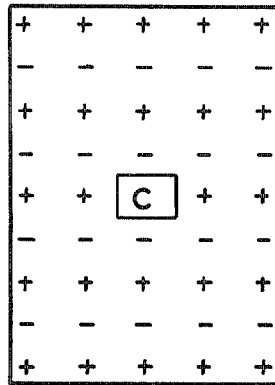
(closed roof and floor) (open sides h doubled)

For all x

$$-w_{iA} + 4w_{iB} = w_{iC} + 2w_{iD}$$

$$\delta_o = \frac{\rho U b h}{2L}(w_i)_{x=o}$$

$$-\delta_{oA} + \delta_{oB} = \delta_{oC} + \delta_{oD} = 0$$

$$\delta_I = \frac{\rho U b h^2}{2L}\left(\frac{\partial w_i}{\partial x}\right)_{x=o}$$

$$-2\delta_{IA} + \delta_{IB} = 2\delta_{IC} + \delta_{ID} = -\delta_{IA}$$

$$\delta_o' = -\frac{\rho U b}{2L}\int_{-\infty}^{o} w_i\,dx$$

$$-\delta_{oA}' + 2\delta_{oB}' = \delta_{oC}' + 2\delta_{oD}' = \delta_{oA}'$$

FIG. 6. Superposition of image systems to relate interference parameters for small wings in different types of rectangular tunnel.

44
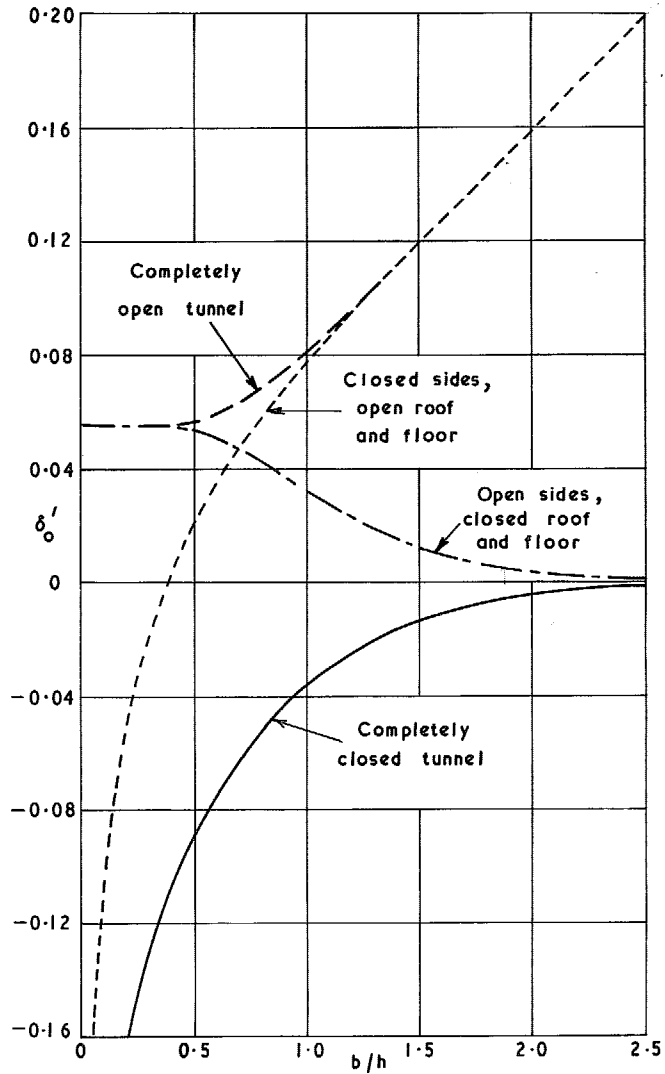
FIG. 7. Unsteady interference parameter for small lifting wings in different types and shapes of rectangular tunnel.
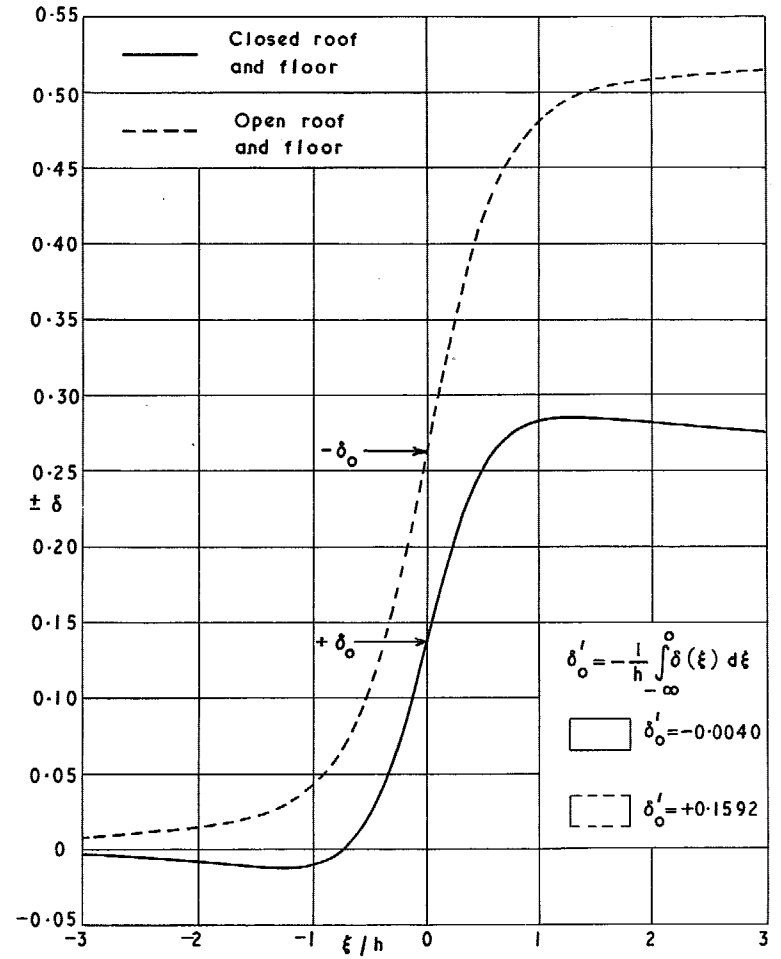
FIG. 8. Streamwise distributions of steady interference upwash in duplex tunnels with solid sidewalls and closed or open roof and floor.
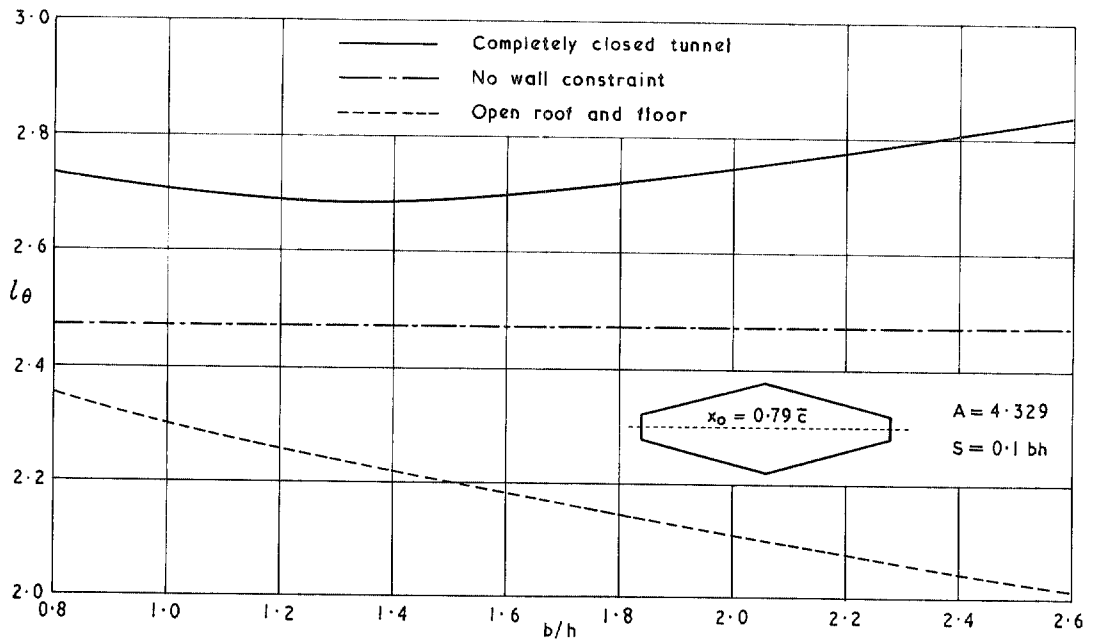
FIG. 9. Calculated steady lift of an unswept
tapered wing at $M = 0.8$ in rectangular tunnels of
constant area.
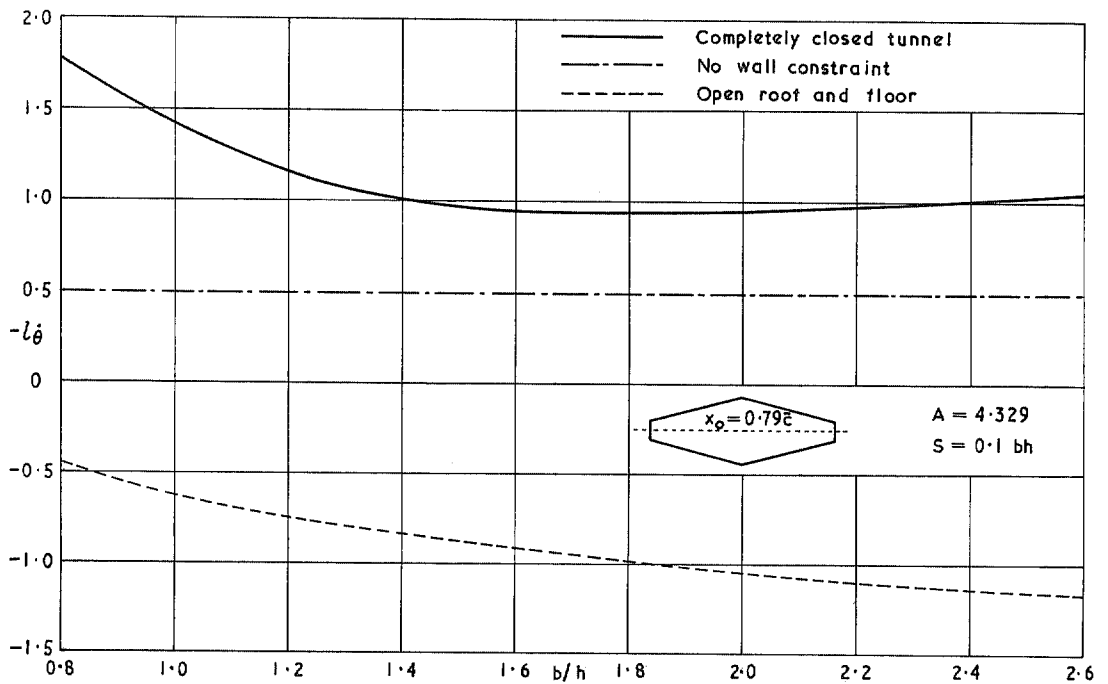
FIG. 10. Calculated cross-damping derivative $l_{\dot\theta}$
of an unswept tapered wing at $M = 0.8$ in. rect-
angular tunnels of constant area.
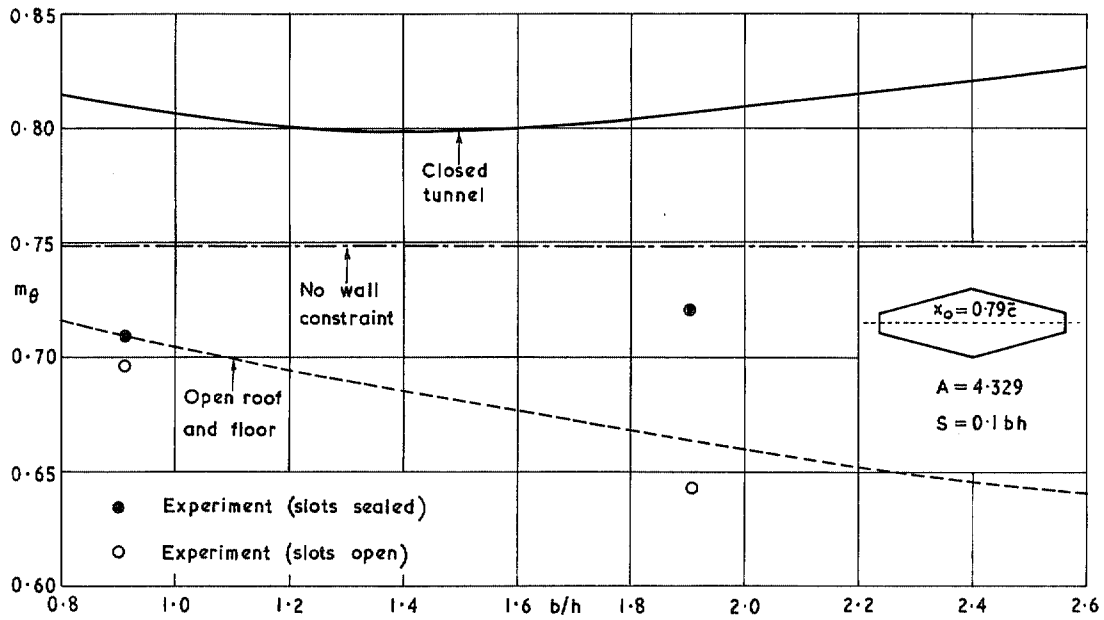
FIG. 11. Calculated and measured pitching stiffness of an unswept tapered wing at $M = 0.8$ in rectangular tunnels of constant area.
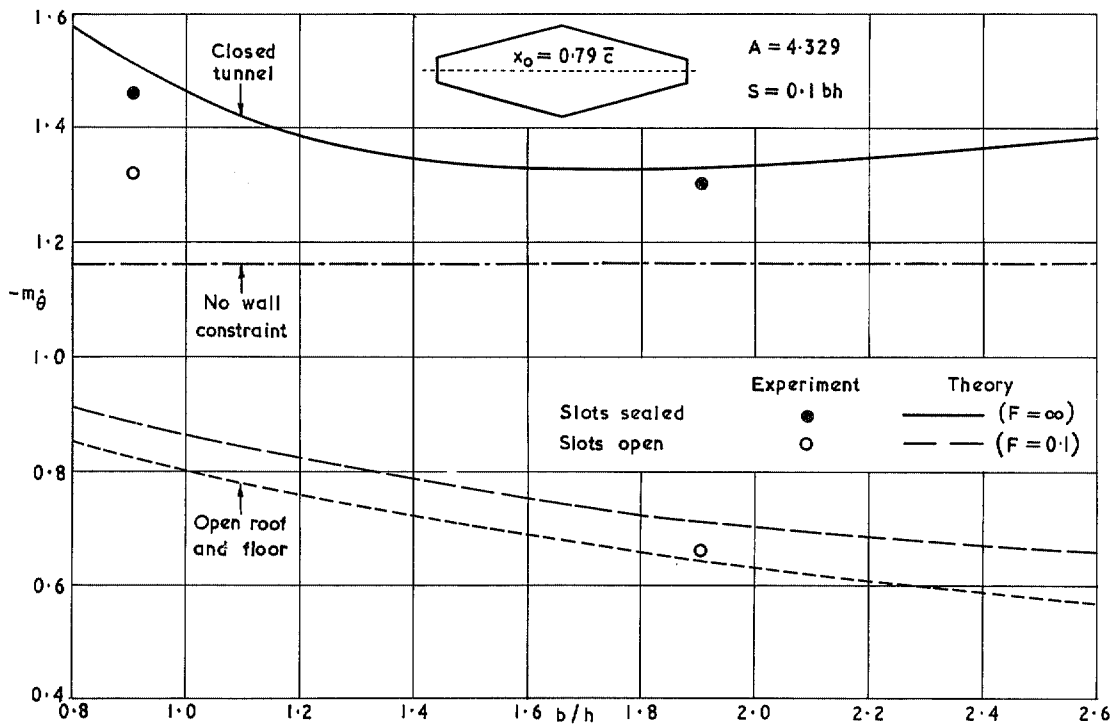
FIG. 12. Calculated and measured pitching damping of an unswept tapered wing at $M = 0.8$ in slotted rectangular tunnels of constant area.

47
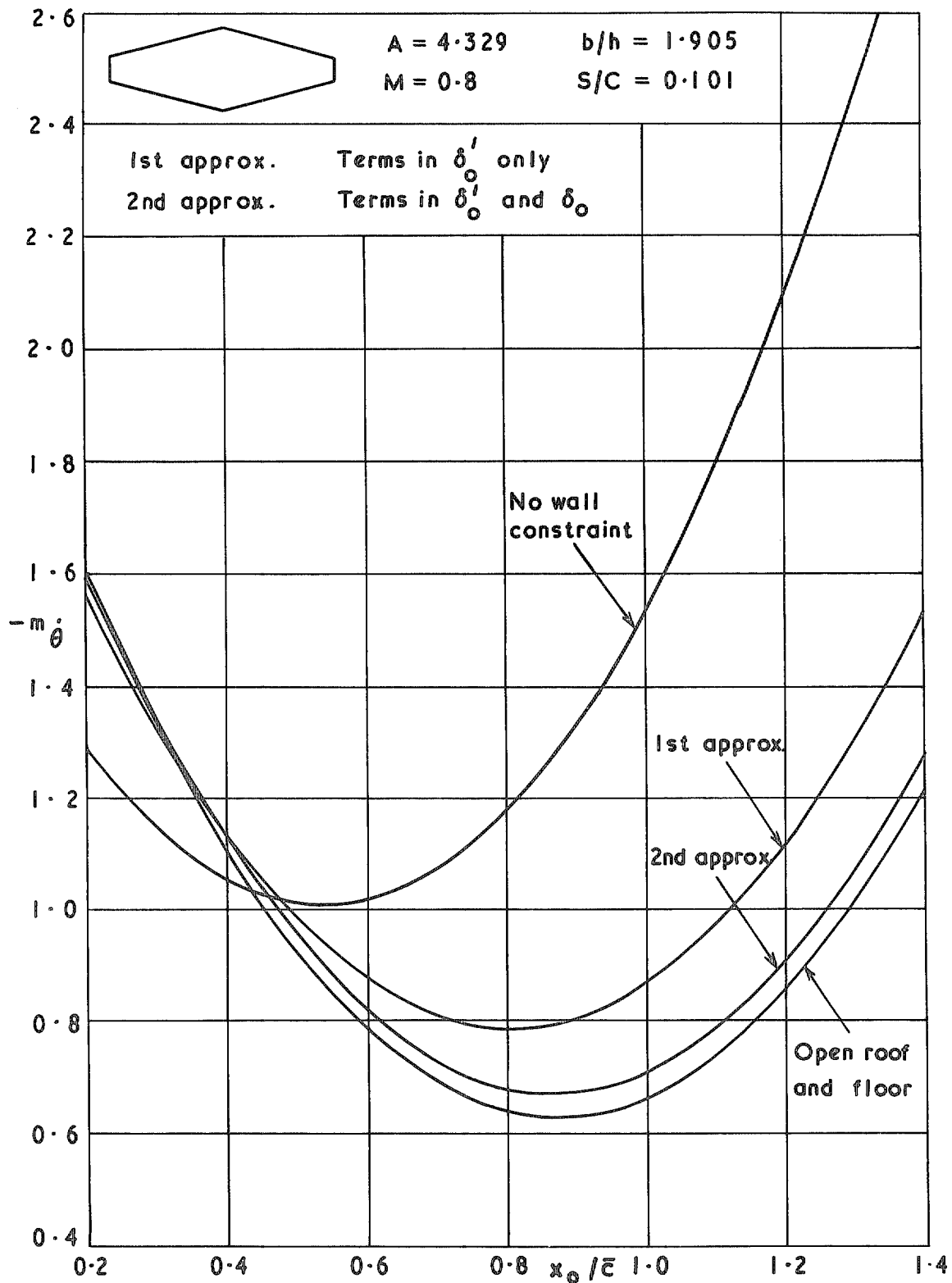
FIG. 13.   Illustration of the relative importance of terms on the right-hand sides of equations (56).

48
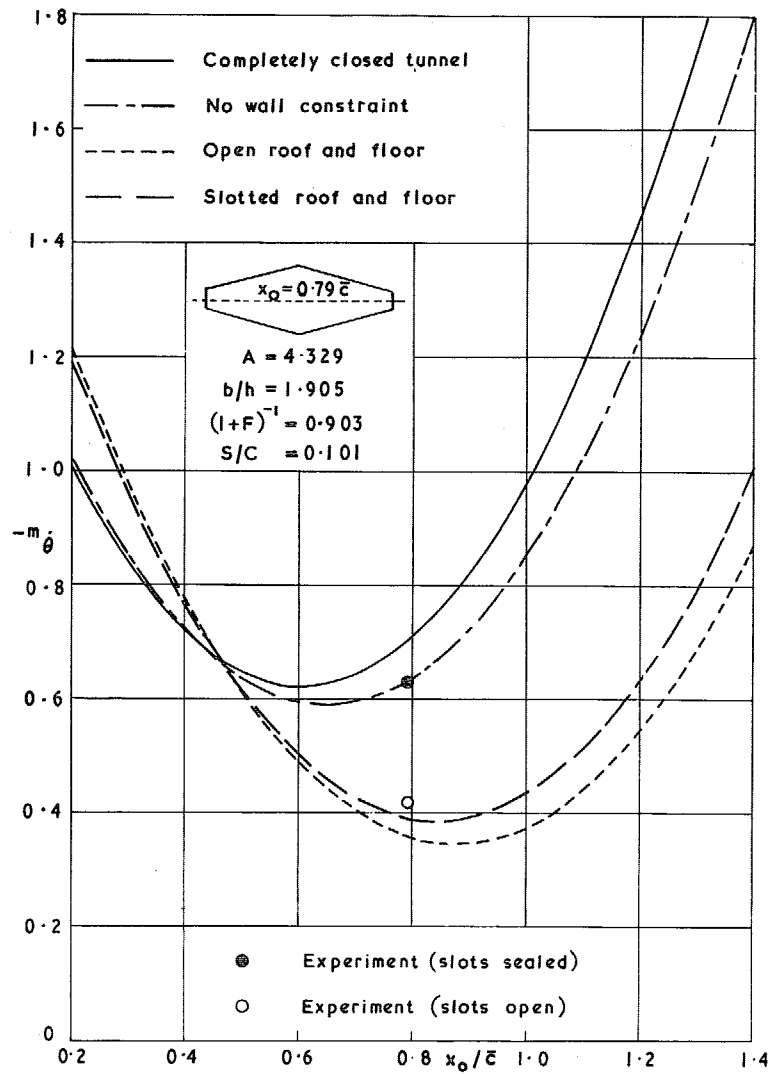
FIG. 14. Calculated and measured pitching damping against axis position for an unswept half-wing in the 25 in. × 20 in. Tunnel at $M = 0.6$.
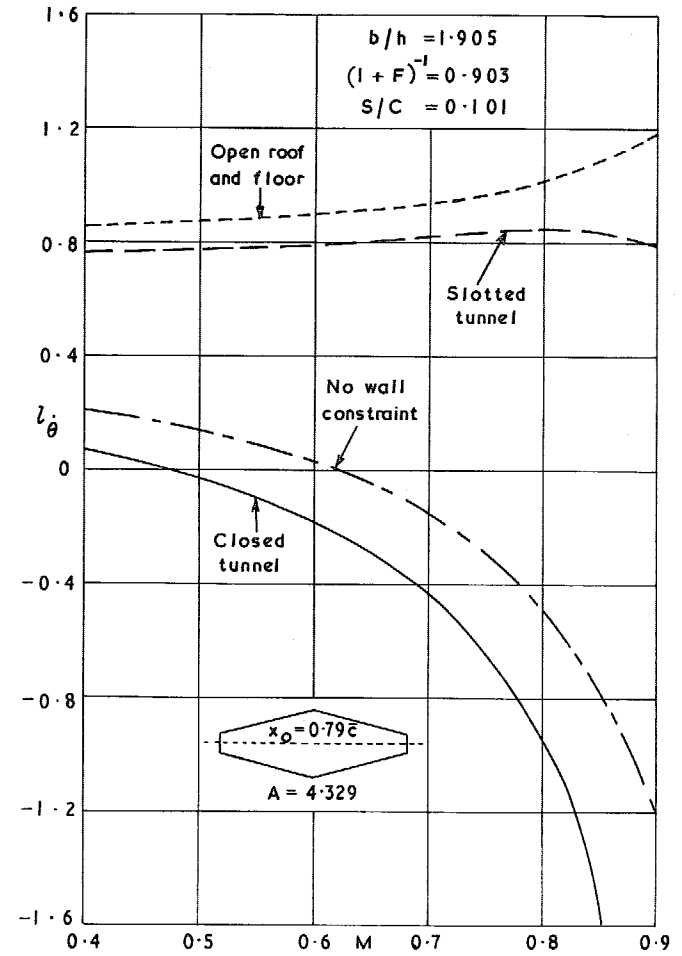
FIG. 15. Calculated $l_{\dot{\theta}}$ against Mach number for an unswept half-wing with and without wall interference in the 25 in. × 20 in. Tunnel.
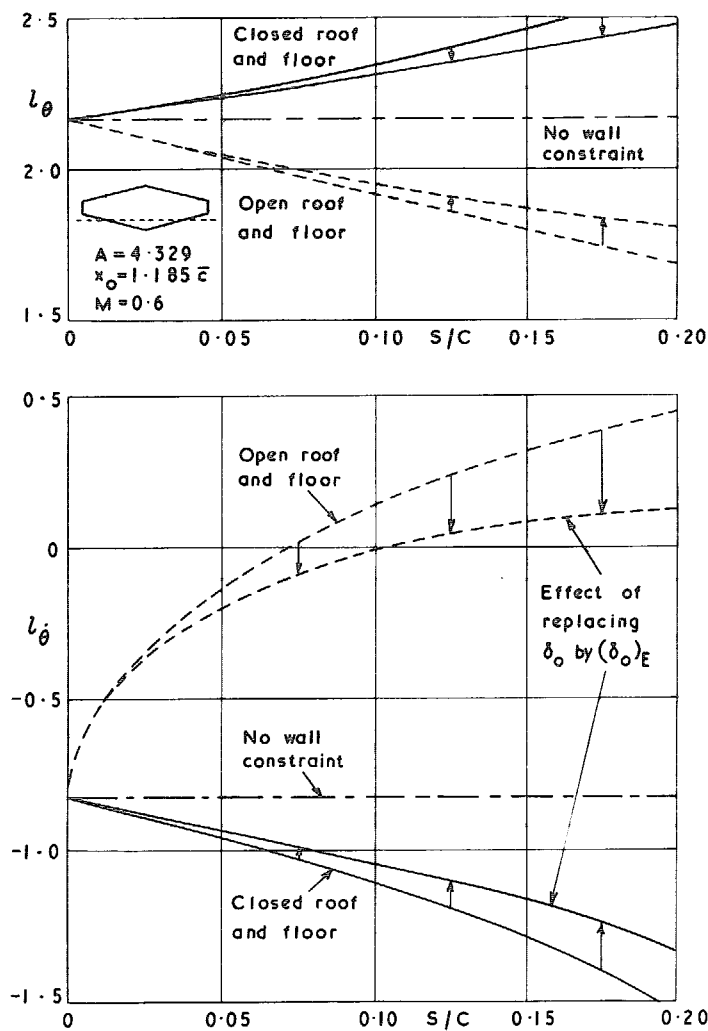
FIG. 16. Effect of model size on lift derivatives of a pitching wing in rectangular tunnels $(b/h = 1.905)$ with solid side-walls.
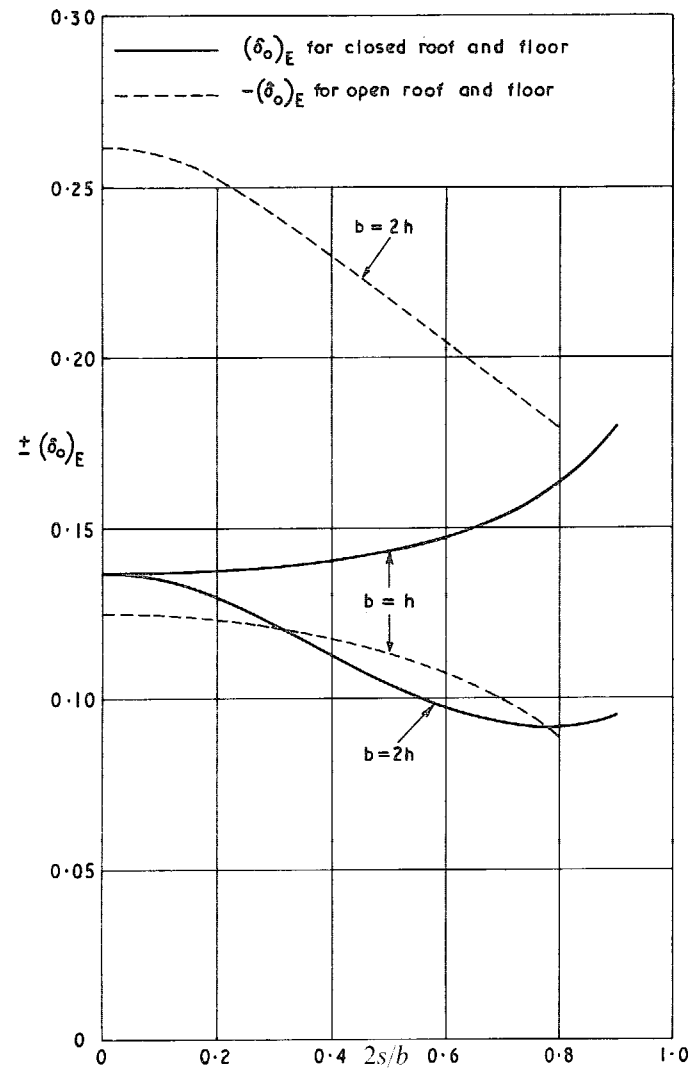
FIG. 17. Steady lift interference parameter for elliptically loaded wings of varying span in rectangular tunnels with solid side-walls.

NPL
36 in. x 14 in.
Tunnel

|← 9·6 in. →| h

|← ½b →|

NPL 9½ in. x 9½ in. Tunnel

|→ 3·6 in. ←|

Delta wings
A = 2·64, A = 3

Unswept wing
A = 4·329

Tunnel	h (in.)	b/h	$(1+F)^{-1}$
36 × 14	30·7$_5$	0·911	0·951
25 × 20	21·0	1·905	0·903
9½ × 9½	7·7	2·468	0·935

NPL
25 in. x 20 in.
Tunnel

|← 11·0 in. →|

M – wing
A = 5·02

The NPL 18 in. x 14 in. Tunnel
is given to scale in Fig. 27.
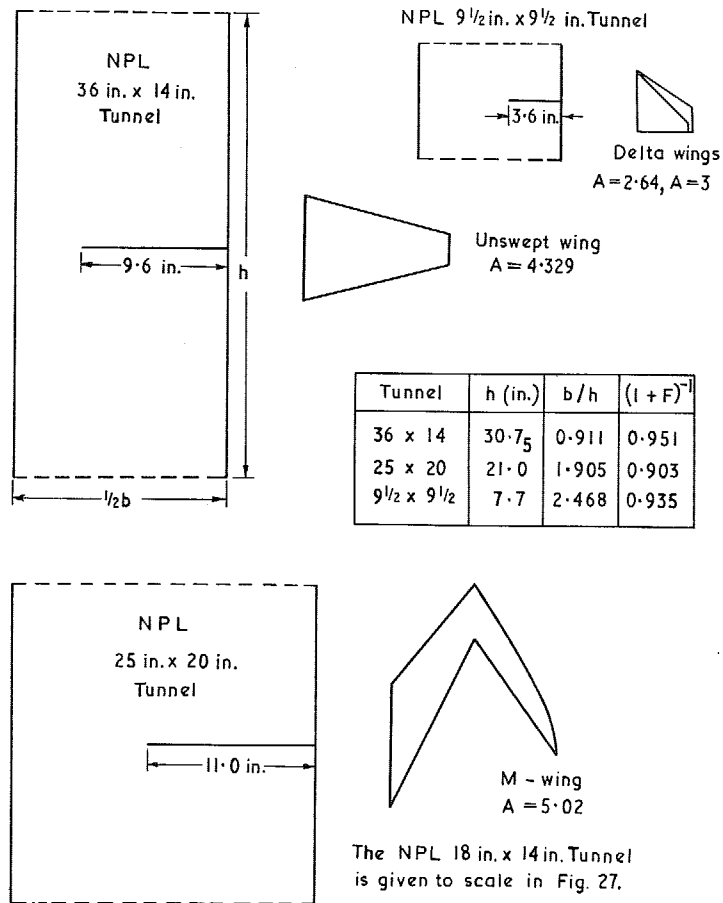
FIG. 18. Slotted-wall tunnels and half-models used in the experiments.

	Expt.	Theory
No wall constraint		—·—
Slots sealed	●	——
Slots open	○	— —
Open roof and floor		— — —

$x_0 = 0.79c$

A = 4·329

S/C = 0·101

$-m_{\dot\theta}$

M
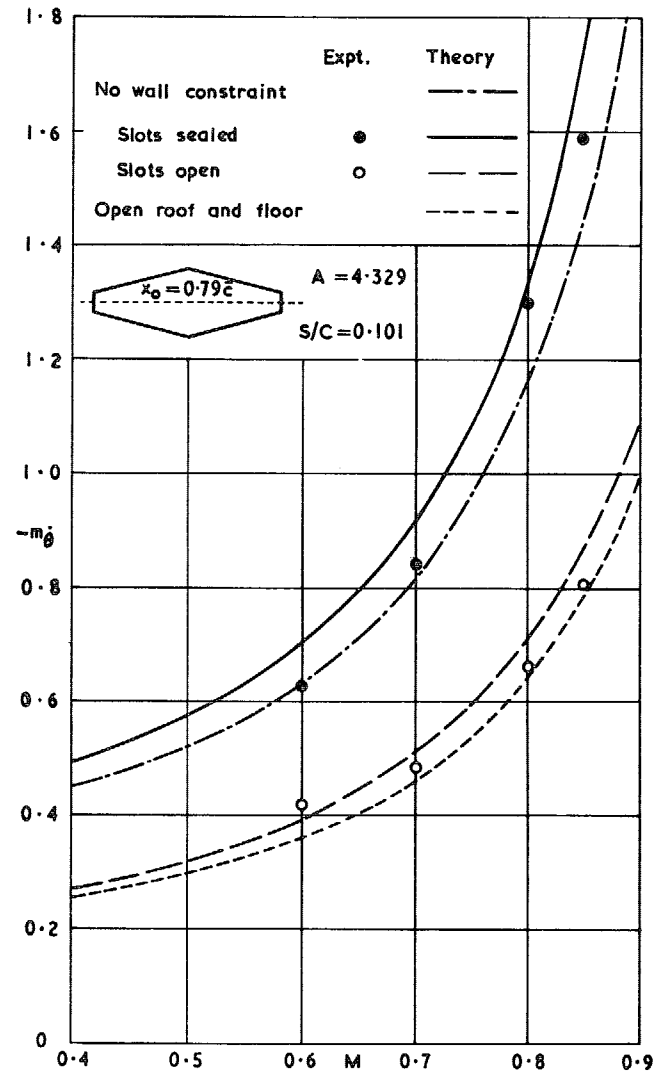
FIG. 19. Pitching damping of an unswept half-wing in the 25 in. × 20 in. Tunnel against Mach number with slots open and sealed.
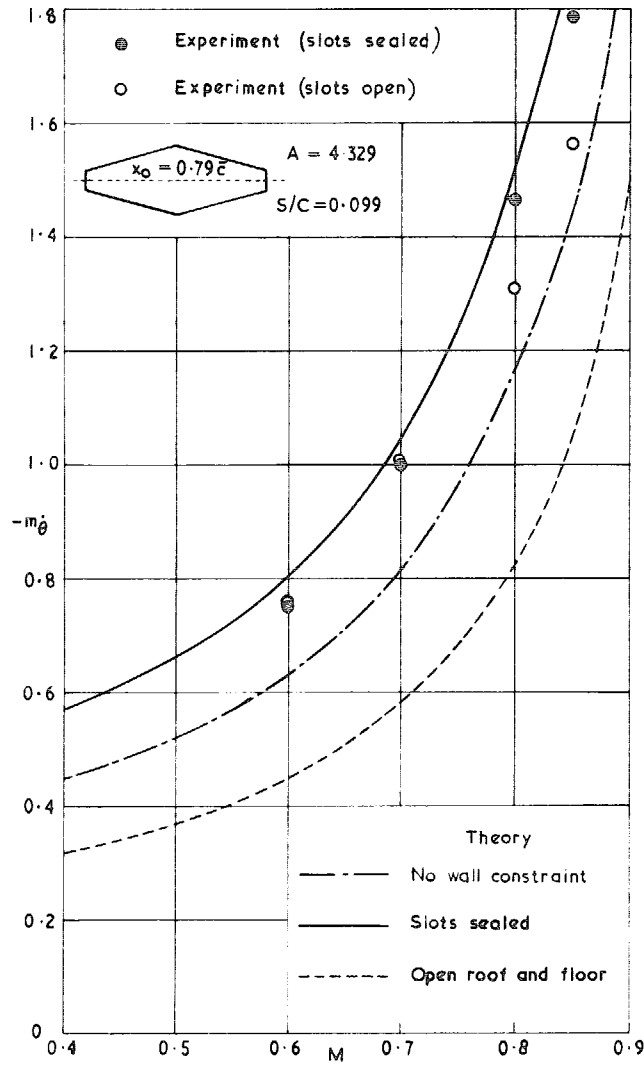
FIG. 20. Calculated and measured pitching damp-
ing of an unswept half-wing in the 36 in. × 14 in.
Tunnel against Mach number.
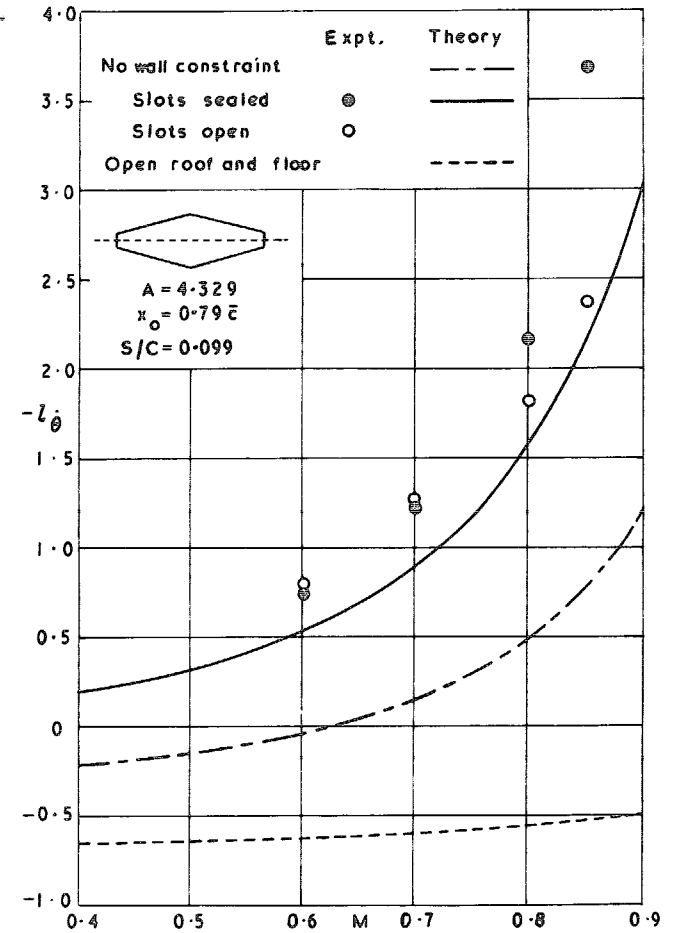
FIG. 21. Calculated and measured $l_{\dot\theta}$ against Mach
number for an unswept half-wing in the 36 in. × 14
in. Tunnel.
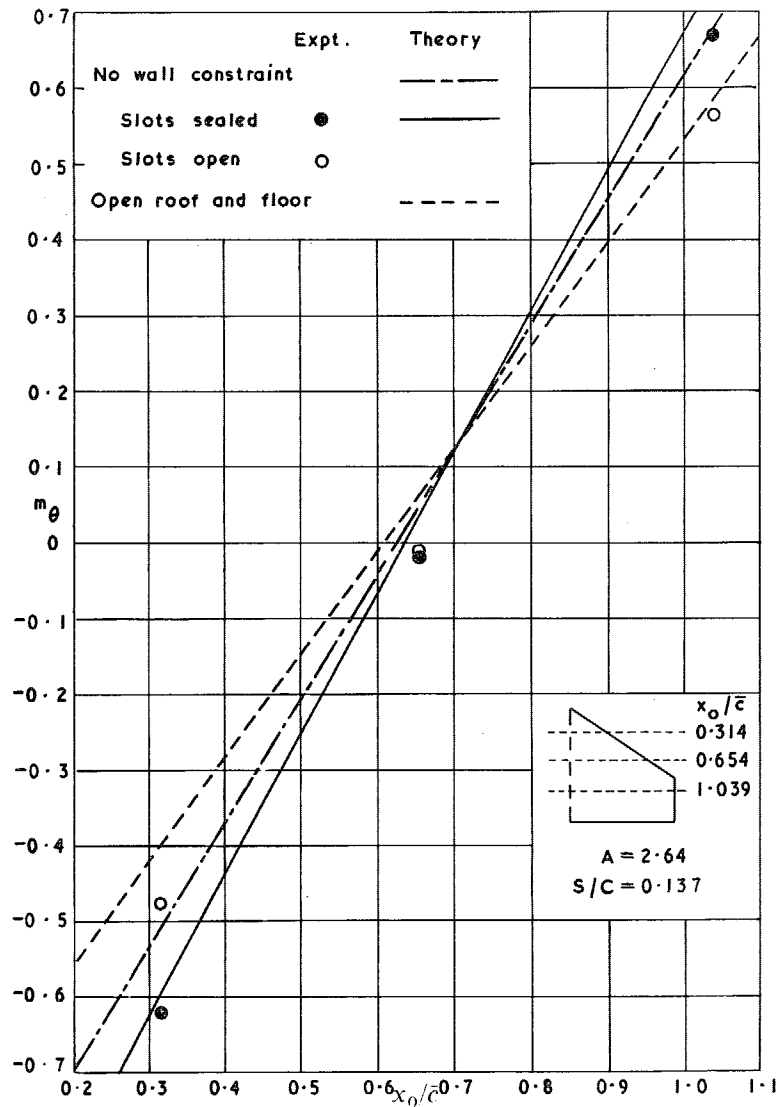
FIG. 22. Calculated and measured pitching stiffness of a half-delta-model in the $9\frac{1}{2}$ in. $\times$ $9\frac{1}{2}$ in. Tunnel against pitching axis at $M = 0.66$.
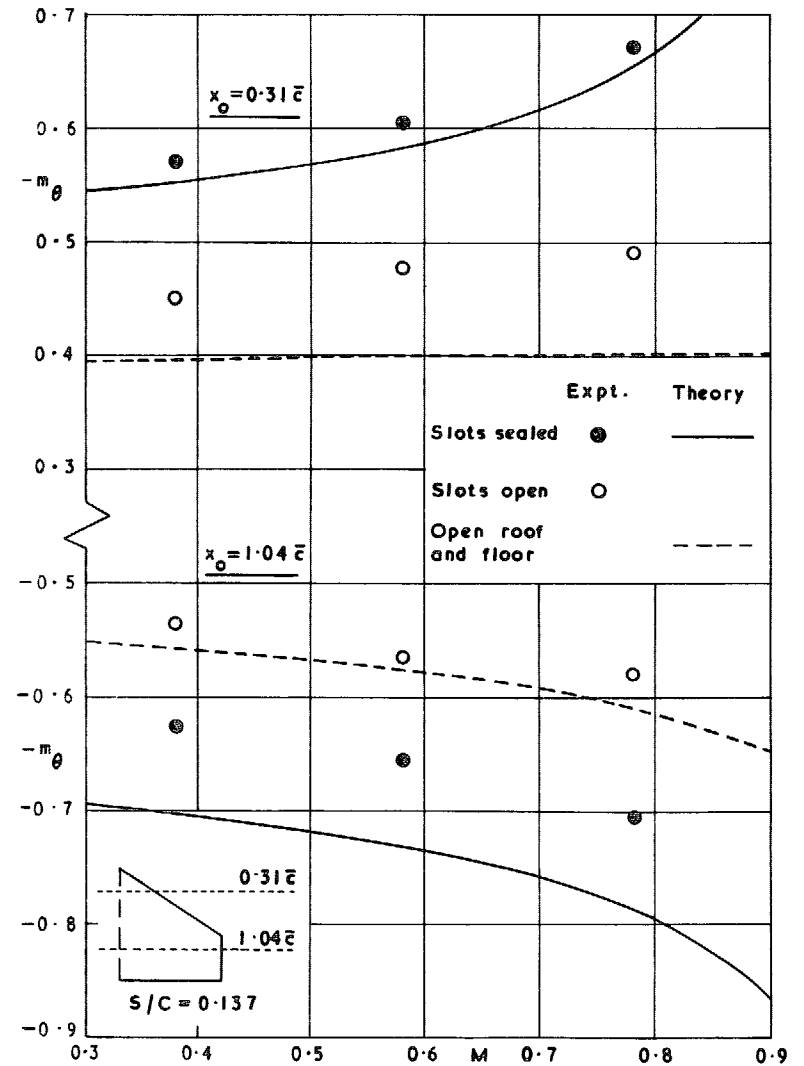
FIG. 23. Pitching stiffness of a half-delta-model ($\Lambda = 2.64$) in the $9\frac{1}{2}$ in. $\times$ $9\frac{1}{2}$ in. Tunnel against Mach number for two pitching axes.
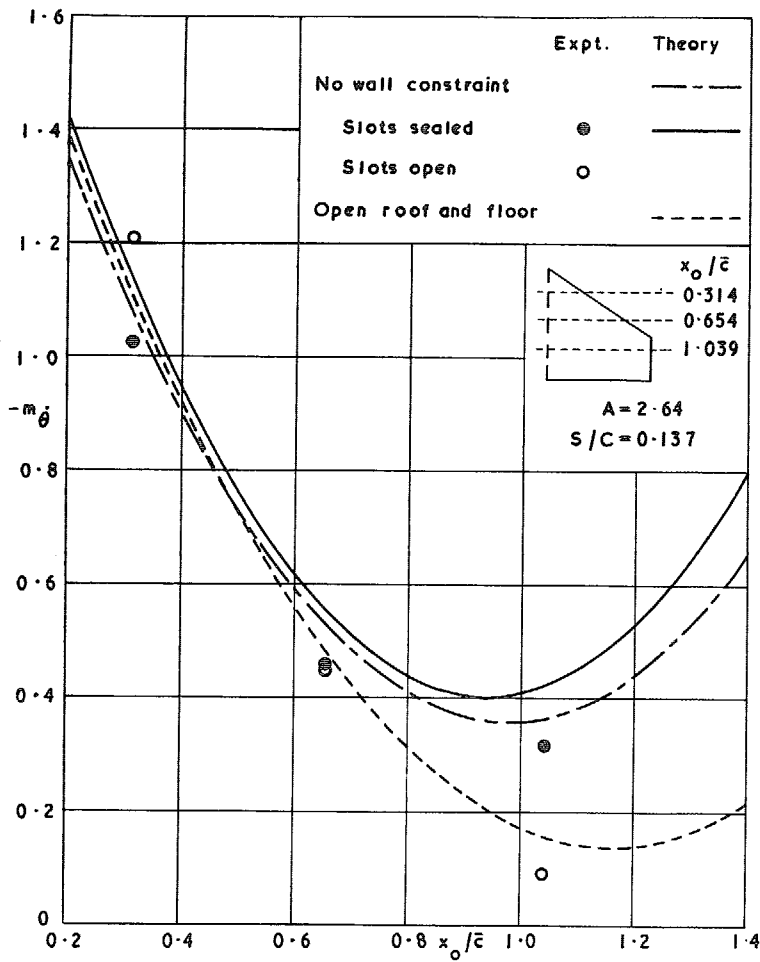
FIG. 24. Calculated and measured pitching damp-
ing of a half-delta-model in the $9\frac{1}{2}$ in. $\times$ $9\frac{1}{2}$ in.
Tunnel against pitching axis at $M = 0.66$.
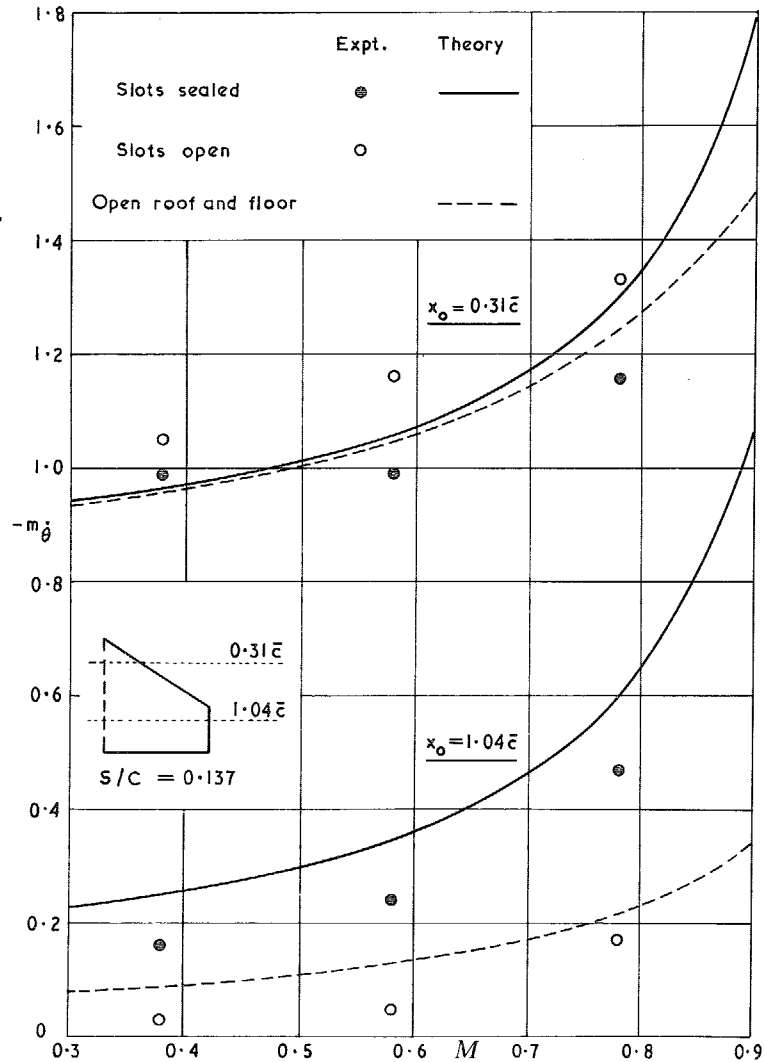
FIG. 25. Pitching damping of a half-delta-model
($A = 2.64$) in the $9\frac{1}{2}$ in. $\times$ $9\frac{1}{2}$ in. Tunnel against
Mach number for two pitching axes.
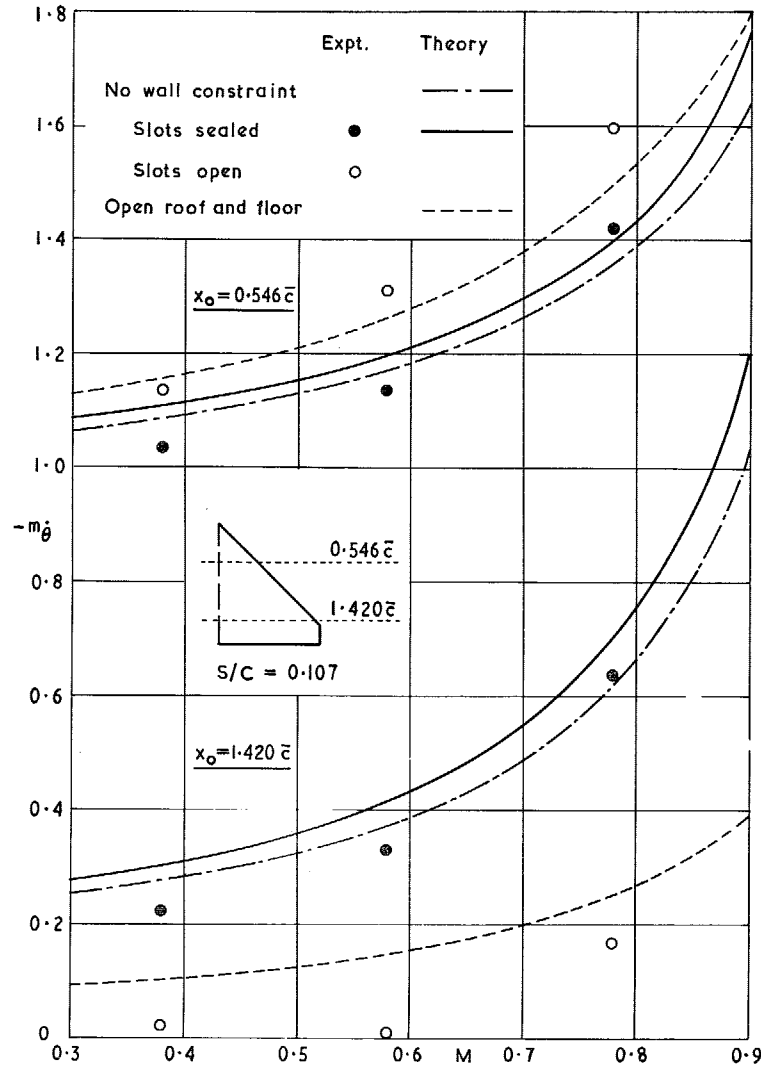
FIG. 26. Pitching damping of a half-delta-model
($A = 3$) in the $9\frac{1}{2}$ in. $\times$ $9\frac{1}{2}$ in. Tunnel against Mach
number for two pitching axes.
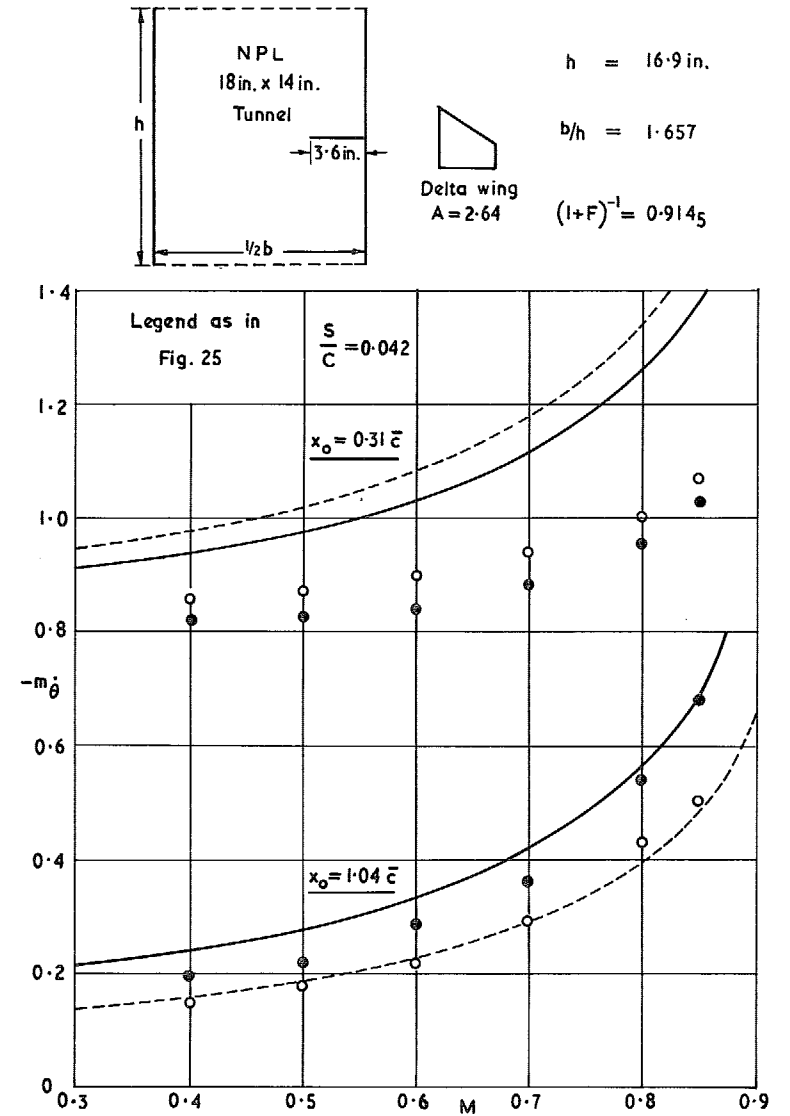
FIG. 27. Pitching damping of a half-delta-model
($A = 2\cdot64$) in the 18 in. $\times$ 14 in. Tunnel against
Mach number for two pitching axes.
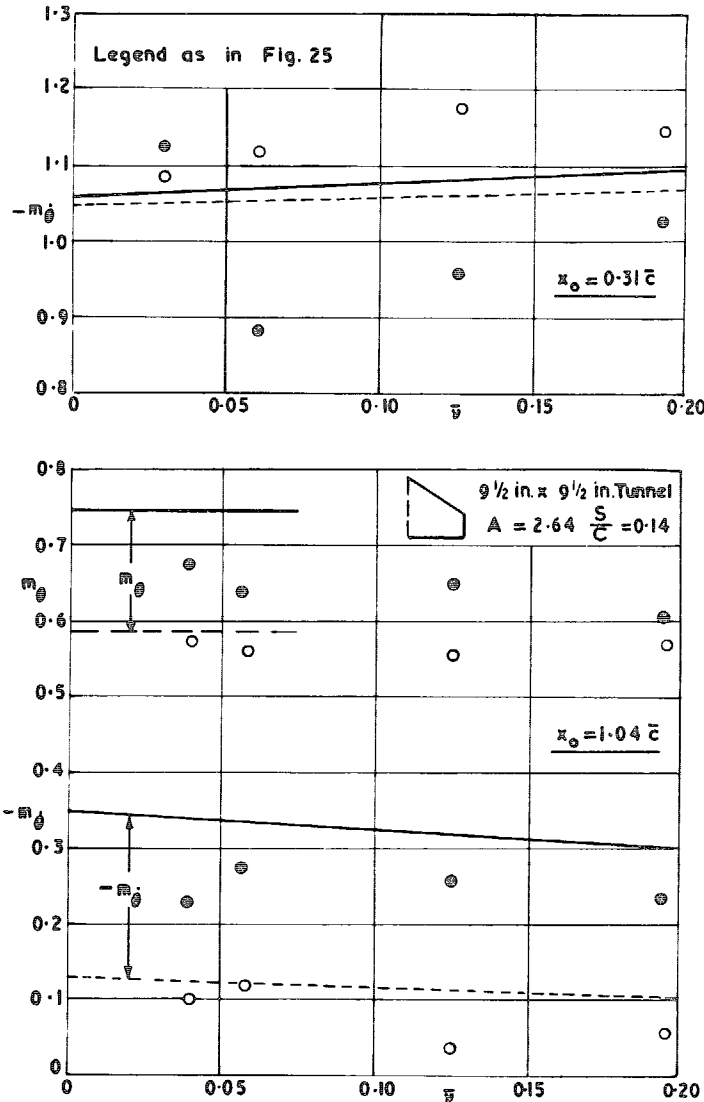
FIG. 28. Measured and calculated direct pitching derivatives for a half-delta-model against frequency parameter ($M = 0.58$).
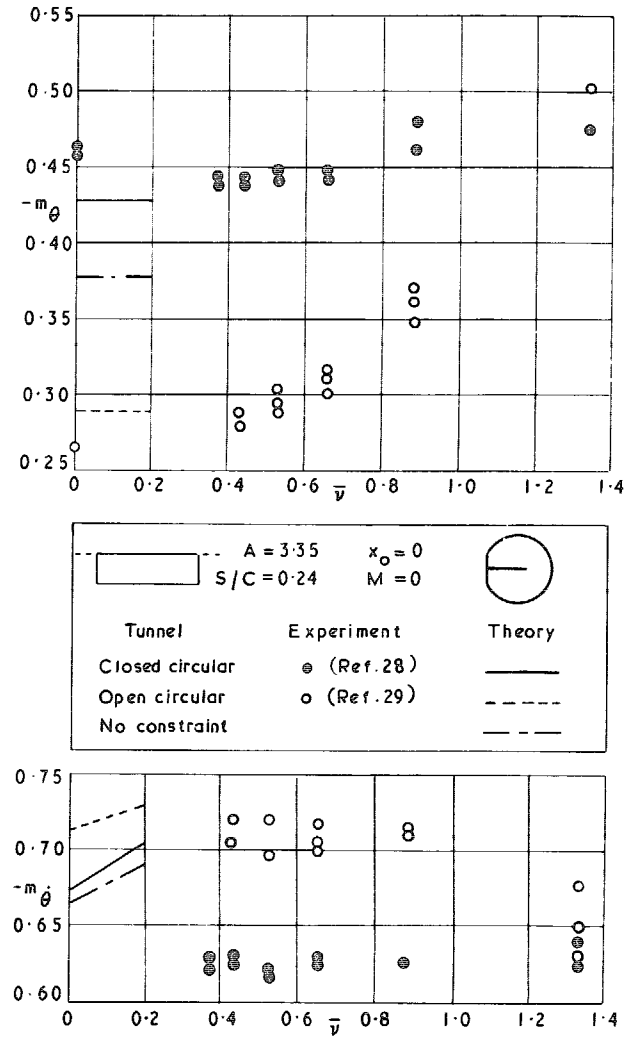
FIG. 29. Direct pitching derivatives for a rectangular half-wing in closed and open circular tunnels with reflection plane.

56
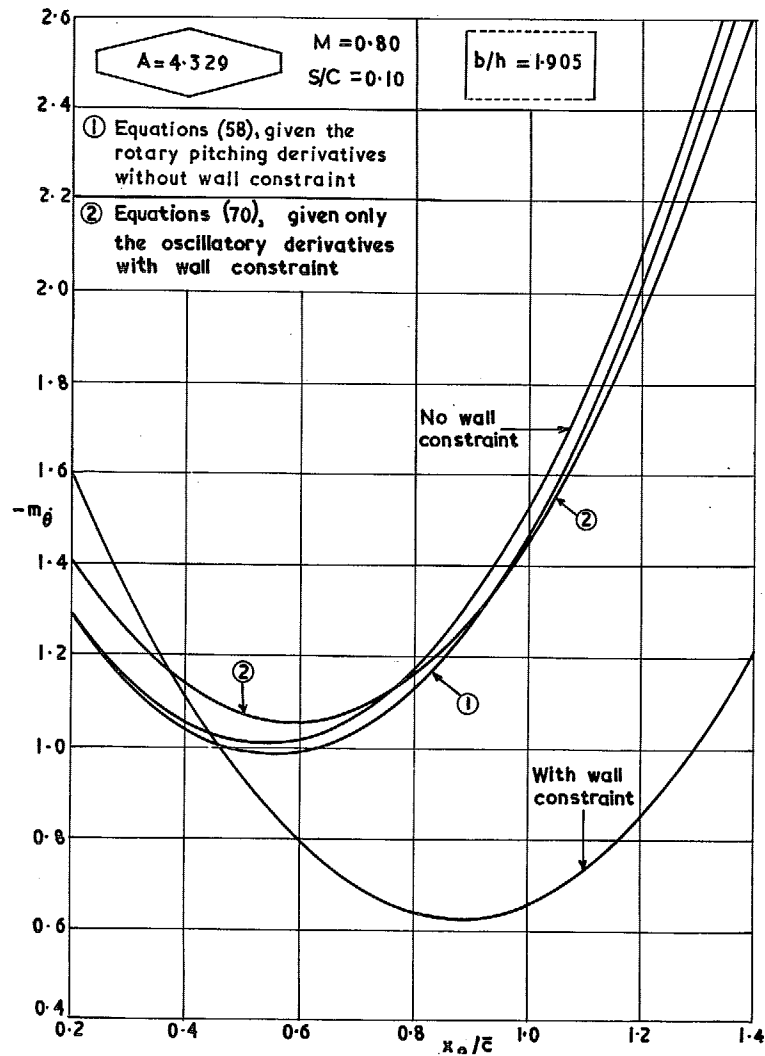
FIG. 30. Practical wall-interference corrections to the pitching damping of an unswept tapered wing against pitching axis.
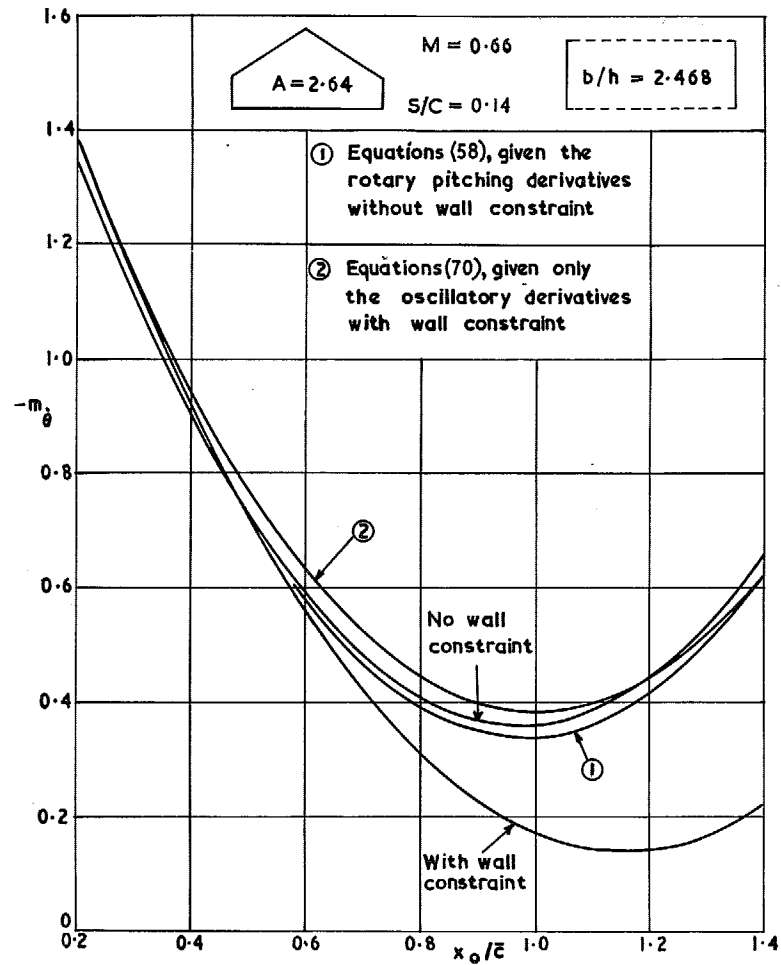
FIG. 31. Practical wall-interference corrections to the pitching damping of a cropped delta wing against pitching axis.
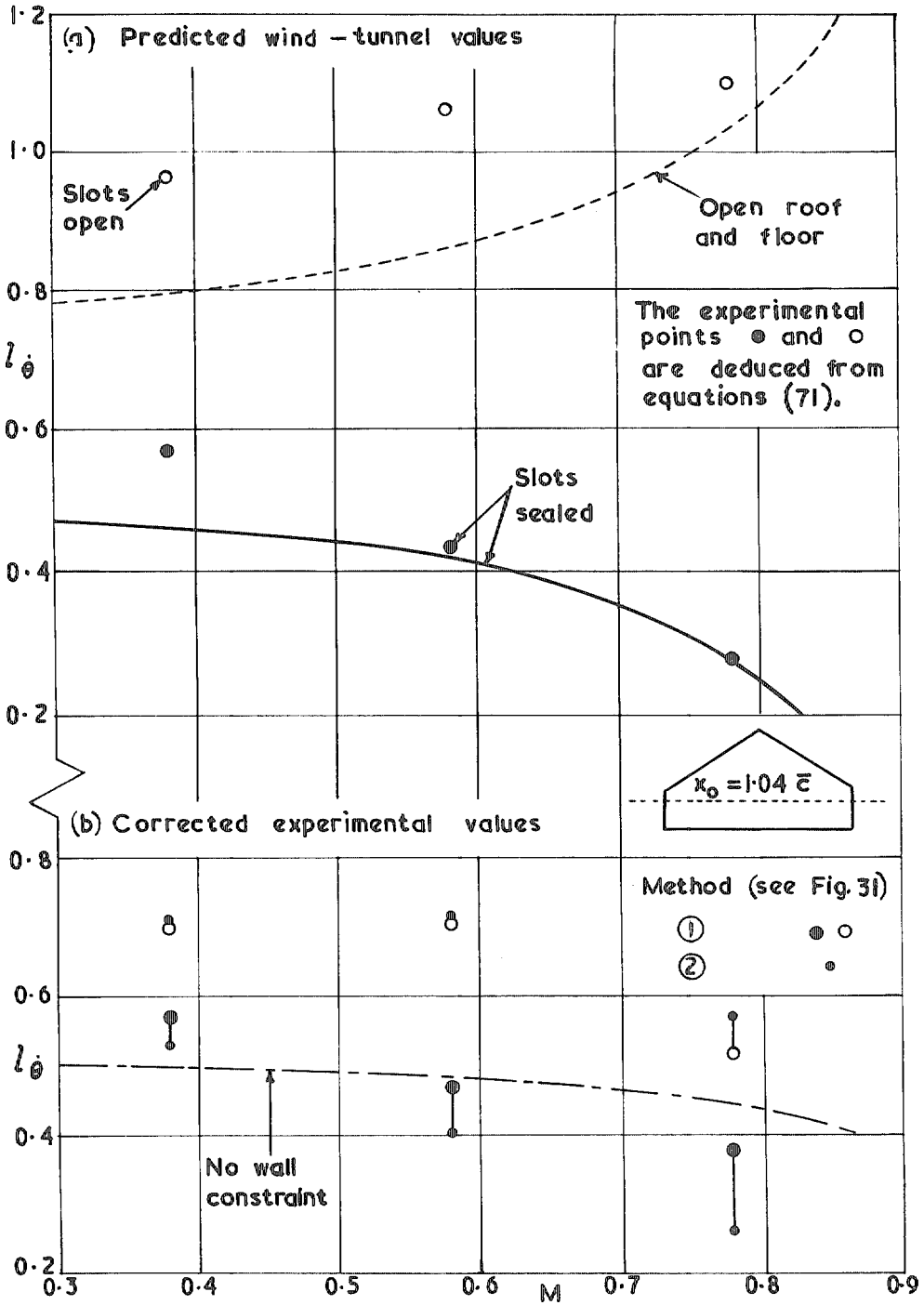
FIG. 32. Estimated l_{θ} against Mach number for a half-delta-model ($A = 2\cdot64$) in the $9\frac{1}{2}$ in. $\times$ $9\frac{1}{2}$ in. Tunnel with and without wall constraint.
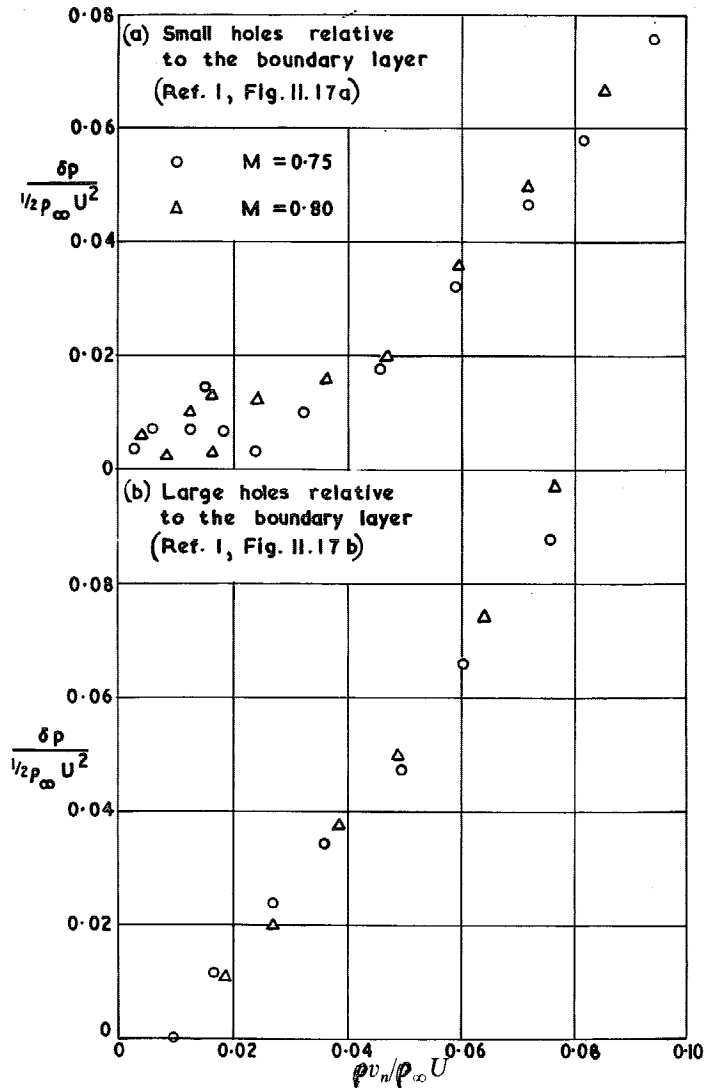
FIG. 33. Pressure-drop coefficient against mass flow ratio across perforated walls of open area ratio 0·225.
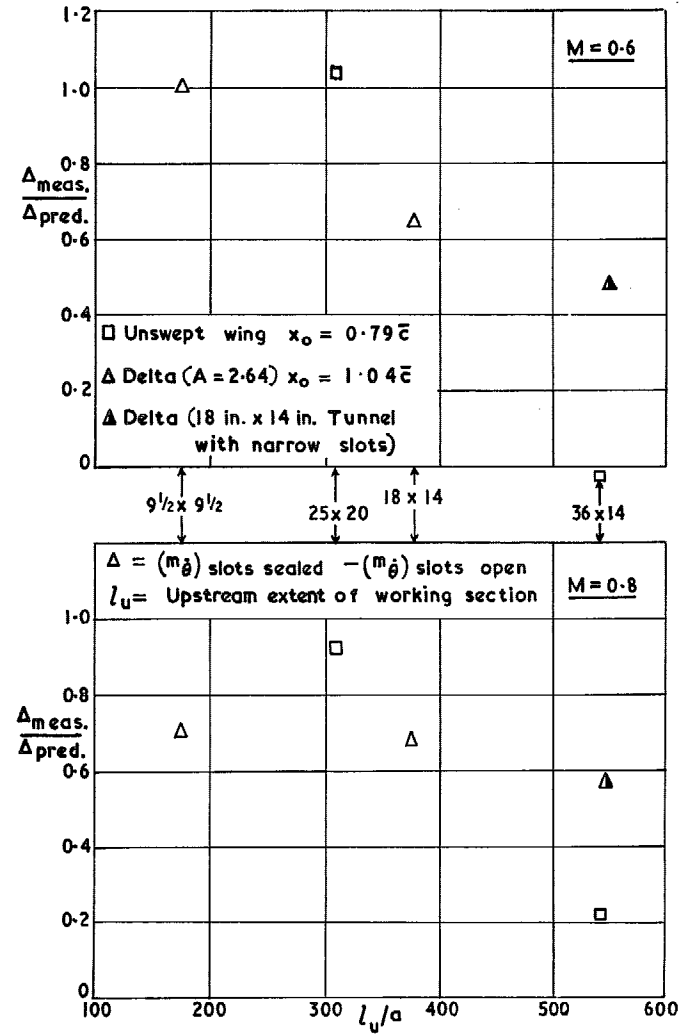

FIG. 34. Effect of relative slot width on the ratio of measured to predicted changes in m_θ due to sealing the slots.